Development of a Novel Continuous Process for Hydrogenation of NBR

by

Lifeng Zhang

A thesis
presented to the University of Waterloo
in fulfillment of the
thesis requirement for the degree of
Doctor of Philosophy
in
Chemical Engineering

Waterloo, Ontario, Canada, 2007

AUTHOR'S DECLARATION FOR ELECTRONIC SUBMISSION OF A THESIS

I hereby declare that I am the sole author of this thesis. This is a true copy of the thesis, including any required final revision, as accepted by my examiners.

I understand that my thesis may be made electronically available to the public.

Abstract

Hydrogenation of nitrile butadiene rubber (NBR) has been carried out industrially for a number of years, producing a material with exceptional resilience to high temperatures and oxidative conditions. Current processes involve a batch reactor which is difficult to optimize further for larger scale production. A continuous process for this particular process is required in order to provide a large volume of production with consistent qualities. The integration of heat balance could be realized in a continuous process. A novel continuous process for hydrogenation of NBR has been developed in the present work.

A multistage agitated contactor (MAC) was proposed as a gas liquid reactor for this process. Comprehensive hydrodynamic data have been acquired under various process conditions. The hydrodynamic behaviour under different operating variables such as stirring speed, liquid flow rate and gas flow rate has been understood through experimental study. It is found that an increase in stirring speed intensifies liquid backmixing while an increase liquid flow rate decreases liquid backmixing. The presence of gas flow helps in reducing liquid back mixing by two coupled effects: liquid entrainment effect due to a cocurrent operation manner and a strengthening effect of liquid flow rate due to its reduction of liquid hold-up. Contradictory conclusions regarding the effect of liquid viscosity on liquid backmixing in a MAC have been resolved through experimental investigation and computational fluid dynamics (CFD) simulations. It is shown that an increase in liquid velocity dampens turbulence which contributes to liquid phase backmixing within the reactor. The established hydrodynamic understanding of MACs in the present work widens its potential application for gas liquid process.

Based on comprehensive understanding of the proposed reactor, a bench-scale prototype was designed and constructed in order to demonstrate hydrogenation performance. One more efficient catalyst for NBR hydrogenation, an osmium-based catalyst, was used in the present work. Hydrogenation degree of NBR in the continuous unit was investigated at operating conditions relevant to industrial applications. It is indicated from the experimental results that a desired hydrogenation degree of over 95% in 2.5% and 5% NBR solutions can be achieved at the conditions investigated. It is also shown that both system pressure and catalyst loading increase hydrogenation conversion. Mathematical modeling of the designed process was established by coupling the intrinsic

catalytic hydrogenation from batch studies and flow behavior of the reactor. A cascade of stirred tanks with back flow (CTB) model was used to characterize the dynamic hydrogenation performance in a MAC. The comparison of experimental results and numerical prediction indicates that the established model could satisfactorily predict the hydrogenation in the designed process with consideration of approximately 30%-50% catalyst deactivated due to impurities and oxygen contamination in the polymer solution. A revised n CSTRs-in-series model was proposed to predict the hydrogenation degree at steady state and a good agreement was found when comparing the predicted results with the experimental data.

A continuous process for hydrogenation at a pilot scale was designed based on the primary results from the bench scale process. A process with a capacity of 50 tons/year was targeted and the hydrogenation efficiency provided by the pilot scale unit has been estimated through the established reactor model.

Acknowledgements

I'd like to express my gratitude to the following individuals:

Professor Garry L. Rempel for his support and guidance of this project. From time to time, his encouragement and precious suggestions help me to get through difficulties experienced through the project. Without this, the project wouldn't have been accomplished.

Professor Qinmin Pan for providing me lots of insightful technical advice during conducting research and writing academic papers.

Dr. N. McManus for sharing the experience and knowledge of catalyst preparation and hydrogenation of NBR.

Professor Stubley for providing CFD software and technical discussion of CFD simulations.

All the friends I made in Waterloo during the past four years, Truth (Zhenli), Mouli, Jialong, Dongyu, Guangwei, Xingwang, Jimmy Liu, Changlin. Life is enjoyable with all of you and the partied we have had together.

My parents, my brothers and my sister for their support and understanding for those years I was studying abroad.

My wife, Qiong, for her sharing of delight and difficulties experienced over the course of this work, and for her unconditional love and support during my study at Waterloo.

The financial support of the Natural Sciences and Engineering Research Council (NSERC) and Lanxess Inc.

To my parents, my wife (Qiong), my brothers and my sister

Table of Contents

List of Figures

List of Tables

Chapter 1 Introduction

1.1 Background

Hydrogenated nitrile butadiene rubber (HNBR) is an elastomer which has been intensively applied in the automotive industry. In particular, it is used as components in engine compartments due to its high thermal and oil resistance. Subsequent benefits can be achieved from its positive impact on the environment and energy saving. An efficient catalytic hydrogenation technique has been developed for the production of HNBR (Rempel, 2000). At present, HNBR is currently produced in industry using a semi-batch process. This is an effective method for its production, allowing small production of a specialized material. However, batch processes are well known to be labour intensive and more difficult to carry out for large volume production due to the time loss during process turnaround. The inability to take advantage of integrating the heat and material balances back into the process is another drawback of the batch process. Like all hydrogenations, a large amount of energy is released during reaction. Since the reaction follows a 1^{st} order kinetics behaviour, approximately 90% of this energy is released during the first half of the reaction. It's difficult to store energy for later use unless a separate part of the process can make use of it during the short period interval in which it is being generated. As the demand for HNBR increases, the batch production strategy may be untenable. The adoption of a continuous process is required to provide a large volume of the production. The advantages of the continuous process lie in that it can provide a good opportunity to integrate the heat and material flows in a process. Excess heat generated during the initial stage of the reaction can be utilized to pre-heat the fresh feed to the reaction temperature. The continuous process enables the large scale production and consequently the product cost will be decreased. The economy and productivity of the continuous process is worthy of the development. A bench-scale packed bed reactor was designed and constructed by Parent (1996) to study the feasibility of conducting the continuous process for HNBR. Kehl (1998) continued to assess the hydrodynamic performance of this packed bed reactor with respect to gas hold-up, liquid dispersion and mass transfer limitations. However, the relatively large length-over-diameter ratio is not practical for an industrial application. Numerical studies have been carried out by Pan and Rempel (2000, 2002, 2003) and the investigation showed that the optimal performance of the designed reactor was achieved by employing a small continuous stirred tank reactor (CSTR) followed by a large plug flow reactor (PFR). The present work is aimed at developing a novel continuous process to efficiently realize the proposed reactor configuration (small CSTR + large PFR) for the catalytic hydrogenation of NBR.

The principal objective of this project is to develop an efficient continuous process for hydrogenation of NBR. A suitable gas liquid reactor is desired to perform the gas liquid process. Hydrodynamic studies were conducted in order to understand the behavior of the designed reactor, such as the phase hold-up, liquid mixing and mass transfer performance. Hydrogenation performance under various operating conditions is attained and mathematical modeling with regard to the coupling behavior between kinetics and flow behavior through the whole reactor were carried out. A pilot scale continuous process was proposed based on the results from the designed bench scale set-up.

1.2 Scope of the Research Work

The project is aimed to develop a novel reactor for a continuous catalytic process for hydrogenation of NBR. The expected characteristics of this reactor include instantaneous mixing of components in the inlet, efficient mixing in the radial direction, and minimum back mixing along the flow direction. Superior gas liquid mass transfer and heat transfer capability should be ensured. Controllable phase hold-up should be another feature of the desired reactor. Therefore, the objectives of this project were to design an efficient reactor which can provide the expected characteristics with simple structures for design and process. The reactor should allow a wide operation range. Depending on operating conditions, both conventional stirred tanks and bubble columns may satisfy some of the requirements but both are ideal mixers with respect to residence time distribution of liquid phase. From the literature study, it is found that a multistage agitated contactor (MAC) is the ideal reactor candidate that can meet all the above requirements, including that of minimal axial mixing of both gas and liquid phase even at low gas loads. However, the hydrodynamic data of this reactor is quite limited and the liquid mixing performance is not well understood when both gas and liquid phases are operated in a co-current manner which has proved to be effective for reduction of pressure drop and minimizing liquid back mixing. More importantly, no unified conclusion is available to describe the liquid mixing behavior in viscous systems, which hinders its potential application in viscous systems. In order to employ a MAC to perform the continuous hydrogenation process, studies on hydrodynamics of MACs are required.

In order to understand liquid backmixing within the designed MAC, a conventional approach was used in an air-water system as discussed in detail in Chapter 3. The liquid residence time distribution (RTD) was investigated under different operating conditions by a pulse input technique. The cascade of stirred tanks with back flow (CTB) model was found to be more suitable to describe the liquid flow behavior in a MAC with few stages while the cascade of non-ideal stirred tank with back flow (CNTB) model exhibited the same performance under turbulent conditions. Two important parameters for a gas liquid process,

namely, gas hold-up and mass transfer coefficient, were also measured in an air-water system. A comparison with literature values was conducted. A new correlation was proposed to predict liquid backmixing in a two-phase flow system from the power input point of view.

After establishing an understanding of the hydrodynamics understanding of MACs in an air-water system, (see Chapter 4) liquid backmixing behavior in viscous systems was investigated by using the same approach in an air-water system. The gas hold-up was also measured in order to correlate liquid backmixing in the presence of gas phase flow. The data obtained from air-viscous systems helped in resolving the existing contradiction about the effect of liquid viscosity on liquid backmixing.

Quite recently, computational fluid dynamics (CFD) has emerged as a powerful tool to tackle chemical engineering problems such as reactor design and process optimization. CFD has the ability to provide more detailed insights. In Chapter 5, liquid residence time distribution in a MAC was predicted via CFD simulations. A suitable simulation strategy was developed and simulation results were validated by experimental data. From this, a certain level of confidence for the application of CFD application was established.

In Chapter 6, the content and the objectives focus on a demonstration of hydrogenation within the constructed continuous set-up. The features and operating flexibility of the self-designed process is elaborated in this chapter. The primary hydrogenation results suggest that the designed reactor can be applied to undertake continuous catalytic hydrogenation. A desired conversion of over 95% can be successfully achieved under certain operating conditions. A macroscopic reactor model is established by coupling reactor flow behavior and intrinsic hydrogenation kinetics. Numerical simulation is performed and compared with the experimental data.

Based on the results obtained from the bench scale set up, a pilot scale unit was designed in Chapter 7 and the hydrogenation performance within the designed unit was predicted by the established model.

Future work is suggested in Chapter 8 based on two aspects. One aspect focuses on hydrogenation performance of the established set-up. Within this aspect, different catalyst systems are proposed to

undertake catalytic studies. Meanwhile, hydrodynamics of the designed reactor at higher pressure conditions is expected to present different behavior from that at ambient conditions. The other aspect is concentrating on CFD simulations of reactive multiphase flow in a MAC. Proper physical models of gas flow in the MAC should be established to predict local information in the reactor. The localized information including hold-up distribution and bubble size distribution should be acquired in order to improve reactor modeling. A population balance equation (PBE) is required to account for bubble flow behavior. Physical models for bubble breakage and bubble coalescence should be implemented in simulations for a better prediction.

Chapter 2 Literature Review

2.1 Hydrogenation of NBR

HNBR is an oil resistant rubber commonly used when physical properties such as tensile strength, modulus and abrasion resistance must be maintained in an environment where the material routinely comes in contact with oils and fuels. Extensive usage can be found in the automotive industry for hoses, seals and timing belts where long term resistance to heat and fuel is crucial.

Nitrile butadiene rubber is produced through emulsion copolymerization of butadiene (Bd) and acrylonitrile (AN). After the polymerization, there is still a residual carbon-carbon double bond left in each Bd segment in the final polymer as shown in Figure 2.1.

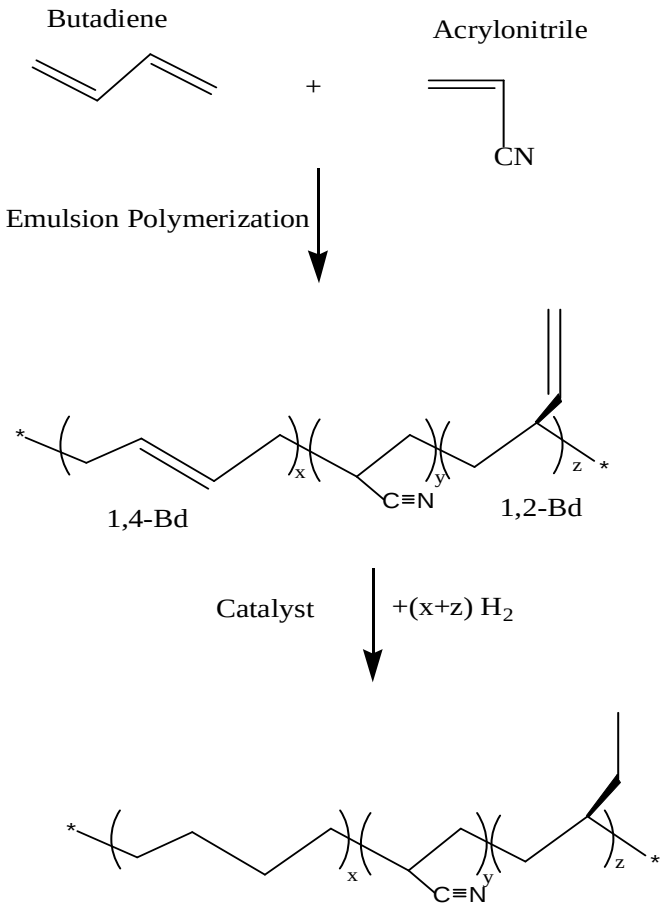

Figure 2. 1 Preparation of hydrogenated nitrile butadiene rubber

The residual unsaturated bond in the polymer backbone is susceptible to breakdown when exposed to heat, light or ozone. By selectively hydrogenating these unsaturated bonds, the performance of the material in resistance to heat and ozone can be significantly improved, as well as its durability over long term exposure to aggressive environments. Any reduction of the polar nitrile group to an imine or amine compromises the oil resistant properties desired. Several catalysts have been developed to selectively hydrogenate the carbon-carbon double bond and leave the nitrile group intact (Rempel, 2000).

2.1.1 Hydrogenation Kinetics

The reaction kinetics and mechanism of the catalyzed hydrogenation of NBR has been intensively studied over a wide range of operating conditions for a rhodium catalyst (Mohammadi and Rempel, 1987; Parent et al., 1996) and for an osmium catalyst (Parent et al., 1998). These extensive investigations showed that the olefin conversion adheres to a first order rate model with respect to carbon-carbon double bond concentration and catalyst concentration. However, with respect to hydrogenation concentration it could vary from zero order to second order, depending on operating conditions such as pressure and the catalytic system employed. In general, the kinetics for the reaction carried out at a given catalyst concentration can be described according to Equation 2.1.

$$-\frac{d[C=C]}{dt} = k'[C=C][H_2]^m \qquad \textbf{Equation 2. 1}$$

wherein the reaction order *m* can be varied from 0 to 2 depending on different catalyst systems applied and different operating conditions under investigation, [C=C] represents carbon carbon double bond concentration, mM, and $[H_2]$ represents hydrogen concentration, mM, while k' is the rate constant,

$mM^{-m}.s^{-1}$.

For homogenous catalyst precursors of the form $RhCl(PPh_3)_3$ and $RhH(PPh_3)_3$, a first-order olefin dependence has been experimentally confirmed. With respect to $[H_2]$, both systems exhibit a first- to zero-order dependence as the system pressure is increased. However, for the $OsHCl(CO)(L)(PCy_3)_2$ (L=vacant or $L=O_2$) catalyst complexes for NBR hydrogenation a second order dependence at low hydrogen pressure changes to zero order dependence as hydrogen pressure exceeds 60 bars (Parent et al., 1998). Strict first order behavior in hydrogen is maintained for the ruthenium analogue $RuHCl(CO)(PCy_3)_2$.

2.1.2 Previous Work on the Development of a Continuous Process of NBR

Several attempts have already been made to develop a continuous process for hydrogenation of NBR. The hydrogenation conversion requirement (95%) precludes an approach of using a single CSTR. A continuous set-up was developed as a packed bed and preliminarily investigated by Parent (1996) and Kehl (1998). Hydrogenation in this established reactor was achieved to some extent. However, it was anticipated that this reactor is not very suitable for a homogeneous hydrogenation operation on a large scale since it possessed a relatively large height-to-diameter ratio (100:1). In addition, the hydrogenation performance of the existing set-up could be simulated by a relatively large portion of CSTR followed by a small portion of plug flow reactor (PFR) (0.83 CSTR+0.17 PFR) according to the previous numerical work conducted by Pan and Rempel (2000). The large portion of CSTR reduced the reactor volume efficiency. However, the hydrogenation degree could be significantly increased when the reactor configuration starts with a small CSTR followed by a PFR. Efficient mixing at the inlet of the targeted reactor is required.

The numerical study of Pan and Rempel (2000) also shows that the coupled behaviors of this process could be described by the parameters: relative capacity of reaction over mass transfer, ability of catalyst in activating molecular hydrogenation, C=C loading level and residence time parameter. Moreover, Pan and Rempel (2003) numerically investigated the effect of phase hold-up on the hydrogenation behavior of a CSTR and a PFR for a continuous hydrogenation process. The optimal liquid hold-up for both CSTR and PFR should not exceed 0.8 under industrial operating conditions. Therefore, an advanced continuous process should be capable of providing a proper phase hold-up either for sufficient liquid residence time or superior gas liquid mass transfer.

2.2 Gas Liquid Reactor Selection

Based on the desired features of the gas liquid reactor for continuous hydrogenation of NBR, efforts have been firstly focused on seeking a suitable gas liquid reactor in the open literature. Since gas liquid process dominates almost 25 percent of current chemical industries, many types of reactors have been developed for gas liquid processes. Amongst those, conventional stirred reactors and bubble column reactors are the most commonly used reactors in chemical industries. Both of them represent ideal mixers with respect to residence time distribution (RTD) of the liquid phase. Their advantages as well as disadvantages have been well addressed in the literature. Conventional stirred reactors have distinguished features such as excellent mixing, high interfacial mass transfer and good heat removal ability. However, the broader

residence time distribution of both phases inhibits its application for a continuous process which requires a relatively long residence time and a narrower RTD. Several CSTRs can be applied to achieve a long residence time but the transportation of reactants from one CSTR to another will be difficult when both gas and liquid phases are involved. In addition, the capital cost will increase. The main advantages of bubble columns are their simple construction, the absence of any moving parts, ease of maintenance and good mass transfer. A relatively long residence time can be obtained under proper operating conditions. However, unexpected axial dispersion occurs in an empty bubble column, which results in a lower conversion rate of the chemical process. Generally two methods have been extensively applied to reduce dispersion (Deckwer, 1982). One approach is incorporation of perforated plates and the other is use of packing material or a static mixer. Incorporation of additional perforated plates into bubble column transforms the single model of bubble column into a multistage cascade version. This new distribution of gas over the perforated plates intensifies mass transfer and reduces the fraction of large bubbles and prevents backmixing in both phases. However, when dealing with viscous liquids, insufficient mixing and gas liquid mass transfer hinders the application of the bubble column. According to the desirable features of a continuous process for hydrogenation of NBR, both conventional stirred tanks and bubble columns may satisfy some but not all requirements for this particular process. Therefore, an alternative gas liquid reactor is pursued to meet the requirements.

A unique reactor, multistage mechanically agitated contactor (MAC), attracts our attention due to its potential application in gas liquid processes. A typical multistage mechanically agitated column is shown as Figure 2.2. The development of this type of this column is based on the drawback of a single stage stirred tank. The single stage tank suffers from substantial gas and liquid backmixing. Moreover, with an increase in the vessel diameter, the power input is ineffective in the wall region and the gas dispersion becomes poor. These limitations can be reduced by using multiple impellers and a height-to-diameter ratio greater than one. In addition, these multistage units can utilize thinner walls as compared with the single stage contactor (SAC) and thus can be advantageously used for high pressure operations. Another advantage of this promising reactor is that different stages can be operated under different conditions. For example, the impeller used in the stirred vessel could be various due to different mixing purposes and the temperature could be operated at different level since the reaction rate could be varied from stage to stage.

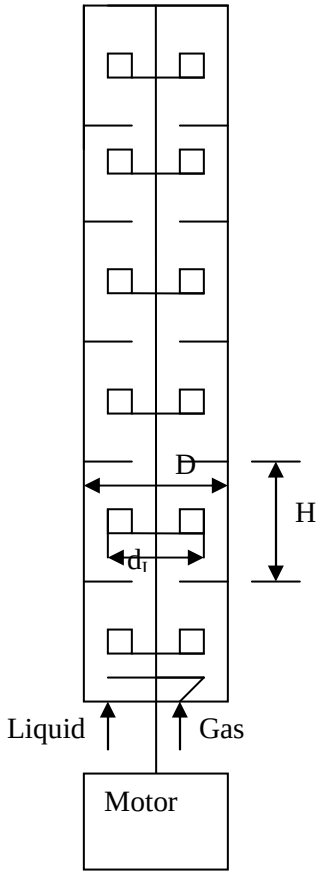

Figure 2. 2 Schematic description of multistage mechanically agitated contactor (MAC)

Most existing multistage agitated contactor applications have been used for liquid-liquid extraction (Oldshue and Rushton, 1952; Bibaud and Treybal, 1966; Miyauchi et al., 1966, Ingham, 1972; Touris and Tavlarides, 1990) or for single liquid phase processing (Lelli et al.1972). MACs have also been applied for gas-liquid absorption due to its potential attractiveness as noted by Joshi et al. (1982). Horizontal baffles with a suitable size are needed to minimize backmixing between impellers, which is different from stirred vessels with multiple impellers. Vadaurri and Sherk (1985) applied an annular opening to reduce the back flow rate and the back flow ratio can be reduced to less than 0.055 when the opening area to column cross section ratio is 0.868 % as shown in Figure 2.3.

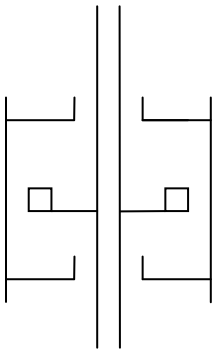

Figure 2. 3 An annular opening applied to a MAC (Vadaurri and Sherk, 1985)

Regarding a MAC industrial application in a continuous manner, only a few cases have been reported. To the best of our knowledge, the earliest application was found to be hydrogenation of fat in a multistage agitated reactor (Perry and Green, 1997); subsequent applications were also disclosed by several patents (US 4,370,470 for continuous production of arylene sulfide polymer with a diameter of 0.203 m and US 4,275,012 for process for continuous refining of oils and fats). However, hydrodynamic data in the open literature for its industrialization or scale up is not sufficiently presented when compared to that for single stage stirred vessels and bubble columns. Only a few studies for air-water are available for a MAC as a gas-liquid contactor (Sullivan and Treybal, 1970; Meister et al., 1979; Breman et al., 1995, 1996a, 1996b; Takriff et al., 1998). The limited studies on MAC are probably due to the high investment costs of a MAC relative to those of a bubble column and stirred vessels. However, this could be compensated by the hydrodynamic advantages of the MAC in various industrial gas-liquid or gas-slurry processes. The following section will thoroughly review and discuss hydrodynamic studies reported in the literature.

2.3 Literature Review of Multistage Agitated Contactors

It has been found in the literature that only a few researchers have investigated hydrodynamic performance of MACs for gas liquid applications. Table 2.1 summarizes reactor geometries and operating conditions reported in those studies.

2.3.1 Liquid Axial Backmixing and RTD

In MACs, a proper design of reactor geometries and operating conditions is required to minimize liquid axial backmixing to achieve high reactor volume efficiency. A suitable reactor flow model is always sought for describing the liquid flow behaviour.

Table 2. 1 Summary of reactor geometric dimensions and operation conditions of MACs

	Meister et al. (1979)	Sullivan and Treybal (1970)	Breman et al. (1995, 1996a, 1996b)	Takriff et al. (1998)
Geometry and Configuration				
d_{vb} (m)	0.015 (4 baffles)	0.013 (4 baffles)	0.009 (4 baffles)	0.02 (4 baffles)
d_{hb} (m)	0.065	0.082	0.04	0.0254 and 0.0521
δ_{hb} (m)	Unknown	0.003/0.013	0.005	unknown
D (m)	0.15	0.152	0.09	0.242
H (m)	0.2	0.083	0.09	0.242
d_I (m)	0.06 (6 bladed)	0.051 (6 bladed)	0.03(12 bladed)	0.0889 and 0.127(6 blades)
N_I	2 (at H_I=0.2H and H_I=0.67H) or 1(at H_I=0.2H)	1 (at H_I=0.5 H)	1 (at H_I=0.5 H)	1 (at H_I=0.5 H)
N_C	9	12	9	2
Operating conditions				
Gases	Air	Air	Air, helium	Air
Liquids	Water	Water	Water, octane, monoethylene glycol (MEG)	Water
Operation manner	Co-current	Counter-current	Single phase flow	Countercurrent and cocurrent
P/(Pa), T(K)	1.0123, 293	1.0123, 278	1.0123, 293	1.0123, 278
N-range (rps)	7-18	3.3-33.3	10-36.7	
u_G (m/s)	0.005-0.03	0.007-0.123	0.01-0.1	0-1 (countercurrent) and0-4 (cocurrent)
u_L (m/s)	0.004-0.012	0.0018-0.0266	0	0-0.05

where d_{vb} is vertical baffle, m, while d_{hb} is the diameter of horizontal baffles, m. δ_{hb} is thethickness of the horizontal baffle, m. D is the diameter of the reactor column, m, while H is the height of each stage, m. d_I is the diameter of the impeller, m. N_I is the number of impellers within one stage whereas N_c is the number of stages in a MAC. N is the stirring speed, rps. P is the system pressure, Pa, and T is the system temperature, K. u_G and u_L represent gas and liquid velocities, m/s.

Where a MAC is concerned, there are two commonly mathematical flow models used to describe the liquid flow behavior. One is the axial dispersion model, which describes an inert tracer as follows:

$$\frac{\partial C}{\partial t} + u_L \frac{\partial C}{\partial z} = D_e \frac{\partial^2 C}{\partial z^2} \qquad \textbf{Equation 2. 2}$$

where C is the concentration of the tracer, kg/m^3. D_e is called the "dispersion coefficient" or "back mixing diffusivity", m^2/s, which servers to represent a quantitative degree of mixing. The analytical solution of the above equation can be obtained at a given boundary condition (Levenspiel, 1999).

The other model is a cascade model of stirred tanks with back flow (CTB) as depicted in Figure 2.4 (a). In this model, perfect mixing is assumed within each stage while there is a constant back flow between consecutive stages. The above assumption is applicable when the stirring speed employed exceeds the critical stirring speed and a complete mixing regime is obtained.

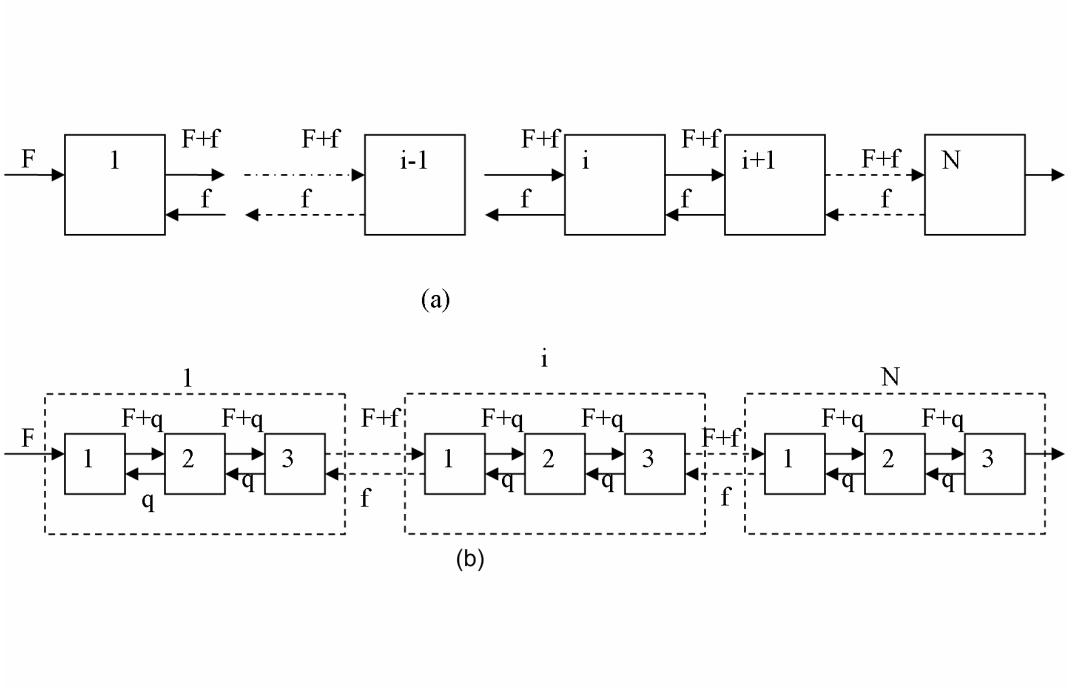

Figure 2. 4 Model of a cascade of stirred tanks with back flow (CTB) (a) (Haug, 1971) and a cascade of non-ideal stirred tanks with back flow (CNTB) (b) (Rehakova and Novosad, 1968)

For an inert tracer component, the mass balance equation at the first stage is

$$V\frac{dC_1}{dt} = F\,C_0 - (F\ +f\ )C_1 + f\,C_2\ ,\quad t>0 \qquad \textbf{Equation 2. 3}$$

C_0 is the inlet tracer concentration, kg/m^3.

For stages $2 \le N_c \le N-1$, the conservation equation reads

$$V\frac{dC_i}{dt} = (F\ +f\ )C_{i-1} + f\,C_{i+1} - (F\ +2f\ )C_i \qquad \textbf{Equation 2. 4}$$

For the stage N_C, it can be expressed as

$$V\frac{dC_{N_C}}{dt} = (F\ +f\ )C_{N_C-1} - (F\ +f\ )C_{N_C} \qquad \textbf{Equation 2. 5}$$

where F is a forward liquid flow rate, m^3/s and f is a back flow rate, m^3/s. C_i is the tracer concentration in the i^{th} stage, kg/m^3. V is the volume of one stage, m^3.

In the CTB model, the assumption of perfect mixing at each stage is sometimes not applicable when non-ideal mixing occurs in an individual stage. A remedy to account for non-ideal mixing is that one stage can be considered to be several vessels in series with an intrastage back flow in turn under imperfectly mixed conditions and the optimal number of vessels in one stage was found to be three (Rehakova and Novosad, 1968) as shown in Figure 2.4 (b). q is the intrastage back flow rate, m^3/s. Both the AD model and the CTB model have been used in various studies. Sullivan and Treybal (1970) and Meister et al. (1979) achieved axial dispersion coefficients for the air-water system at gas superficial velocities u_G: 0.005-0.03 m/s; N:7-18 rps and u_G: 0.007-0.123 m/s; N: 3.3-33.3 rps. However, the AD model assumes the extent of liquid mixing to be constant anywhere in the column. This is not consistent with current knowledge about liquid flow patterns in single stage agitated contactors (Tatterson, 1991). Therefore, the CTB model was preferably adopted to describe the liquid mixing in MACs by Haug (1971), Lelli et al. (1972, 1976), Breman et al. (1996a, 1996b), Takriff et al. (1998) and Xu et al. (2005). In the CTB model, fluid exchange between the lower and upper circulation flows within one stage is assumed to be high enough to provide ideal liquid mixing in that compartment. In contrast, fluid exchange between two consecutive compartments will be significantly lower due to the addition of the horizontal baffles reducing the free area between the compartments. In Table 2.2 a summary of empirical relations for f or D_e with operating variables and/or reactor geometries proposed by various research groups is provided.

The liquid backmixing parameters, D_e and f, can be related shown in following equation (Miyauchi et al., 1966):

$$f = \left(\frac{D_e}{u_L H} - \frac{N_C}{2N_C - 1}\right) u_L A \qquad \textbf{Equation 2. 6}$$

where A is cross-sectional area of the column, m^2.

Table 2. 2 Literature equations for liquid backmixing in MAC

Equation Number	Relation	Authors
BE 1	$f = \frac{0.038\mu_L d_I}{2\rho_L}\mathrm{Re}_1(1+19.5(\frac{\mathrm{Re}_2}{\mathrm{Re}_1}))^{-1}$ for $\mathrm{Re}_1>5000$	Lelli et al. (1972)
BE 2	$D_e = (0.449 + 0.0118\frac{d_I N}{u_L})u_L H$	Bibaud et al. (1966)
BE 3	$f = 0.0098(\zeta\frac{Nd_I}{u_L}[\frac{d_I^2 A_{hb}}{HDA}]^{0.5})^{1.24}u_L A$ ζ is the impeller correction factor and A_{hb} is the horizontal baffle area, m^2.	Haug (1971)
BE 4	$f = 0.027Nd_I(\frac{H}{D})^{0.5}$	Miyauchi et al. (1966)
BE 5	$D_e = 0.375(1-\varepsilon_d)Nd_I\frac{d_{hb}}{D}H$ ε_d is the disperse phase holdup.	Ingham (1972)
BE 6*	$f = f^{\varepsilon_G=0}(1-\varepsilon_G)$ ε_G is the gas holdup.	Nocentini et al. (1988)
BE 7++	$D_e = (0.239 + 0.014\frac{d_I N}{u_L})u_L H$ for $\varepsilon_G = 0$ $D_e = 227.6N\ d_I H(\frac{\rho_L N(1-\varepsilon_G)^2}{\mu})^{-0.928}$ for $\varepsilon_G \neq 0$	Sullivan and Treybal (1970)
BE 8 ++	$f = f^{entr} + (1-\varepsilon_G)^3 f^{ma}$ $f^{ma} = 0.07(\frac{\mu_L d_I^2}{\rho_L})^{0.75}N^{0.28}$ $f^{entr} = 3.14\times10^4\mu_L^{1.2}\sigma^{3.4}N^{-1.4}u_G^{0.61}$	Breman et al. (1996b)

*without horizontal baffle

++ gas liquid system

In BE 1, Re_1 is the Reynolds number with respect to the impeller while Re_2 is the Reynolds number with respect to liquid bulk flow. μ_L is the liquid viscosity, Pa.s. In BE 8, σ is the surface tension, N.m, and ρ_L is the liquid density, kg/m^3. f^{ma} and f^{entr} are back flow rates due to mechanical agitation and entrainment effect, m^3/s.

In Table 2.2, all equations predict that D_e and f increase linearly or almost linearly with the agitation speed. Equations BE 5 and BE 6 predict that D_e and f decrease linearly with increasing dispersed phase holdup ε_d. In contrast, equation BE 7 predicts that the back flow rate will increase strongly with increasing gas holdup ε_G, (f is proportional to $(1-\varepsilon_G)^{-1.86}$). This scenario is also observed by Meister et al. (1979) for an air-water system at relatively low stirring speed, while at higher stirring speed the back flow decreases with increasing ε_G. Equation BE 8 incorporates the effects of fluid properties such as viscosity and surface tension on the back flow rates. However, equation BE 8 was generated based on the experiments of non-flow operations and the effect of liquid velocity on axial liquid mixing was not included, which could be significant as indicated in BE 2, BE 3 and BE 7. Both equations BE 2 and BE 7 show that increasing the liquid velocity increases back flow rates while the opposite influence is observed in equation BE 3. In equation BE 4, the effect of liquid flow rate is also assumed to be zero and the correlation is based on non-flow experiments or the experiments in which the flow effects are small. Ingham (1972) investigated the entrainment effect of drops in a liquid-liquid extraction column. The larger drops have stronger capacity for liquid entrainment. The entrainment could considerably affect the backmixing at a low stirring speed while at a high stirring speed the eddy turbulence generated by agitation is predominant on backmixing. The lack of an accurate dependency of liquid velocity on back flow rate is a hindrance with respect to industrial applications.

2.3.2 Gas Hold-up

The gas hold-up in mechanically agitated reactors is an important parameter for gas liquid flow systems and suitable gas hold-up not only ensures sufficient gas liquid contacting but also provides a reasonable residence time for liquid reactants in the reactor. In general, gas hold-up is a function of the geometric parameters, fluid properties such as viscosity and surface tension, the electrolyte nature of the solution, and the foaming characteristics of the liquid. Many empirical correlations have been developed to describe relations between gas hold-up and operational variables as shown in Table 2.3. Among those relations, the one proposed by Van Dierendock et al. (1970) is considered suitable to predict the gas holdup in single

stage agitated tanks with diameters ranging from 0.165 m to 2.60 m and can be applied for scale-up purposes. Breman et al. (1995) modified this relation by including the viscosity of liquid and influence of gas density on ε_G. The resulting relation predicted quite well the data provided for a MAC. In addition, the relation modified by Breman et al. (1995) was also extended to other systems beyond the air-water system.

Table 2. 3 Empirical correlations for gas hold-up

Reference	Correlation
Meister et al. (1979)	I=1: $\varepsilon_G = 1.21\times10^{-2} N^{0.54} u_G^{0.35}$ for one impeller per stage I=2: $\varepsilon_G = 3.16\times10^{-3} N^{0.63} u_G^{0.56}$ for two impellers per stage
Loiseau et al. (1977)	$\varepsilon_G = 0.011 u_G^{0.36} (\frac{P_G}{V})^{0.27} \sigma^{-0.36} \mu_L^{-0.056}$ P_G is the power input under aeration, W.
Sullivan et al. (1972)	N=0-8.33 rps $\varepsilon_G = 8.876\times10^{-4} N + 1.874 u_G + 2.31 u_L + 0.052$ N=8.33-33.3 rps $\varepsilon_G = 2.315\times10^{-2} N + 0.691 u_G + 0.137 u_L + 0.052$
Van Dierendock (1970)	$\varepsilon_G = \left(0.31 \left[\frac{u_G}{\left(\frac{g\sigma}{\rho_L}\right)^{0.25}} \right]^{0.67} + 0.33 \frac{d_I^2}{D(gD)^{0.5}} (N - N_0)^{0.67} \right)$ Critical stirring speed: $N_0 = 0.15 g^{0.5} D^{1.5} d_I^{-2}$; g is the gravity constant, m/s^2.
Breman et al. (1995)	$\varepsilon_G = \left(0.16 \left[\frac{u_G}{\left(\frac{g\sigma}{\rho_L}\right)^{0.25}} \right]^{0.67} + 0.32 \frac{d_I^2}{D(gD)^{0.5}} (N - N_0) \right) \times \left(\frac{g\mu_L^4}{\rho_L \sigma^3} \right)^{-0.042} (\frac{\rho_G}{\rho_{air}})^{0.12}$ ρ_G and ρ_{air} are the densities for gas and air, kg/m^3.

2.3.3 Volumetric Mass Transfer Coefficient

Many efforts have been made on characterizing volumetric mass transfer coefficient, $k_L a$, s^{-1}, in mechanically agitated gas liquid contactors. Most of them are attributed to single stage vessels. Only a few studies are available for MACs. Sullivan and Treybal (1972) and Meister et al. (1979) have investigated gas liquid mass transfer with a stationary method for air-water only in a MAC. Sullivan and Treybal (1972) did not obtain a reliable $k_L a$ because their mass transfer rate was almost entirely determined by the gas side resistance against mass transfer due to the high solubility of the tracer (ammonium) used in their study. A well-known correlation proposed by Van't Reit (1979) is frequently applied for single stages. However, this correlation is only valid for turbulent conditions and doesn't include the effects of liquid properties. In contrast, various authors have proposed $k_L a$ relations or individual relations for mass transfer coefiicient, k_L, m/s and interfacial area, a, m^2/m^3, for pure liquids, which incorporates the influence of physical properties on $k_L a$. Table 2.4 summarizes correlations for mass transfer coefficient in gas liquid reactors.

Table 2. 4 Empirical correlations for mass transfer coefficient in stirred vessels

References	Correlation
Meister et al. (1979)*	I=2: $k_L\alpha = 69.6(P_G/V)^{0.707}(u_G)^{0.305}$ I=1: $k_L\alpha = 104.9(P_G/V)^{0.801}(u_G)^{0.248}$
Van't Riet (1979)	$k_L a = 0.026(\frac{P_G}{V})^{0.4} u_G^{0.5}$
Breman et al. (1996a)*	$a = 51.1(\frac{P_G}{V})^{0.283}\sigma^{-0.19}(\frac{u_G}{v_B})^{(0.127+0.211\mu_L)}$ $v_B = 1.53(\frac{g\sigma}{\rho_L})^{0.25}$
Calderbank (1958)	$k_L = 0.42(\frac{\mu g}{\rho_L})^{1/3}(\frac{D_L\rho_L}{\mu_L})^{0.5}$ where D_L is molecular diffusivity, m^2/s. $a = 1.44(\frac{P_G}{V})^{0.4}\sigma^{-0.6}\rho_L^{0.2}(\frac{u_G}{v_B})^{0.5}$
Yagi and Yoshida (1975)	$k_L a = 0.06(\frac{D}{d_I^2})(\frac{d_I^2 N\rho_L}{\mu})^{1.5}(\frac{d_I N^2}{g})^{0.19}(\frac{\mu_L}{\rho_L D_L})^{0.5}(\frac{\mu_L u_G}{\sigma})^{0.6}(\frac{Nd_I}{u_G})^{0.32}$

* correlation based on MACs while others for single stage stirred vessels

The correlation with Meisters' parameter values for a MAC predicts $k_L a$ to be hardly affected by superficial gas velocity. Breman et al. (1996a) proposed a correlation for the interfacial area, which takes into account a combined effect of superficial gas velocity and the liquid viscosity on *a*. The derivation of the correlation was based on mass transfer measurement with three gas liquid systems (air-water, air-Monoethylene Glycol, Helium-n-octane). The overall influence of u_G on $k_L a$ in this relation was such that $k_L a$ was hardly affected by u_G both for water and n-octane while $k_L a$ was predicted to increase significantly with increasing u_G for more viscous systems.

2.3.4 Impeller Selection

Impeller types used are very crucial for gas liquid agitated vessels because of power performance, flow patterns generated and gas handling capability of impellers which determine the whole performance of the stirred vessel. Impellers are typically classified according to mixing regime, laminar or turbulent mixing. For laminar mixing, the impeller diameters approach the size of the tank since the transport of momentum by laminar flow is poor. The impeller is required to bring fluid motion to the entire contents of the tanks. In most laminar flow applications, baffles are not needed and can cause poor mixing behaviour. In turbulent mixing, large-diameter impellers are not used since turbulent flow transports momentum well and the impellers are typically one fourth to one half of the tank diameter. In the turbulent flow regime, classifications are further refined into axial and radial flow impellers. It is found that radial flow impellers disperse the feed more rapidly than axial flow impellers. This is attributed to less turbulence at the liquid surface generated by axial flow impeller (Tatterson, 1991). Therefore, a typical radial impeller, standard Rushton turbine, is commonly used in industry. The Rushton turbine is a six-bladed disk turbine as shown in Figure 2.5.

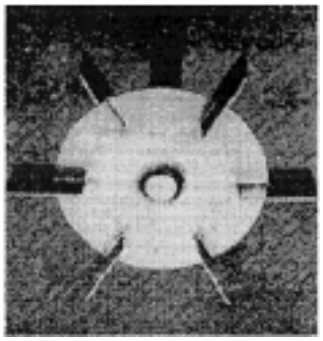

Figure 2. 5 Schematic description of Rushton turbine

A preliminary impeller screen was conducted before commencing a hydrodynamic study on a continuous set-up (Zhang, 2004). The experimental investigation included gas hold-up and mass transfer coefficient characterization by using three disk turbines, Rushton turbine (RT), concave blade disk turbine (CBDT) and Scaba, respectively. The impellers were tested in water and 0.5 % CMC solution. It was found that a RT generally exhibited the highest performance in gas hold-up and mass transfer coefficient under the same operting conditions since a RT has the highest power number (N_p=5) while CBDT and Scaba have power numbers of 4 and 1.5, respectively. As a consequence, RTs of different scales relative to MACs were primarily used as impellers.

2.4 Computational Fluid Dynamics (CFD)

A computational fluid dynamics (CFD) technique was introduced to chemical engineering community about two decades ago (Harris et al., 1996; Delnoij et al., 1997). The application of CFD to reactor design has significantly progressed since then with the development of CFD techniques. Without the aid of CFD, the reactor design procedure is closer to an art than science due to the complexity of fluid mechanics prevailing in reactors, particularly in stirred vessels. CFD offers the possibility of predicting the detailed flow and turbulence characteristics of the reactor under different geometries and operating conditions by governing equations. A fully predictive CFD simulation is able to present a spatial and temporal variation of velocity, pressure, and temperature and concentration distribution in stirred vessels with single phase flow or multiphase flow.

Several recent publications have established the potential of CFD for describing hydrodynamics of the stirred tank and improving the knowledge of local information about turbulent field, gas hold-up, interfacial area, bubble size and reaction rates (Bakker and Van Den Akker, 1994; Hjertager, 1998; Lane et al., 2002, 2005; Kerdouss and Proulx, 2006). The approach of Euler-Euler has been commonly used. In this approach, both gas and liquid phases are treated as interpenetrating continua and conservation equations are solved for each phase. In order to predict gas hold-up in sparged reactors, a constant bubble size is usually adopted (Deen et al., 2002; Ranade, 1997). However, local information about gas hold-up and bubble size can not be obtained by the above approach. Therefore, Bakker and Van Den Akker (1994) and Venneker et al. (2002) used a conservation equation of bubble volume and population balance equations for turbulent gas dispersion in stirred tanks, respectively. However, the two-phase flow field and turbulence properties were simulated in one-way coupling by scaling single phase flow obtained by CFD simulations and the impeller was modeled with imposed boundary conditions via experimental data.

Often, this data is too difficult to obtain in the case of multiphase flow and does not capture the detailed information between blades. Lane et al. (2002, 2005) carried out a fully three dimensional CFD simulation to model a gas sparged tank equipped with a single Rushton turbine using multiple references of frame (MFR) model for impeller and bubble number density equation, including various expressions for drag and dispersion forces. Kerdouss and Proux (2006) predicted gas dispersion and bubble size in a double turbine stirred tank. A bubble number density equation was implemented in order to account for the combined effect of bubble breakage and coalescence in the tank.

From the literature survey, it can be concluded that CFD can be utilized to help in understanding the flow behavior prevailing in the designed reactor and provide the detailed information about mixing, gas dispersion as well as reaction performance.

Chapter 3 Hydrodynamic Studies in MACs with Air/Water System

3.1 Introduction

In the literature, limited studies of hydrodynamic characteristics of MACs have been reported for gas liquid processes. Liquid backmixing, gas hold-up and mass transfer in MACs have been reported by only a few groups (Meister et al., 1979; Sullivan and Treybal, 1970; Breman et al., 1995, 1996a, 1996b; Takriff et al., 1998). The former two research groups used the axial dispersion (AD) model to describe the axial liquid backmixing in the MACs and obtained relatively good RTD fitting with a large number of stages. The number of stages for MACs used by Meister et al. (1979) and Sullivan and Treybal (1970) are 9 and 12, respectively. However, when the number of stages is fairly low, the AD model is not applicable to describe the liquid flow behaviour (Takriff et al., 1998; Zhang et al., 2005a, 2005b). The level of liquid backmixing determines the stage efficiency, which is defined as the equivalent number of CSTRs over the number of actual stages. For instance, when the CTB model is employed, a MAC with a back flow ratio of 1 has only a 38% actual stage efficiency; a value of less than 0.06 for back flow ratio is required to achieve 90% stage efficiency. Therefore, a MAC with low liquid backmixing is desired in order to maintain high stage efficiency. Many efforts have been made to develop mathematical relations between liquid backmixing with operating variables, as summarized in Table 2.2 of Chapter 2. However, only limited data have been available for gas liquid systems, in particular, for gas viscous systems. Meister et al. (1979) reported some quantitative data about liquid backmixing for a MAC as a gas liquid contactor. However, the axial backmixing hasn't been explored under a relatively long liquid residence time. The liquid residence time investigated was less than 10 minutes (Meister et al., 1979; Sullivan and Treybal, 1970). Breman et al. (1996b) and Takriff et al. (1998) applied non-flow technique to study interstage backmixing and as a consequence the effect of liquid flow on liquid backmixing was automatically excluded.

In summary, the liquid backmixing study for a gas liquid system is scarce and no general correlation can be used to predict the liquid backmixing in a MAC for a gas liquid process specifically when gas and liquid phases are operated in a co-current manner. Based on the literature survey, one objective of this chapter was to investigate the influences of operating parameters such as liquid flow rate, gas flow rate, stirring speed, and gas hold-up on liquid backmixing in order to provide the fundamental data for the application of the MAC as a gas liquid contactor operated in a co-current fashion. The study was also

aimed at providing fundamental data for the application of a MAC to a continuous gas liquid process with a relatively long residence time. In this chapter, liquid backmixing was characterized through residence time distribution (RTD) studies over a large range of operating conditions. Model discrimination was conducted by comparing experimental RTD curves with those predicted from the models. A suitable backmixing parameter was extracted from the experimental RTDs under various operating conditions. In a two-phase flow system, the gas hold-up is an important parameter to characterize gas liquid contact and is also considered to play an important role on liquid backmixing. Therefore, the gas hold-up was also investigated in order to achieve comparable data with the literature values. The gas hold-up was measured by a stop-flow approach as described the following section. Mass transfer coefficients were evaluated through a steady state approach. The detailed experimental description is given in the following section.

3.2 Experimental Section

3.2.1 Experimental Set-up and Operation Conditions

A schematic diagram of the experimental set-up of the multistage agitated contactor is shown in Figure 3.1. Two MACs consisted of 6 stages (H/D=1) separated by horizontal baffles with central circular opening of 0.02 m I.D and the thickness of 2 mm. The diameters for two reactors are 0.10 m and 0.15 m, respectively. Each compartment was provided with a standard Rushton Turbine agitator attached to a long shaft within the MAC. The dimension and geometries of impellers are shown in Figure 3.2 and the diameter of the impeller is 0.05 m. Four vertical baffles with a width of 1/10 D are also supplied and equally spaced. A conductivity cell was installed at the outlet of the set-up for measurement of tracer concentrations.

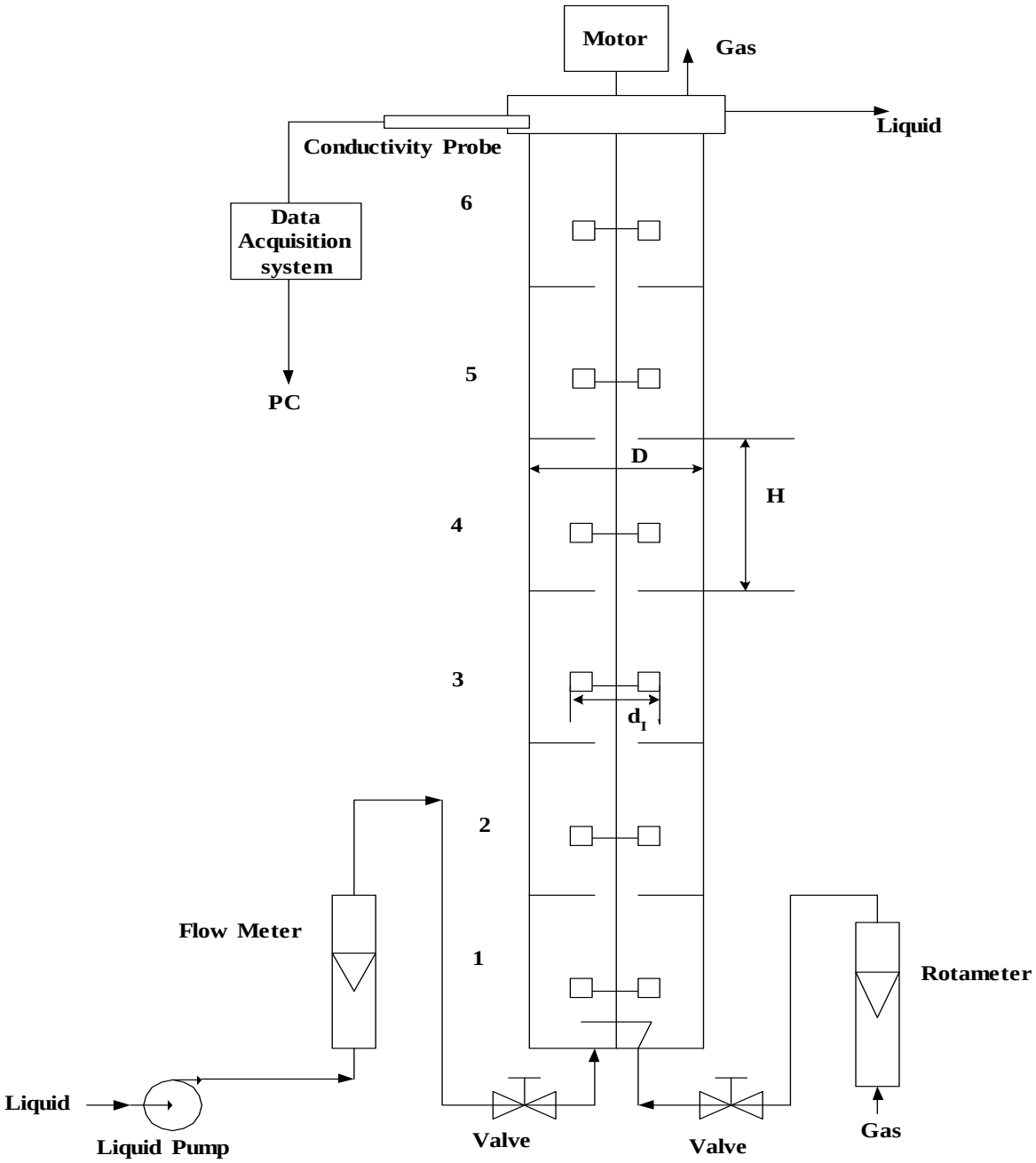

Figure 3. 1 Schematic description of the continuous set-up

Figure 3. 2 Impeller geometric description

In a typical RTD experiment, a particular set of parameters were chosen and a known liquid flow rate was allowed into the column co-current to a particular gas flow rate. A pulse input of a tracer (3 ml of NaCl solution) was injected just at the inlet of the liquid flow by a syringe with the shortest time period possible. The injection time was usually less than a second and the mixing time within one stage was generally several seconds (3~5 seconds) at the operating conditions. In addition, the average residence time for a single stage was usually several minutes. Therefore, the influence of the injection period on RTD curves was negligible. The tracer concentration was recorded by a data acquisition system (VWR). The experimental procedure was repeated for various gas and liquid flow rates, stirring speeds, number of stages. The same impeller was used for both MACs. Therefore, the ratios of impeller diameter over the diameter of the MACs were 1/2 and 1/3, respectively. The liquid superficial velocity varied from 0.0005 m/s to 0.006 m/s and the gas superficial velocity was ranged from 0.01 m/s to 0.1 m/s. In addition, the stirring speed ranged from 10 rps to 30 rps for $d_I/D=1/3$ and 5 rps to 15 rps for $d_I/D=1/2$. All experimental studies were carried out in a MAC of 6 stages except for the investigation of the effect of stage number. Air was chosen as a gas phase and distilled water was used as the continuous liquid phase. When the mass transfer measurement was conducted, oxygen was stripped by nitrogen in distilled water. An oxygen probe (YSI 5739) and a dissolved oxygen meter (YSI 52) were used to measure the oxygen concentration at steady state.

3.2.2 Experimental Approach

3.2.2.1 RTD Measurement

The residence time distribution curves can be obtained from the tracer concentration measured at the outlet of the reactor under given operation conditions. A residence time distribution is usually characterized by several numerical values. One of them is the averaged residence time or mean residence time, $\bar{t}$ (second). The averaged residence time can be evaluated as follows:

$$\bar{t} = \frac{\int_0^\infty C\ t dt}{\int_0^\infty C dt} = \frac{\sum t_i C_i \Delta t_i}{\sum C_i \Delta t_i} \qquad \textbf{Equation 3. 1}$$

The residence time function, E(t) (s^{-1}), can be defined as follows:

$$E(t) = \frac{C}{\int_0^\infty C dt} = \frac{C_i}{\sum C_i \Delta t_i} \qquad \textbf{Equation 3. 2}$$

Another important parameter is the variance representing the spread of the distribution. The variance can be evaluated as follows:

$$\sigma^2 = \frac{\int_0^\infty (t-\bar{t})^2 C dt}{\int_0^\infty C dt} = \frac{\int_0^\infty t^2 C dt}{\int_0^\infty C dt} - \bar{t}^2 = \frac{\sum t_i^{\,2} C_i \Delta t_i}{\sum C_i \Delta t_i} - \bar{t}^2 \qquad \textbf{Equation 3. 3}$$

The normalized residence time distribution

$$E(\theta) = \bar{t}\, E(t) \qquad \textbf{Equation 3. 4}$$

The normalized variance is calculated by the following equation,

$$\sigma_\theta^{\,2} = \frac{\sigma^2}{\bar{t}^2} \qquad \textbf{Equation 3. 5}$$

For each residence time curve obtained from the experiment, the averaged residence time and the normalized variance were evaluated according to the above equations.

3.2.2.2 Gas Hold-up Measurement

The gas gold-up was measured by a stop-flow method. The liquid level was recorded before and after aeration. The gas hold-up was calculated as follows:

$$\varepsilon_G = \frac{(H_1 - H_0)}{H_1} \qquad \textbf{Equation 3. 6}$$

where H_1 is the liquid level before aeration, m, and H_0 is the height of liquid after aeration, m. The measurement was taken by simply stopping both gas and liquid flows after a steady state of operation is achieved under given conditions.

3.2.2.3 Mass Transfer Measurement

Another objective of the present study is to investigate the volumetric mass transfer coefficient in a MAC. The volumetric mass transfer coefficient in MACs has been studied using a steady state method (Tsuge et al., 1995) and a dynamic approach (Sullivan and Treybal, 1972; Meister et al., 1979). A steady state method was employed due to its simplicity of measurement and equivalent accuracy. The rational of the steady state approach lies in the CTB model which describes mass balance of oxygen concentration in one stage as follows:

$$(1-\varepsilon_G)V\ \frac{dc_i}{dt} = (F+f)c_{i-1} - (F+2f)c_i + fc_{i+1} + k_L aV\ (1-\varepsilon_G)(c^* - c_i)$$

Equation 3. 7

At steady state, the term on the left side of the above equation disappears and the analytical solution is obtained by Hibino and Tsuge (1978) as follows:

$$\gamma_i = 1 - \frac{(1-x)\gamma_0}{x^{N_C-1}}\left(\frac{G_1 m_1^{\,i-N_C} - G_2 m_2^{\,i-N_C}}{G_1^{\,2} m_2^{N_C-1} - G_2^2 m_1^{N_C-1}}\right) \qquad \textbf{Equation 3. 8}$$

with

$$\gamma_i = \frac{c^* - c_i}{c^*} \qquad \textbf{Equation 3. 9}$$

$$G_1 = (1+\lambda) - m_1 x \qquad \textbf{Equation 3. 10}$$

$$G_2 = (1+\lambda) - m_2 x$$ **Equation 3. 11**

$$\lambda = \frac{k_L aL(1-\varepsilon_G)}{u_L N_C (1+\alpha)}$$ **Equation 3. 12**

$$m_1 = \frac{(1+x+\lambda) + [(1+x+\lambda)^2 - 4x]^{0.5}}{2x}$$ **Equation 3. 13**

and

$$m_2 = \frac{(1+x+\lambda) - [(1+x+\lambda)^2 - 4x]^{0.5}}{2x}$$ **Equation 3. 14**

The modified back flow ratio is

$$x = \frac{f}{f+F}$$ **Equation 3. 15**

The back flow ratio can be described as

$$\alpha = \frac{f}{F}$$ **Equation 3. 16**

where c* is the saturated oxygen concentration, kg/m^3, N_C is the number of stages, and c_i is the oxygen concentration in the ith stage, kg/m^3.

If back flow rate and gas hold-up are given, the volumetric mass transfer coefficient can be evaluated by minimizing the deviation of the values calculated by using Equation 3.8 from the experimental values measured at the steady state.

3.3 Experimental Results and Discussion

3.3.1 Effect of Variables on RTD

In order to understand the effect of operating variables on mixing behavior of the reactor of interest, various RTD curves have been attained by varying operation variables. The variables under investigation

were superficial gas velocity, liquid velocity, stirring speed and number of stages. Repeated experimental runs indicated that the experimental data possess a deviation of <5% for average residence times and normalized variances.

3.3.1.1 Effect of liquid velocity on RTD

The effect of liquid flow rate on RTD is shown in Figure 3.3. From the experimental curves, the averaged residence times obtained for three different liquid flow rates are 290 seconds, 412 seconds and 880 seconds, respectively. Similarly, the normalized variances indicating the spread of residence time distribution can be evaluated according the standard approach (Levenspiel, 1999). The normalized variances for three different flow rates are 0.170, 0.175 and 0.182. The averaged residence time decreases with an increase in the liquid flow rate as expected. However, an increase in liquid flow rate leads to a decrease in variances, indicating that the distribution is narrower at a higher liquid flow rate. When using n-CSTRs-in-series model is used, the number of equivalent CSTRs increases. More specifically, the stage efficiency increases. For instance, when a liquid flow rate increases from 0.001 m/s to 0.003 m/s, the stage efficiency increases from 91% to 95%. It is indicated that backmixing decreases with an increase in liquid velocity, which is reflected in the spread of RTD. It can be interpreted that the interstage back flow is suppressed by the bulk flow. This is consistent with the studies by Meister et al. (1979) and Sullivan and Treybal (1970). Increasing liquid flow rate is usually not a practical way to reduce back flow between consecutive stages because a sufficient residence time or reaction time is sometimes required to maintain a desired reaction conversion.

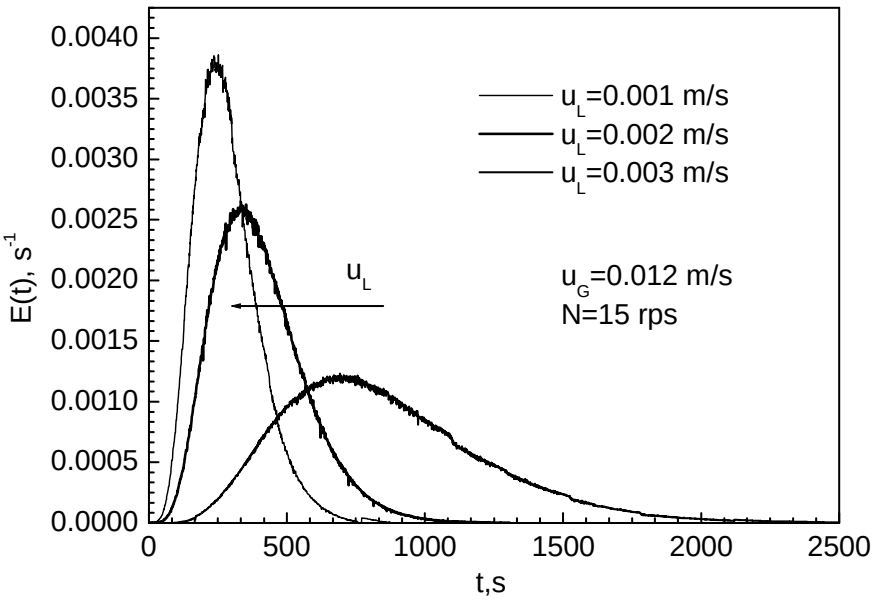

Figure 3. 3 Effect of liquid velocity on residence time distribution (D=0.15m and d_I/D=1/3)

3.3.1.2 Effect of Stirring Speed on RTD

The stirring speed is an important parameter to determine the mixing level in agitated vessels. The effect of stirring speed on RTD is shown in Figure 3.4. The averaged residence time for three stirring speeds of 15, 20 and 25 rps are 880 seconds, 865 seconds and 836 seconds, respectively and the corresponding variances are 0.182, 0.188 and 0.209, respectively. It can be seen that increasing stirring speed results in a decrease in residence time because an increase in stirring speed leads to a decrease of liquid hold-up and as a consequence the averaged residence time decreases. A higher variance means a broader residence time distribution because increasing stirring speed intensifies the turbulence level by increasing the power input. Therefore, a stirring speed plays a complex role can be interpreted that an increase in stirring speed increases the spread of RTD due to the turbulence generated by mechanical agitation.

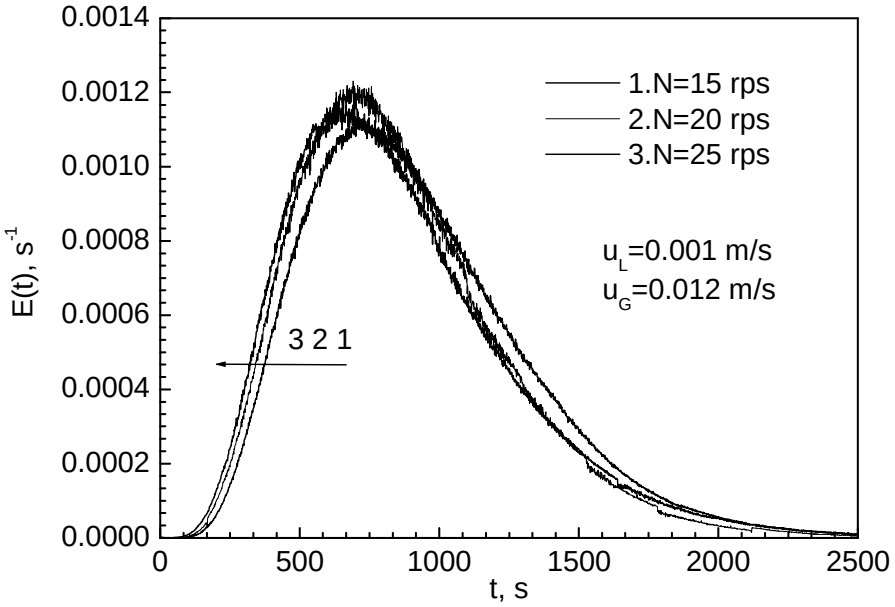

Figure 3. 4 Effect of stirring speed on RTD (D=0.15 m and d_I/D=1/3)

However, a complex dependency of axial backmixing on stirring speed in a two-phase flow system was observed by Meister et al. (1979) and Breman et al. (1996b). The complexity occurs because stirring speed increases the gas hold-up as well as liquid backmixing. An increase in gas hold-up will cause a drop in backmixing owing to the hindrance effect of disperse phase and straightening effect on liquid flow rate (Breman et al., 1996b; Nocentini et al., 1988).

3.3.1.3 Effect of gas flow rates on RTD

Figure 3.5 shows the effect of gas velocity on RTD curves. The averaged residence times for three gas superficial velocities of 0.012, 0.022 and 0.038 m/s are 880 seconds, 830 seconds and 780 seconds, respectively. The corresponding normalized variances are 0. 182, 0.175 and 0.170. It can be seen that with an increase in gas flow rate, the spread of RTD becomes narrower as reflected in the normalized variances, indicating that back flow between stages becomes lower. An increase in superficial gas velocity results in an increase in the gas hold-up, which virtually strengthens liquid flow rate and reduces back flow ratio (Breman et al., 1996b).

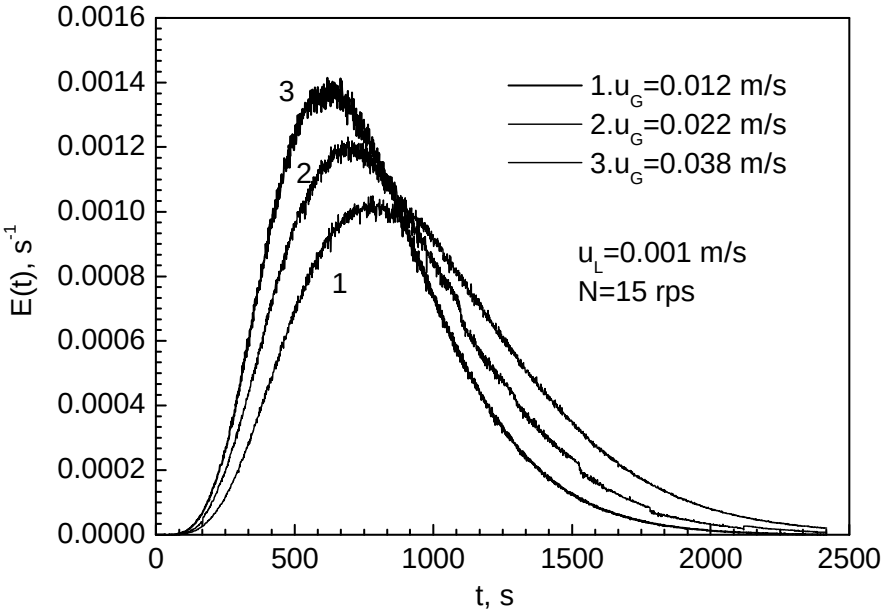

Figure 3. 5 Effect of superficial gas velocity on residence time distribution (D=0.15 m and d_I/D=1/3)

In a co-current flow application, the direction of entrainment of the disperse phase coincides with the main direction of the bulk flow, resulting in a decreasing effect on back flow ratio.

3.3.1.4 Effect of number of stages on RTD

In order to achieve the same residence time with a different number of stages, the liquid flow rate varies accordingly. Figure 3.6 shows that the spread of the normalized RTD becomes narrower when a larger number of stages are used. It is reasonable that more stages can be applied to obtain plug flow behavior, which is consistent with the theory that plug flow can be mimicked by an infinite number of CSTRs.

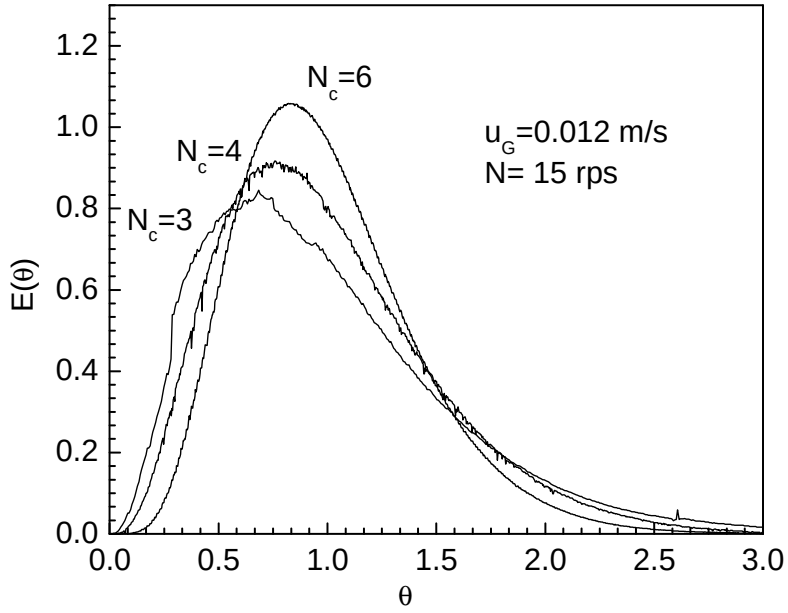

Figure 3. 6 Dimensionless RTD curves in different number of stages (D=0.15 m and d_I/D=1/3)

3.3.2 Model Discrimination

It is known that the AD model and the CTB model have been commonly used to describe the liquid flow behavior in MACs. The expression of the normalized variance from the AD model varies according to different boundary conditions. Since the diameters of the inlet and outlet are relatively small compared to the diameter of the contactor, a close-close boundary condition is applicable. As a consequence, the normalized variance can be expressed in the following equation when a close-close boundary condition is applied to the AD model (Levenspiel, 1999)

$$\sigma_\theta^{\,2} = \frac{2D_e}{u_L L}\left\{1 - \frac{D_e}{u_L L}\left(1 - \exp\left(\frac{-u_L L}{D_e}\right)\right)\right\} \qquad \textbf{Equation 3. 17}$$

When the CTB model is employed to describe the liquid flow within the reactor, the variance of residence time distribution for N_c stages is obtained, using Laplace transforms and the method of moments, as follows:

$$\sigma_\theta^{\,2} = \frac{1 - x^2 - \frac{2x}{N_c}(1 - x^{N_C})}{N_c (1-x)^2}$$ **Equation 3. 18**

The solution was first developed by Van der Lann (Vidaurri and Sherk, 1985). The back flow ratio can be evaluated by solving Equation 3.18 from a given normalized variance.

The suitability of the above two models was investigated by a comparison of the experimental RTD curve with the curves predicted by the two models as shown in Figure 3.7. In this figure, a RTD curve is predicted by the AD model with an axial dispersion coefficient evaluated from Equation 3.17 if an experimental variance is given. It is apparent that the AD model shows a considerable deviation from the experimental data while the CTB model fits the data well due to that the AD model has less plausible physical meaning in MACs with few stages.

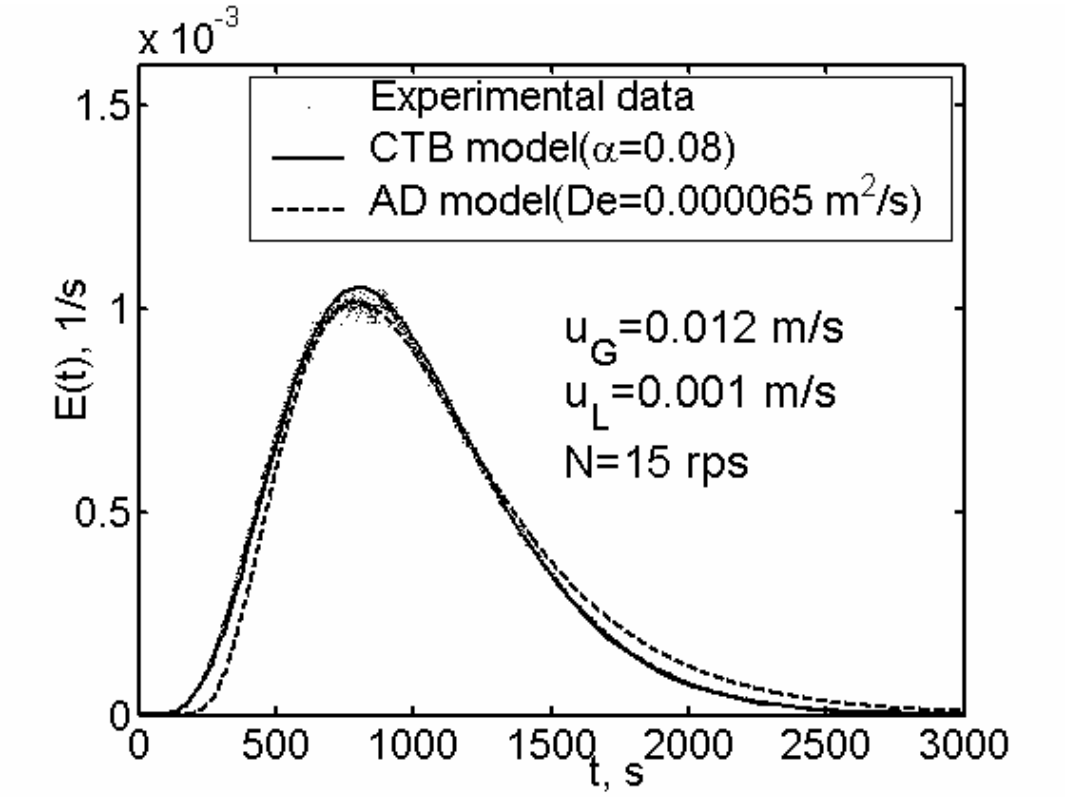

Figure 3. 7 Comparison of the experimental curve with the values predicted by the AD model with different axial dispersion coefficient and the CTB model

Therefore, the CTB model was used to characterize liquid flow in the designed MAC through this chapter.

3.3.3 Effect of Operating Variables on Back Flow Ratio

3.3.3.1 Effect of Liquid Velocity on Back Flow Ratio

Different RTD curves can be obtained by varying operating variables. The back flow ratio can be evaluates from the resultant normalized variance according to Equation 3.18. The effect of liquid flow rate on back flow ratio was investigated in two different columns and the results are shown in Figure 3.8 and Figure 3.9. It can be seen that back flow ratio decreases considerably with an increase in liquid velocity from these two figures. This was also observed by Haug (1971), Ingham (1972) and Meister et al. (1979) in a single phase and two-phase system. The back flow is considerably suppressed by the liquid bulk flow. In a single phase system, back flow ratio was proportional to $u_L^{-1.24}$ according to Haug's correlation.

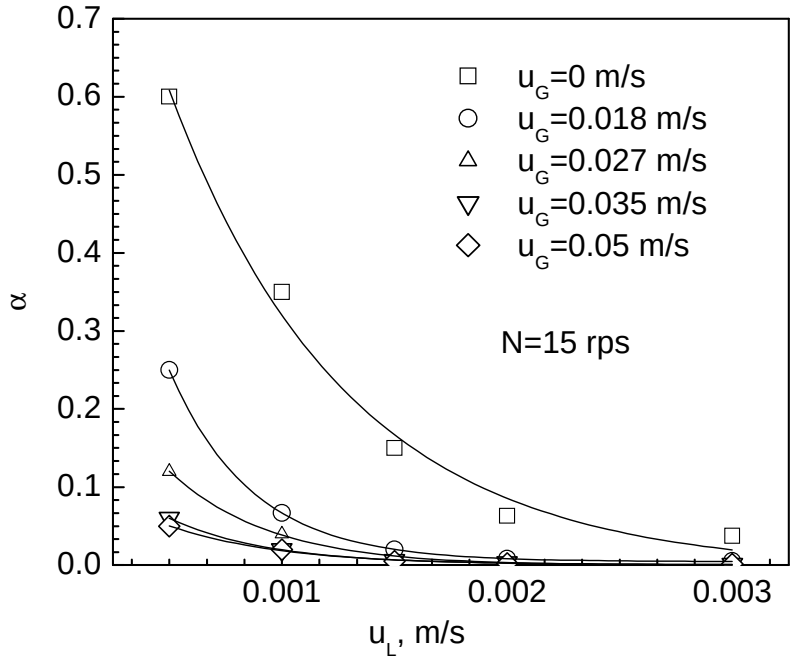

Figure 3. 8 Effect of liquid velocity on back flow ratio (D=0.1 m and d_I/D=0.5)

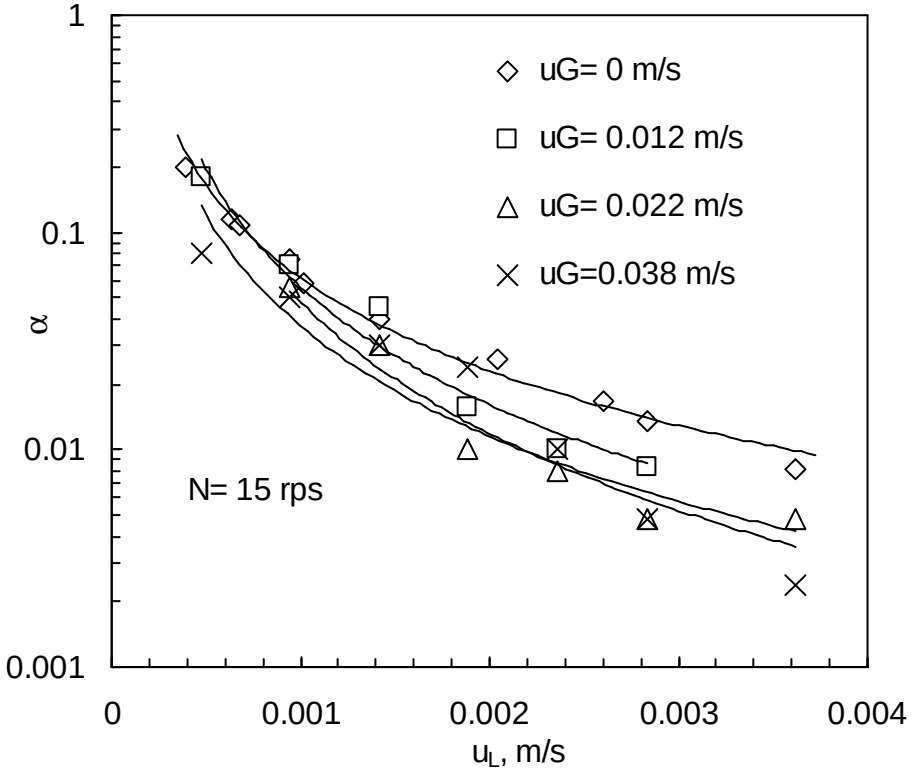

Figure 3. 9 Effect of liquid velocity on back flow ratio (D=0.15 m and d_I/D=1/3)

It is also seen in the figures that the majority of the back flow ratios in a two-phase system are lower than that obtained in a single phase system because the presence of the gas phase hinders liquid backmixing. With an increase in the gas flow rate, a decrease in backmixing is observed due to the increase in gas hold-up. The presence of gas phase reduces the liquid hold-up by virtually increasing the liquid flow rates. In addition, the entrainment effect of gas phase mitigates back flow due to the co-current operation manner as shown in Figure 3.10.

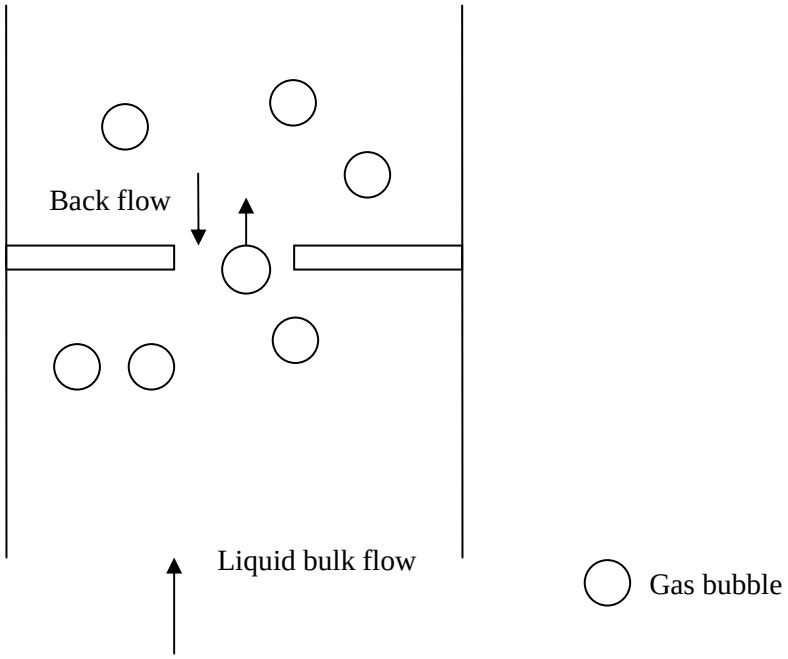

Figure 3. 10 Entrainment effect of gas bubbles in a co-current manner

The entrainment effect of the gas phase on back flow in a multistage agitated contactor was previously discussed in the literature (Breman et al., 1996b; Ingham, 1972). For a counter-current operating manner, the liquid entrainment by gas phase deteriorates back mixing whereas the effect should be the opposite in a co-current operation. The magnitude of entrainment effect is determined by bubble diameter and the number of bubbles. A larger bubble size favors the entrainment effect owing to a larger gas liquid contact area it possesses and a larger number of bubbles definitely facilitate entrainment effect too.

3.3.3.2 Effect of Stirring Speed on Back Flow Ratio

Back flow ratio increases with an increase in stirring speed as shown in Figure 3.11 and Figure 3.12 for a single phase system. As expected, increasing stirring speed intensifies the eddy turbulence in the system. In the literature, many correlations show a similar trend.

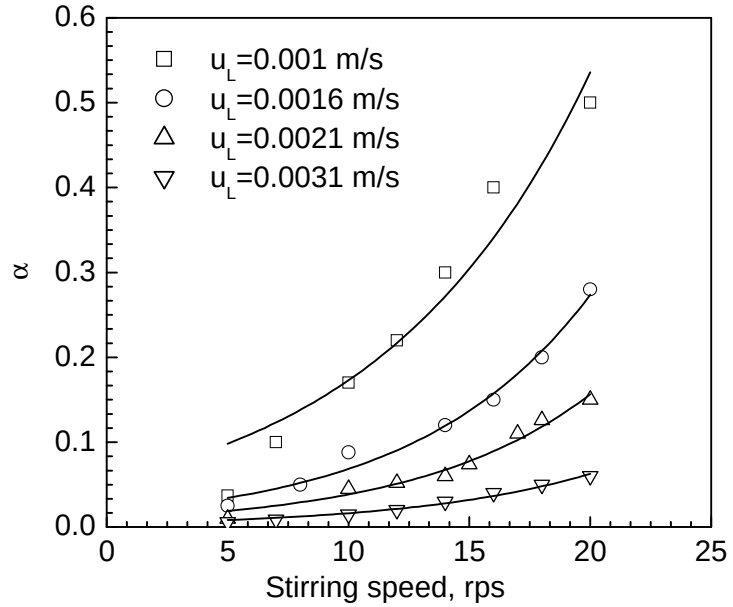

Figure 3. 11 Effect of stirring speed on liquid backmixing in a single phase system (D=0.1 m and $d_I/D=0.5$)

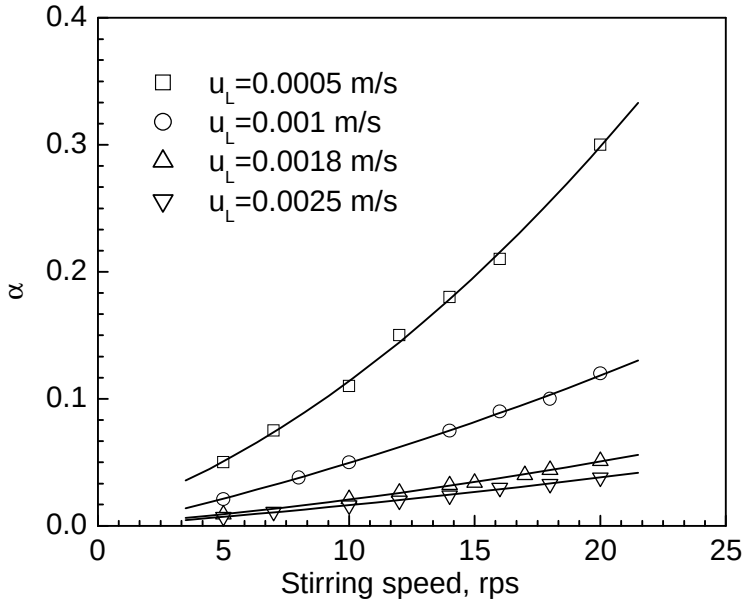

Figure 3. 12 Effect of stirring speed on liquid backmixing in a single phase system (D=0.15 m and $d_I/D=1/3$)

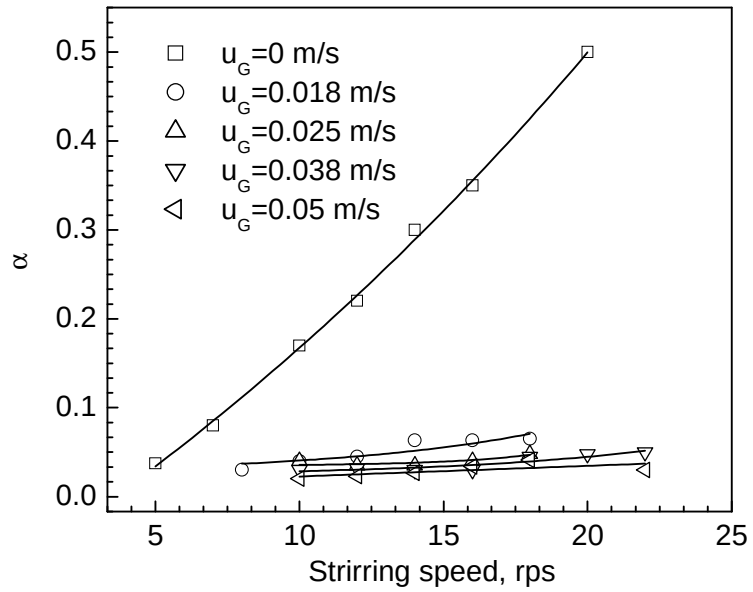

Figure 3. 13 Effect of stirring speed on back flow ratio (u_L=0.001 m/s, D=0.1 m and d_I/D=0.5)

The effect of stirring speed on back flow ratio in the presence of the gas phase is shown in Figure 3.13 and Figure 3.14 for the two columns of 0.1 m and 0.15 m in diameter, respectively. It is found that increasing gas superficial velocity decreases the back flow ratio due to the resulting increase in gas hold-up, which favors the hindrance of back flow of the liqiuid phase by the gas phase. The gas holdup increases the actual velocity of the liquid phase, thus constituting a flow straightening phenomena, and reducing the magnitude of the back flow. The similar phenomena were observed by Ingham (1972) in a multi-mixer liquid-liquid extraction and by Tariff et al. (1998) in a gas liquid MAC of two stages. It also can be seen from the two figures that the effect of stirring speed on back flow ratio at high superficial gas velocity is not as significant as what happens at a low gas velocity, indicating that stirring speed plays a complex role on back flow. No significant effect of stirring speed on back flow rate was reported by Breman et al. (1996b) due to the profound effect of gas phase in their relation. Increasing stirring speed also increases the gas hold-up and decreases the drop size which is considered to influence the liquid entrainment through the opening.

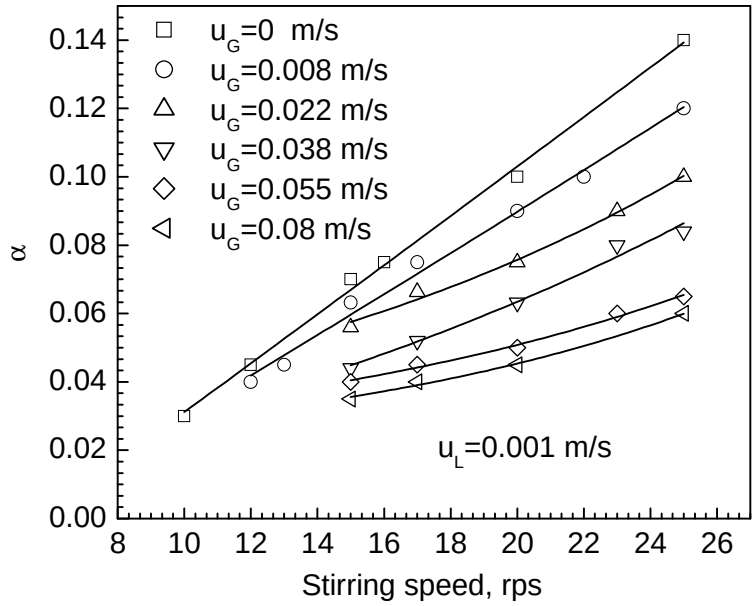

Figure 3. 14 Effect of stirring speed on back flow ratio at various superficial gas velocities (u_L=0.001 m/s, D=0.15m and d_I/D=1/3)

3.3.3.3 Effect of Impeller Position on Back Flow Ratio

Impeller location determines flow patterns in stirred vessel, which leads to different mixing behavior. In a standard stirred vessel, an impeller is usually positioned at 1/3 of the liquid height of the vessel. However, in a MAC, the impeller position varies depending on different operating requirements and reactor geometries. In the literature, it ranged from 1/5 to 2/3 of the stage height as indicated in Table 2.1. However, in most cases, the impeller was located at half of the height of each stage. Although a variety of impeller locations are reported in many studies, the effect of impeller location on liquid backmixing is rarely discussed. From the hydrodynamics prospective, the location of the impeller governs flow patterns and further liquid mixing performance. Therefore, a study on the influence of impeller location on backmixing was carried out in the MAC of D=0.15 m. Three locations were examined at the same operating conditions, namely, stirring speed, liquid and gas flow rate. The results are shown in Figure 3.15.

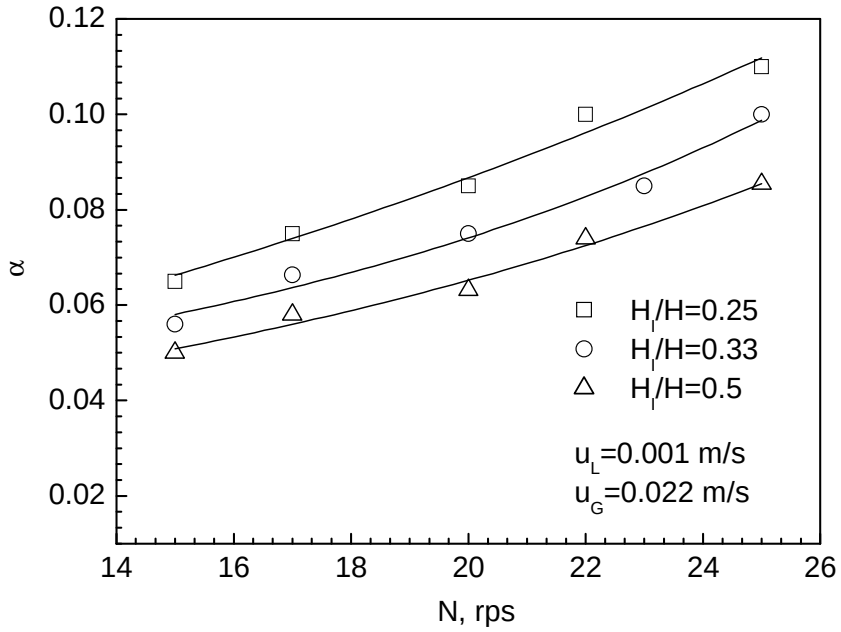

Figure 3. 15 Effect of impeller location in one stage on back flow ratio (D=0.15 m and d_I/D=0.33)

Figure 3.15 clearly shows that at an impeller location of 0.25 H gives the highest back flow between stages among three different locations under investigation. It can be interpreted that when the impeller approaches the opening, the influence of impeller is more significant as discussed in our study (Zhang et al., 2005a). Therefore, in order to minimize back flow and generate symmetric flow patterns within one stage, an impeller location of 0.5 H was exclusively used in this work.

3.3.3.4 Effect of Stage Number on Back Fow Ratio

The back flow ratio in MACs with different number of stages was investigated under the same liquid flow and stirring speed. A similar back flow ratio was observed when the number of stages was increased from 3 to 6 as it can be seen from Figure 3.16. The back flow ratio is expected to be constant since the number of stages only changes the variance of RTD. The independent effect of stage number on back flow ratio is consistent with the theoretical foundation of using the CTB model.

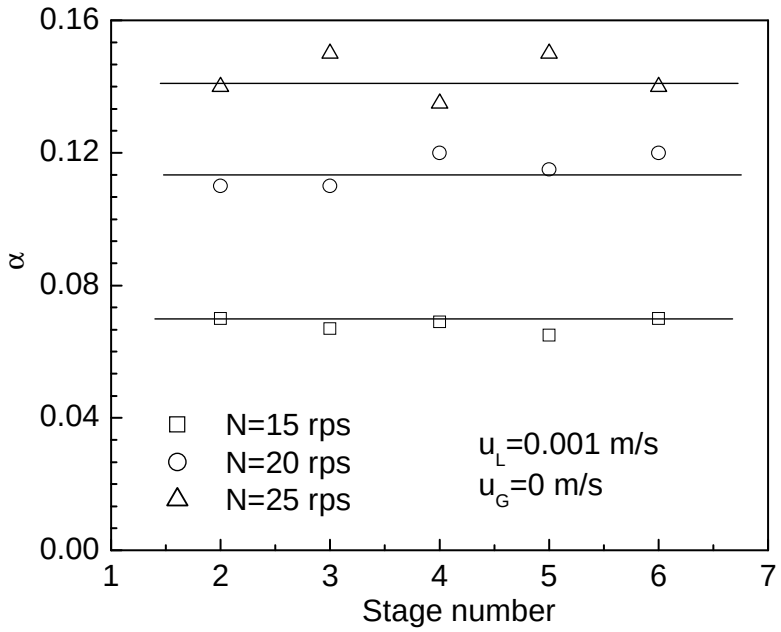

Figure 3. 16 Effect of number of stages on back flow ratio (D=0.15m and d_I/D=1/3)

From the literature study and experimental data, back flow rate in an air-water system is considered to be a function of gas hold-up, bubble size and other operating variables.

3.3.4 Gas Hold-up in Air-water System

Since gas hold-up plays an important role on back flow in two-phase flow systems, it is necessary to understand gas hold-up under different operating conditions in the designed MAC. In addition, gas hold-up is also an important parameter to characterize mass transfer capability in gas liquid processes. Unlike hydrodynamic behavior in bubble columns, the preliminary experimental study shows that the response of gas hold-up to liquid flow rates under investigation (u_L < 0.01 m/s) is marginal since the energy input due to liquid bulk flow is minimal compared to that from mechanical agitation. Therefore, the effects of other parameters such as gas flow rate and stirring speed are considered in this section.

Figure 3.17 and Figure 3.18 show that gas hold-up increases when increasing stirring speed and superficial gas velocity, which is consistent with previous works at this point (Meister et al., 1979; Breman et al., 1995).

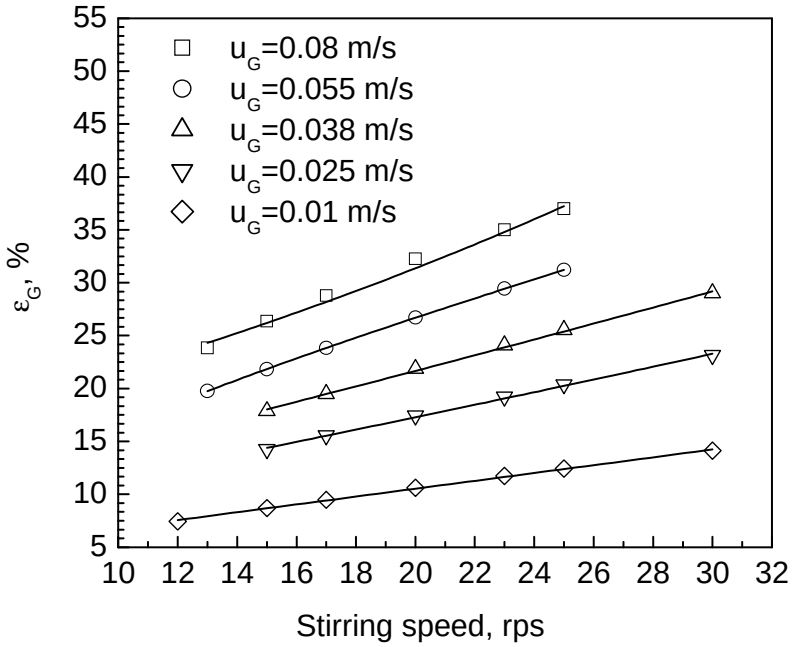

Figure 3. 17 Effect of stirring speed on phase hold-up under various u_G

(u_L=0.001 m/s, D=0.15 m and d_I/D=1/3)

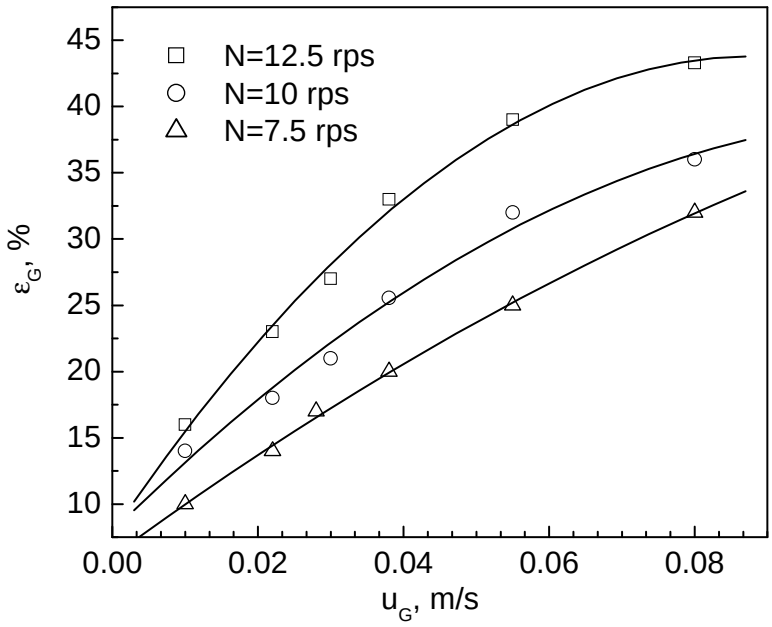

Figure 3. 18 Effect of superficial gas velocities under various stirring speed

(u_L=0.001 m/s, D=0.15 m and d_I/D=0.5)

In order to qualitatively describe a relation between gas hold-up and operation variables, a general form is introduced as follows:

$$\varepsilon_G = p1N^{p2}u_G^{p3} \qquad \textbf{Equation 3. 19}$$

where p1 is the coefficient, $(rps)^{-p2}(m/s)^{-p3}$, p2 and p3 are exponents with respect to stirring speed and gas velocity.

The accuracy of the relation between a correlation and experimental data is expressed in terms of mean average absolute relative residual (MARR):

$$MARR = \frac{1}{N_d}\sum\left|1-\frac{\varepsilon_G^{Cal}}{\varepsilon_G^{Exp}}\right|\times 100\% \qquad \textbf{Equation 3. 20}$$

where N_d is the number of experimental points.

The coefficients in Equation 3.19 are optimized by minimizing the MARR function at a confidence level of 95%. Two correlations with a MARR of 6 % and 7 % are achieved for two different impellers, respectively. The relations are shown in Figure 3.19.

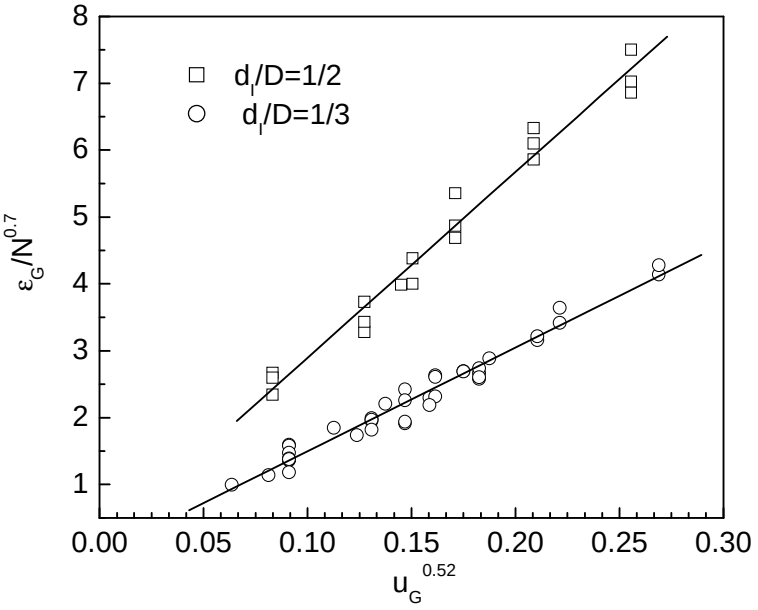

Figure 3. 19 Correlations for two different impellers (D=0.15 m)

The equation for $d_I/D=1/3$ is as follows:

$$\varepsilon_G = 17.2 N^{0.7} u_G^{0.52}$$ **Equation 3. 21**

while the correlation for $d_I/D=0.5$ is as follows:

$$\varepsilon_G = 29.4 N^{0.7} u_G^{0.52}$$ **Equation 3. 22**

Development of the coefficients in Equation 3.19 is also conducted by nonlinear least–squares curve fitting for purpose of comparison. A MATLAB function, NLINFIT, is used to estimate the coefficients at a confidence level of 95%. The resultant parameters are shown in Table 3.1.

Table 3. 1 Optimal values and confidence intervals at a confidence level of 95% for the parameters of the gas holdup relation (Equation 3.19)

	p1	p2	p3
$d_I/D=1/2$	21.27 ± 7.48	0.81± 0.14	0.51± 0.049
$d_I/D=1/3$	15.38± 0.69	0.69± 0.014	0.52± 0.0063

Using the above parameters, A MARR of 4.5% and 3% from the experimental data has been achieved for the impeller of $d_I/D=1/2$ and 1/3, respectively. The parameters obtained by minimizing MARR function are similar to those as shown in Table 3.1, indicating that two different approaches can essentially generate equivalently accurate predictions.

For comparison purposes, the phase hold-up predicted by the proposed correlations and literature correlations are shown in Figure 3.20.

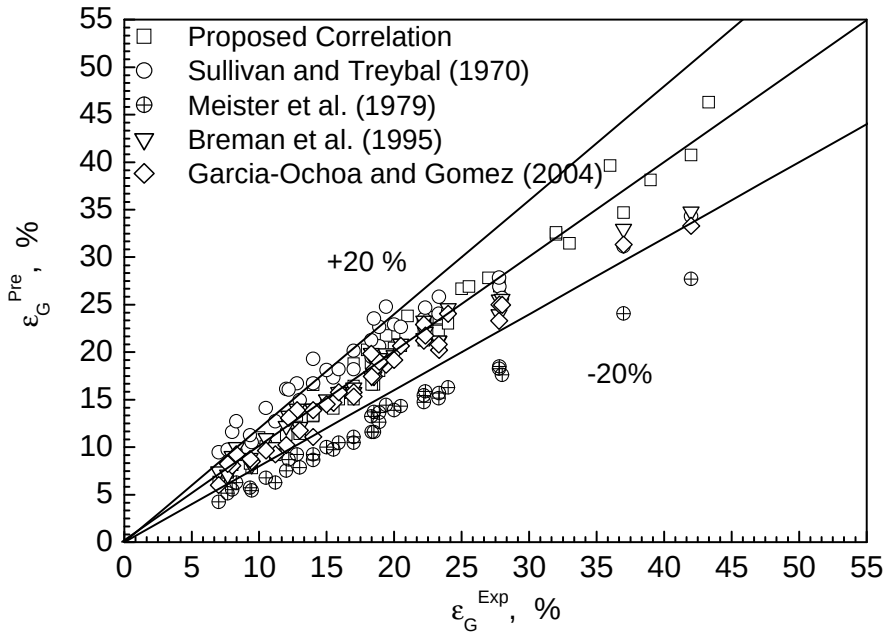

Figure 3. 20 Comparison of experimental data with the literature data

Meister et al. (1979) has the largest MARR (33%) from our experimental data due to its lower impeller position (H_I=0.2 H). The correlation proposed by Breman et al. (1995) has a very small deviation of 6%. The correlation proposed by Sullivan and Treybal (1970) has a deviation of 19% due to their smaller volume for each compartment (D=0.15 m and H=0.083 m). A comparison is also conducted with the values for a single agitated tank theoretically predicted by Garcia-Ochoa and Gomez (2004). A deviation of 8% is observed. It is reasonable owing to that each stage of a MAC virtually resembles a single agitated tank. The experimental work suggests that phase hold-up data in the present study is comparable with the literature values and can be predicted by the values for a single stage contactor.

3.3.5 Empirical Correlation for Back Flow Ratio

An attempt was made to develop a correlation to describe the back flow ratio in a MAC for the gas liquid process. When using the relation proposed by Haug (1971) to predict back flow ratio in our experimental set-up, the predicted values are generally 3-5 times higher than that obtained from the present experimental work for a single phase as shown in Figure 3.21.

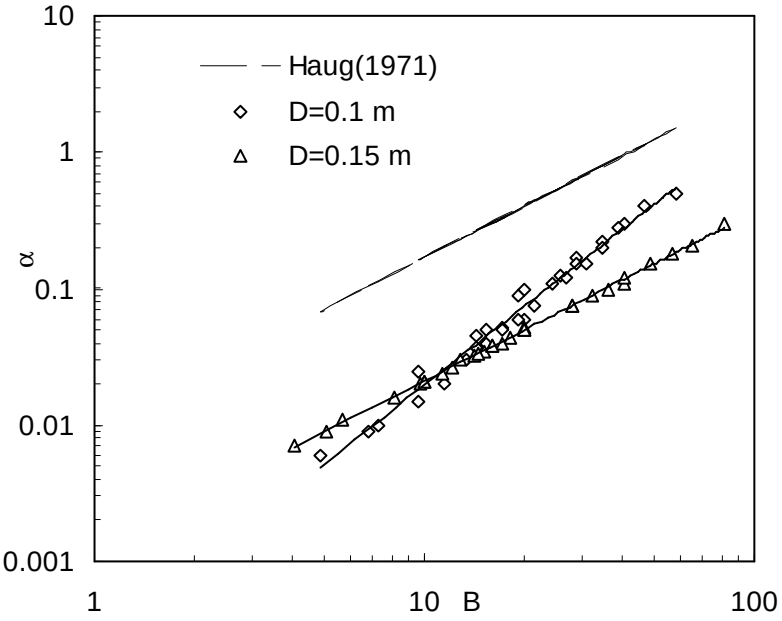

Figure 3. 21 Backmixing in a single phase ($B = \frac{Nd_I}{u_L}(\frac{d_I{}^2 A_{hb}}{HDA})^{0.5}$ **)**

The difference possibly results from the relatively longer residence times in the current study and smaller horizontal opening ($A_{hb}/A=0.015$) as well as different scales. Most of the existing correlations for backmixing in a MAC are empirically based. The lack of a firm theoretical foundation leads to the diversities of correlations. Miyauchi et al. (1969) introduced a local isotropic turbulence theory to explain liquid backmixing between stages. However, the contribution of main stream flow was ignored due to their experimental technique which employed non-flow fashion. No correlation is generated from the power input point of view, which is a characteristic parameter for pumping capacity and the turbulence under turbulent conditions.

Based on experimental data, a new correlation from a power input point of view by minimizing a MARR function is proposed as follows:

$$\alpha = 6*10^{-5}(\frac{P_0}{V})^{0.6} u_L^{-1.4} (\frac{A_{hb}}{A})^{0.6}$$ **Equation 3. 23**

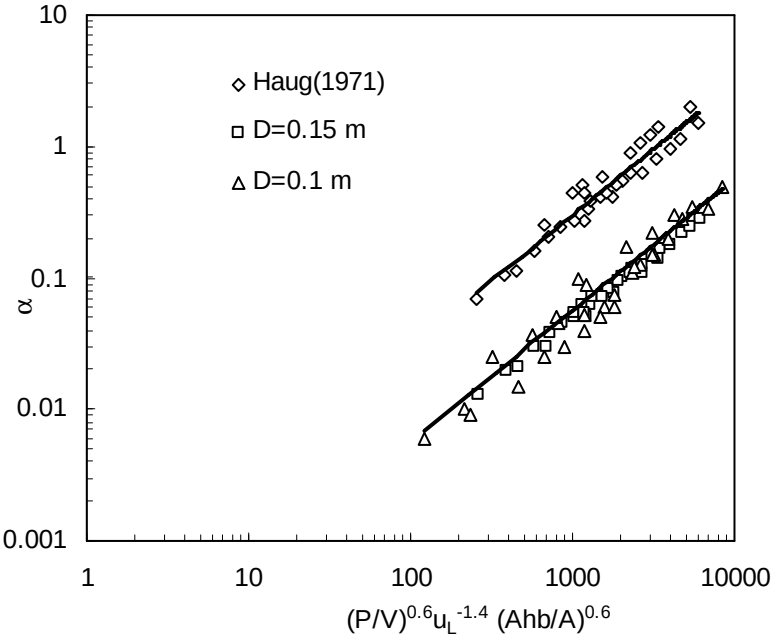

Figure 3. 22 A correlation for a single phase system

It is already noted that back flow is also a function of gas hold-up and bubble size in a two-phase system. As a result, back flow ratio in a gas liquid system can be expressed as follows.

$$\alpha_{GL} = p1(1-\varepsilon_G)^{p2}\alpha_L d_B{}^{p3} \qquad \textbf{Equation 3. 24}$$

where p1 is the coefficient, m^{-p3}, p2 and p3 are the exponents with respect to phase holdup and bubble size. d_B is the bubble size, m. However, bubble sizes are not measured in the present study. The average bubble size can be predicted by the correlation proposed by Bhavaraju et al. (1978):

$$d_B = 0.7\frac{\sigma^{0.6}}{(P_G/V)^{0.4}\rho_L{}^{0.2}}(\frac{\mu_L}{\mu_G})^{0.1} \qquad \textbf{Equation 3. 25}$$

Power consumption under aeration is evaluated by the relation proposed by Michel and Miller (1962).

$$P_G = 0.95(P_0 N d_I{}^3/Q_G^{0.56})^{0.43} \qquad \textbf{Equation 3. 26}$$

where P_0 is the power input in unaerated systems, W, and Q_G is the gas flow rate, m^3/s.

$$P_0 = N_P N^3 d_I^5 \qquad \textbf{Equation 3. 27}$$

where N_p is the power number of the impeller and N_p=5 is applied for a standard Rushton turbine. The prediction of bubble sizes using Equations 3.25, 3.26 and 3.27 are shown in Figure 3.23.

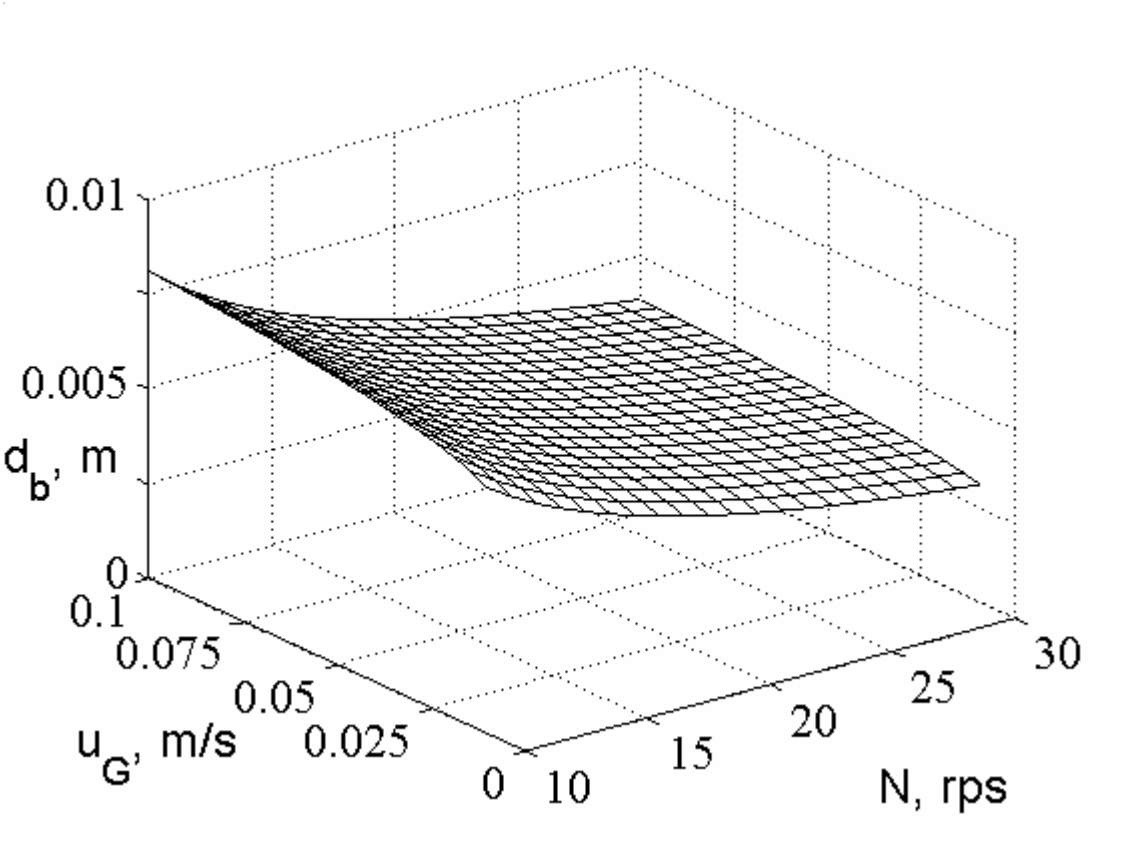

Figure 3. 23 Effect of stirring speed and gas velocity on bubble size

As can be seen in Figure 3.23, the predicted bubble sizes show a slight increase with an increase in gas flow rate while it decreases significantly when the stirring speed is increased.

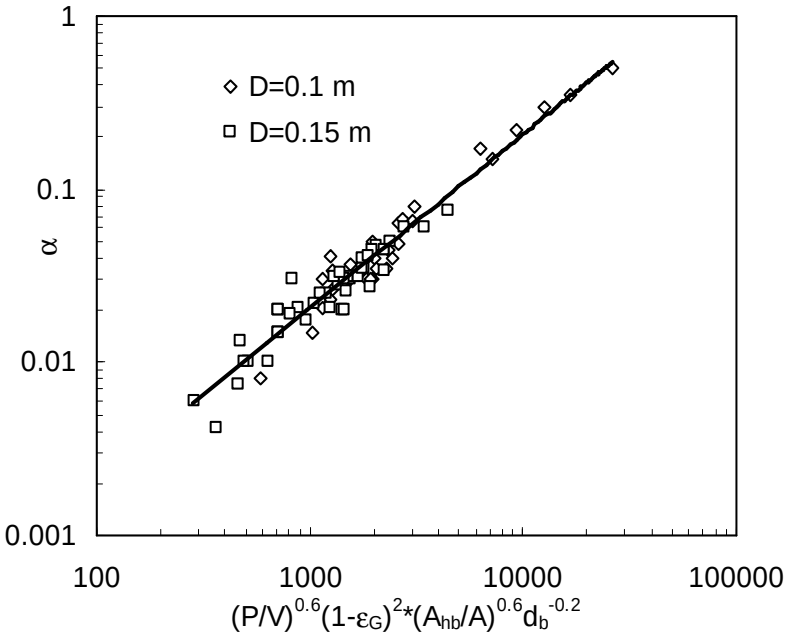

Figure 3. 24 Correlation for back flow ratio in gas liquid system

The following equation is obtained by optimizing the coefficients in equation 3.24 with an average relative deviation of 15%.

$$a_{GL} = 0.34(1-\varepsilon_G)^2 a_L d_B^{-0.2} \qquad \textbf{Equation 3. 28}$$

The prediction of back flow ratio in two experimental contactors by using the above equation is shown in Figure 3.24.

Similarly, the parameters involved in Equation 3.24 are also estimated from nonlinear least-square fitting. The resultant parameters at a confidence level of 95% are given in Table 3.2. The values in the parenthesis are obtained from minimizing a MARR function at a confidence level of 95%.

Table 3. 2 Optimal values and confidence intervals at a confidence level of 95% for the parameters in Equation 3.24

Parameters	p1	p2	p3
	0.27±0.068 (0.34)	1.51±0.31 (2)	-0.22±0.033 (-0.2)

It is apparent that the two approaches can generate the close predictions with difference within 25%.

3.3.6 Volumetric Mass Transfer Coefficient

The mass transfer coefficient is a determinative factor for gas-liquid processes. Superior gas liquid mass transfer is always desirable. Considerable efforts have been expended to develop relations of $k_L a$ with operating variables either via an empirical approach or theoretical prospective. However, most of them are dedicated to single stage agitated contactors (SACs) and limited efforts have been made on a MAC (Meister et al., 1979; Breman et al., 1996a). The correlations proposed by the two research groups can not accommodate each other without taking into account different reactor structures and different operating conditions. The correlation proposed by Meister et al. (1979) is considered to have limited application due to its significant low impeller position. Therefore, the mass transfer coefficient in the designed reactor under various conditions was investigated. The oxygen concentration in different stages was measured and normalized with the saturated oxygen concentration c^* under given operating conditions. A typical comparison of experimental oxygen concentration with theoretical calculation is shown in Figure 3.25.

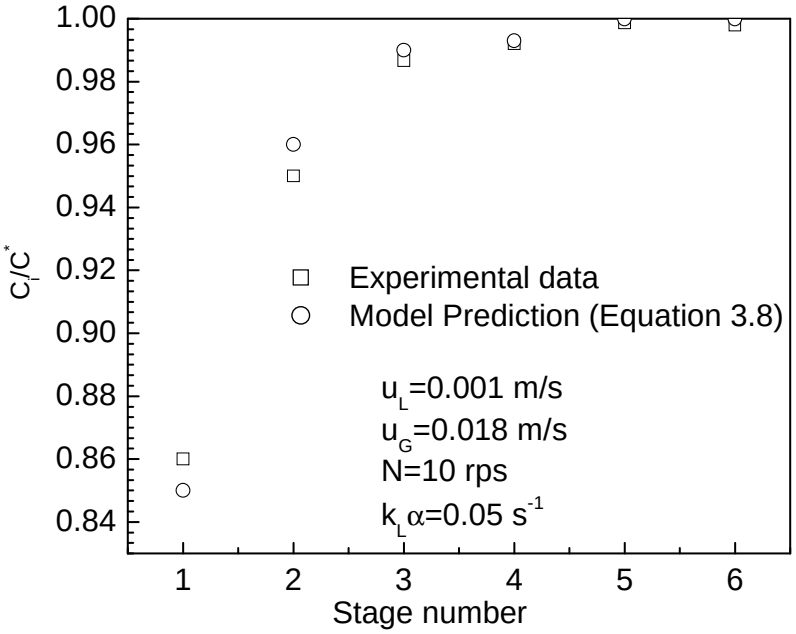

Figure 3. 25 Oxygen concentration in different stages at steady state (D=0.1 m and d_I/D=1/2)

The mass transfer coefficient under different operating conditions is shown in Figure 3.26.

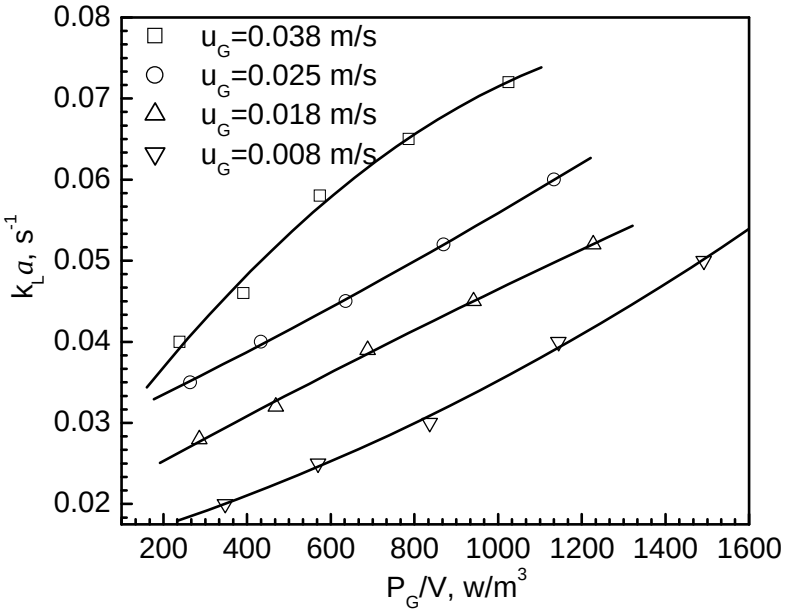

Figure 3. 26 Relation of $k_L a$ with power input under different gas velocities (u_L=0.001 m/s and D=0.1m)

From Figure 3.26, it can be seen that the mass transfer coefficient increases with an increase in power input as well as an increase in gas flow rate. The observation agrees with many previously reported studies. A comparison with literature values was also carried out and the results are shown in Figure 3.27, where $k_L a^{exp}$ are the data from the present study and $k_L a^{cal}$ are calculated based on the different correlations from the literature as indicated in Figure 3.27. These figures show that there are small mean deviations of 12.5% and 7% based on the equation of SACs of Van't Reit (1979) and Calderbank (1958), respectively. This implies that the values from a SAC are also applicable for a MAC with an acceptable level of confidence. The large deviation (33%) based on the equation of Meister et al. (1979) may be due to their significant lower impeller position (1/5H). The theoretical model based on the penetration model and Kolmogoroff's theory on isotropic turbulence (Garcia-Ochoa and Gomez, 2004) presents a deviation of 19% from the experimental data and the relatively high deviation can possibly be attributed to the existence of gas hold-up or bubble size profile along with the column.

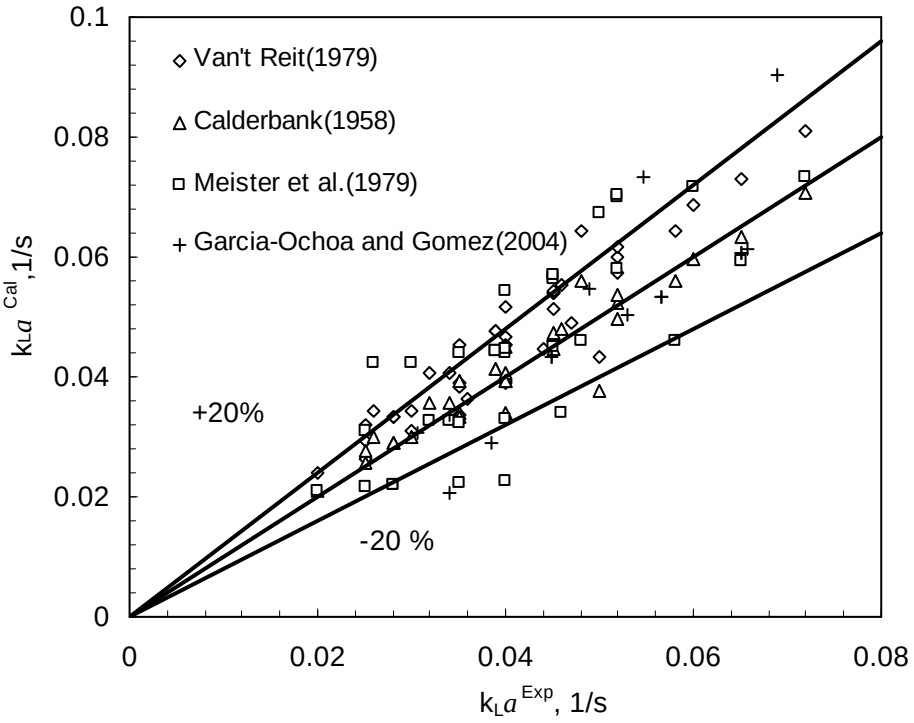

Figure 3. 27 Comparison of k_La values calculated from literature values with the experimental data

3.4 Concluding Remarks

The liquid phase backmixing characteristics of MAC were studied through RTD investigation for different phase velocities, stirring speed and number of stages. For the purpose of interpreting backflow ratio in air-water system, gas phase hold-up was also investigated. The gas hold-up achieved in this work is comparable to literature data. This present study provides the fundamental data for the application of a MAC to a gas liquid process with relatively long residence time and very low backmixing. A new correlation was proposed to predict liquid back flow from the power input point of view.

Based on the experimental studies, it can be concluded that the backmixing in the liquid phase increases with the stirring speed while it decreases with an increase in liquid velocity and gas velocity. The experimental RTD data are satisfactorily fitted by the CTB model. The back flow ratios obtained in present study are relatively low and present a design of a MAC with high stage efficiency.

Using the present data, a correlation is proposed to predict back flow ratios of the continuous phase in a MAC from power input point of view.

Chapter 4 Hydrodynamics Studies in MACs with Air/viscous Fluids

4.1 Introduction

As discussed in Chapter 2, hydrodynamic studies of MACs in gas liquid processes are very limited, in particular, in systems other than air-water. The hydrodynamic behavior in a MAC with a viscous system is not well studied. With regard to the effect of the viscosity on liquid back flow, it was found that back flow rate increases with increasing viscosity under the same stirring speed (Breman et al., 1966 b). Miyauchi et al. (1966) made the same observation for a rotating disk contactor. It was interpreted that increasing power input at constant stirring speed, N, with increasing viscosity intensifies the turbulence and the back flow rate was proposed to be proportional to the power number $Np^{1/3}$ (Miyauchi et al., 1966). However, their correlation was only based on a water system and the effect of viscosity was not fully taken into account. In contrast, back flow ratio, back flow rate over the continuous phase flow, was found to be dependent on $\mu_L^{-1/2}$ (Vidaurri and Sherk, 1985). Backmixing between stages at a very low Reynolds number with respect to the impeller (Re<340) could be reduced to zero (Xu et al., 2005). The dampening effect of the viscosity on turbulence should be considered as an important factor for the back flow in viscous systems. In a non-standard stirred vessel with multiple impellers, a model of "compartments in series with back flow" is used (Vasconcelos et al., 1995, 1996). Under turbulent conditions, namely, Reynolds number > 20000, back flow rate, f, is proportional to the stirring speed N (Fajner et al., 1982; Vasconcelos et al., 1995) when the CTB model is applied to describe the liquid flow behavior. The parameter indicating back flow between impellers, f/Nd_I^3, is independent of agitation under turbulent conditions while it decreases with a decrease in Re and this effect is more significant when Re falls down to transitional and laminar regions (Vasconcelos et al., 1996). It is interpreted that back flow is directly linked to the pumping capacity of the impeller. From a hydrodynamics point of view, the back flow should possess a similar trend in MACs due to the similar internal structure with a vessel with multiple impellers except for horizontal baffles applied in MACs.

From the literature study, it can be concluded that the hydrodynamic data in MACs with an air/viscous phase flow system is lacking and particularly the effect of viscosity on liquid backmixing is not well explored. The disparity for this aspect may arise from many aspects such as different flow regimes, experimental technique, liquids employed and reactor scales under investigation. The primary objective of this chapter was to investigate liquid backmixing in an air-viscous system operated in a co-current manner.

Various aqueous sugar solutions were used as simulating fluids. The residence time distribution technique was also used as a tool to evaluate the reactor mixing performance. From the experimentally determined RTD curves, flow model discrimination was conducted and a suitable back mixing parameter to describe reactor flow behavior was determined from the experimental curves. The influence of operating variables on mixing performance was investigated. Those variables included stirring speed, gas and liquid flow rates, and different liquids. The gas hold-up in viscous systems was also measured in this chapter since it is expected to show an important impact on backmixing under aerated conditions.

4.2 Experimental Section

The same set-up was used as that in air/water system in Chapter 4 except that the MAC with a diameter of D=0.1 m was exclusively considered. Air was still used as the disperse phase while sugar solutions with different concentrations were used as the continuous viscous liquid media. The viscosity was measured using an Ubbelohde viscometer and the surface tension was measured by Axisymmetric Drop Shape Analysis-Profile (ADSAP). The liquid density was measured using a volumetric flask of 500 ml. The mass of the volumetric flask was measured before the liquids were filled. The difference between before and after the addition of the liquids gave the density after dividing by the flask volume. The physical properties of the liquids used are given in Table 4.1.

Table 4. 1 Physical properties of the liquid phase

	Density, kg/m^3	Viscosity, Pa.s (at 25 °C)	Surface tension, N/m (at 25 °C)
water	1000	0.001	0.073
25% sugar	1090	0.0042	0.068
50% sugar	1210	0.0125	0.059
60% sugar	1370	0.0195	0.055

The gas hold-up was estimated using the same approach adopted in an air/water system. A deviation of < 5% after a few experimental trials at a condition indicates a good reproducibility.

The residence time distribution was measured by using the same approach detailed in Chapter 3. The effect of operating variables such as stirring speed, liquid and gas velocities were studied in order to understand hydrodynamic behaviour of the designed MAC with viscous liquids.

4.3 Experimental Results and Discussion

4.3.1 Gas Hold-up

The effects of stirring speed on gas hold-up are shown in Figure 4.1 and Figure 4.2. Gas hold-up increases with an increase in stirring speed or superficial gas velocity for all the liquid solutions employed as expected. In addition, Figure 4.1 also shows that the gas hold-up, ε_G, is higher in the solutions with lower liquid viscosity, indicating that the viscosity has a negative impact on gas hold-up. It was reported that gas hold-up is proportional to $\mu^{-0.1\sim-0.33}$ in SACs (Loiseau et al., 1977; Nocentini et al., 1993; Garcia-Ochoa et al., 2004) and it will be shown below that the dependence of the gas hold-up on the viscosity in this work is also located within this range. However, slightly increasing the liquid viscosity at a constant density and interface tension may lead to an increase in gas hold-up (Paglianti et al., 2000). This phenomenon does not occur in the present work as well as many other works presumably owing to that a large change in other physical properties of the liquid associated with the change in the viscosity automatically shields the effect.

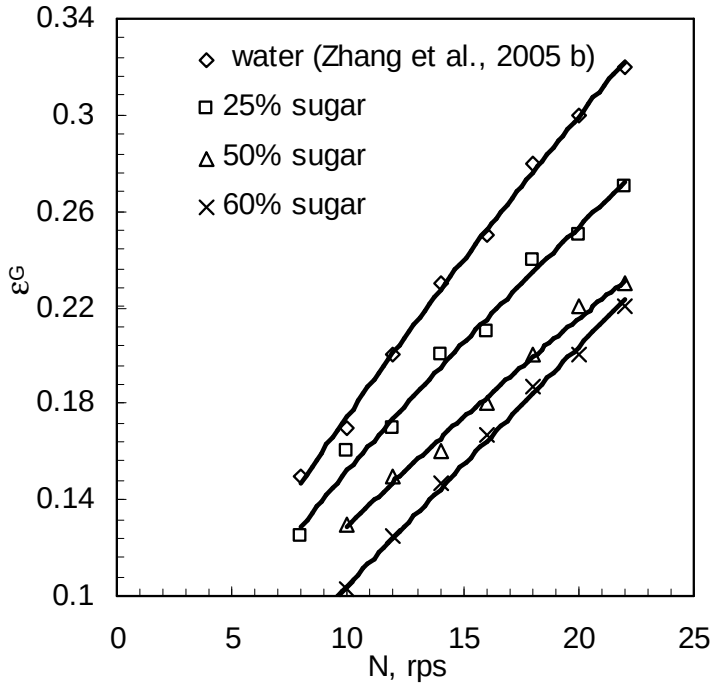

Figure 4. 1 Effect of stirring speed on gas hold-up under different viscosities

(D=0.1 m, u_G=0.018 m/s and u_L=0.001 m/s)

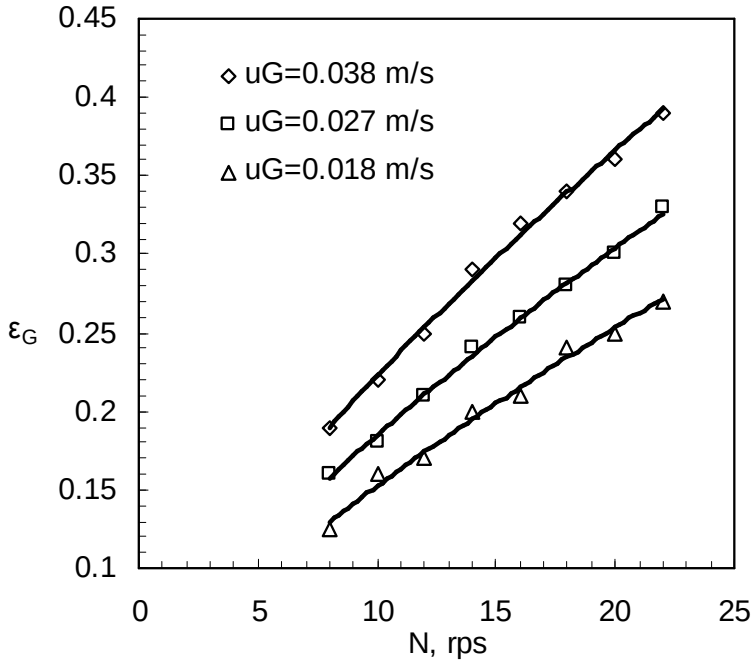

Figure 4. 2 Effect of stirring speeds under different gas velocities

(25% sugar solution and u_L=0.001 m/s)

Regarding gas hold-up in stirred vessels, many correlations have been proposed. However, most of them are focused on single stage and air-water systems. Only a few investigations which involved the influence of viscosity have been reported either from a theoretical point of view (Kudrewizki and Rabe, 1986; Garcia-Ochoa and Gomez, 2004) or from an empirical perspective (Loiseau et al., 1977; Smith, 1991; Nocentini et al., 1993; Breman et al., 1995) as shown in Table 4.2.

All of the equations in this table show that the viscosity has a negative effect on gas hold-up. According to our previous study in an air-water system (Zhang et al., 2005a, 2005b), ε_G is proportional to $N^{0.7}u_G^{0.52}$ with a proportionality constant of 0.32. This relation still holds for the viscous systems investigated in the present work, as shown in Figure 4.3 although the coefficients are different, which are affected by the physical properties of the liquids employed.

Table 4. 2 Gas hold-up correlations used in this work

Garcia-Ochoa et al. (2004)	$\frac{\varepsilon_G}{1-\varepsilon_G} = 0.819 \frac{u_G^{2/3} N^{2/5} D^{4/15}}{g^{1/3}} (\frac{\rho_L}{\sigma})^{1/5} (\frac{\rho_L}{\rho_L - \rho_G})(\frac{\rho_L}{\rho_G})^{-1/15} (\frac{\mu_L}{\mu_w})^{-1/4}$
Loiseau et al. (1977)	$\varepsilon_G = 0.011 u_G^{0.36} (\frac{P_G}{V})^{0.27} \sigma^{-0.36} \mu_L^{-0.1}$
Nocentini et al. (1993)	$\varepsilon_G = (\frac{P_G}{V})^{0.333} u_G^{0.667} (\frac{\mu_L}{\mu_w})^{-\delta}$ δ varies with different fluids
Smith (1991)	$\varepsilon_G = 1.25 \times 10^{-2} (\mathrm{Re} \times Fr \times Fl)^{0.35} (d_I / D)^{1.25}$
Breman et al. (1995)*	$\varepsilon_G = \left(0.16 \left[\frac{u_G}{\left(\frac{g\sigma}{\rho_L} \right)^{0.25}} \right]^{0.67} + 0.32 \frac{d_I^2}{D(gD)^{0.5}} (N - N_0) \right) \times \left(\frac{g\mu_L^4}{\rho_L \sigma^3} \right)^{-0.042} (\frac{\rho_G}{\rho_{air}})^{0.12}$ $N_0 = 0.15 g^{0.5} D^{1.5} d_I^{-2}$

* Based on multistage agitated contactor, others are for SAC

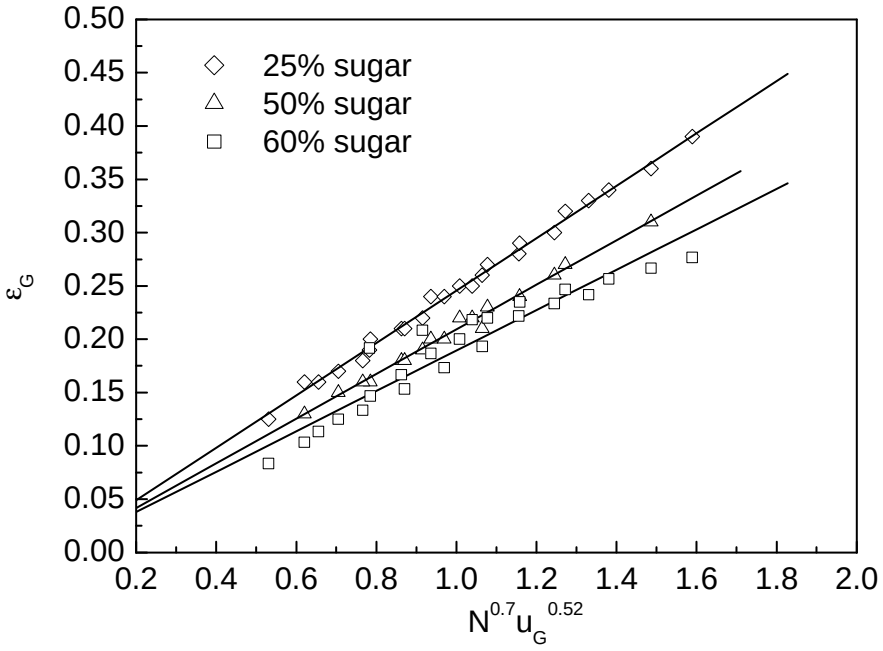

Figure 4. 3 A correlation for phase hold-up in viscous systems

A relationship to describe the viscosity effect on gas hold-up is proposed as follows:

$$\varepsilon_G \propto N^{0.7} u_G^{0.52} \left(\frac{\mu_L}{\mu_w}\right)^{\delta} \qquad \textbf{Equation 4. 1}$$

where δ is the exponent which characterizes the effect of viscosity. A relationship is established by minimizing MARR with a resultant small variance of 5% as follows:

$$\varepsilon_G = 0.31 N^{0.7} u_G^{0.52} \left(\frac{\mu_L}{\mu_W}\right)^{-0.19} \qquad \textbf{Equation 4. 2}$$

A very similar equation is developed through nonlinear fitting at a confidence level of 95% as shown in the following equation:

$$\varepsilon_G = 0.32 N^{0.69} u_G^{0.53} \left(\frac{\mu_L}{\mu_W}\right)^{-0.15} \qquad \textbf{Equation 4. 3}$$

A comparison of experimental data with values predicted from literature correlations was carried out and the results are shown in Figure 4.4.

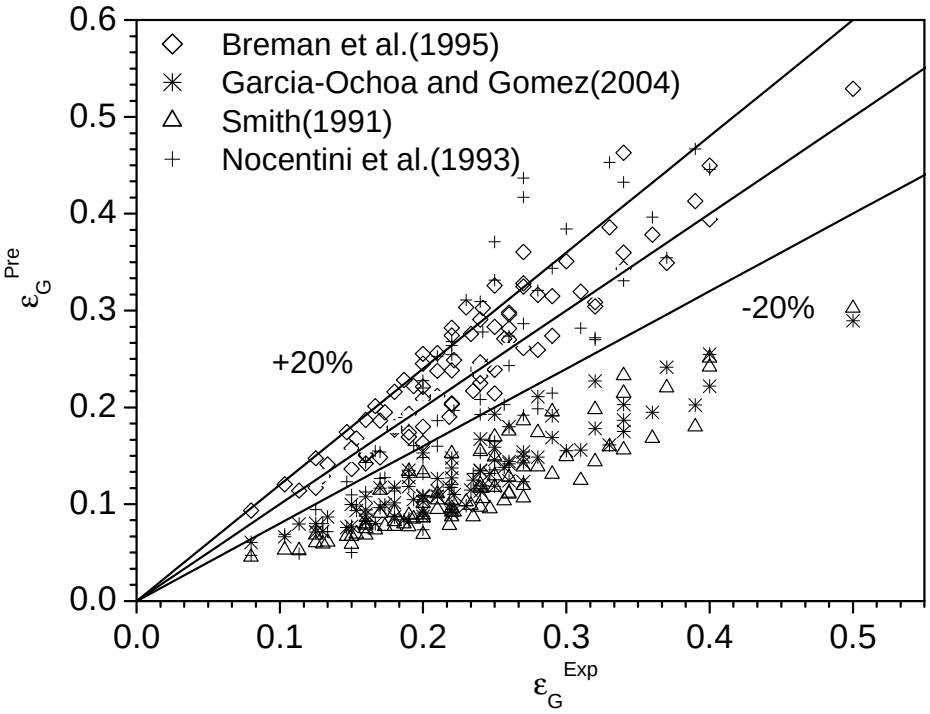

Figure 4. 4 Comparison of experimental data with literature values

A mean absolute relative residue (MARR) was still used to characterize the deviations of the predictions with experiments. The best agreement is from Breman et al. (1995) with a MARR of 11% where the physical properties of the liquid solutions and reactor geometry are taken into account in their relations while both relations of Garcia-Ochoa and Gomez (2004) and Smith (1991) present a poor fit with a MARR of 45% and 50%, respectively. The dimensionless form proposed by Smith (1991) does not include the influence of surface tension which is an important factor for the bubble size and in turn influences the phase hold-up and the correlation gives a relationship that ε_G is proportional to $\mu^{-0.35}$, resulting in a larger scatter. The relation provided by Garcia-Ochoa and Gomez (2004) correlates well with our data for an air-water system in a standard reactor configuration (D=0.15 m and d_I/D=1/3) (Zhang et al., 2005a). However, it poorly fits the present work presumably due to the non-standard configuration in the existing set-up (d_I/D=1/2 and D=0.01 m). A MARR of 24% results from Nocentini et al.(1993)

correlation which is generated in a reactor of 0.232 m in the diameter with four turbines ($d_I/D=1/3$) and $(\mu_L/\mu_w)^{-1/3}$ in their relation is generalized from water-glycerol solutions which is different from the sugar solutions ($(\mu_L/\mu_w)^{-0.19}$) used in the current study. The discrepancy might be attributed to some unknown different physical properties amongst the various liquids used.

4.3.2 Liquid Phase RTD in Viscous Media

The collected conductivity data were converted to RTD curves as detailed in Chapter 3 and a typical curve is shown in Figure 4.5.

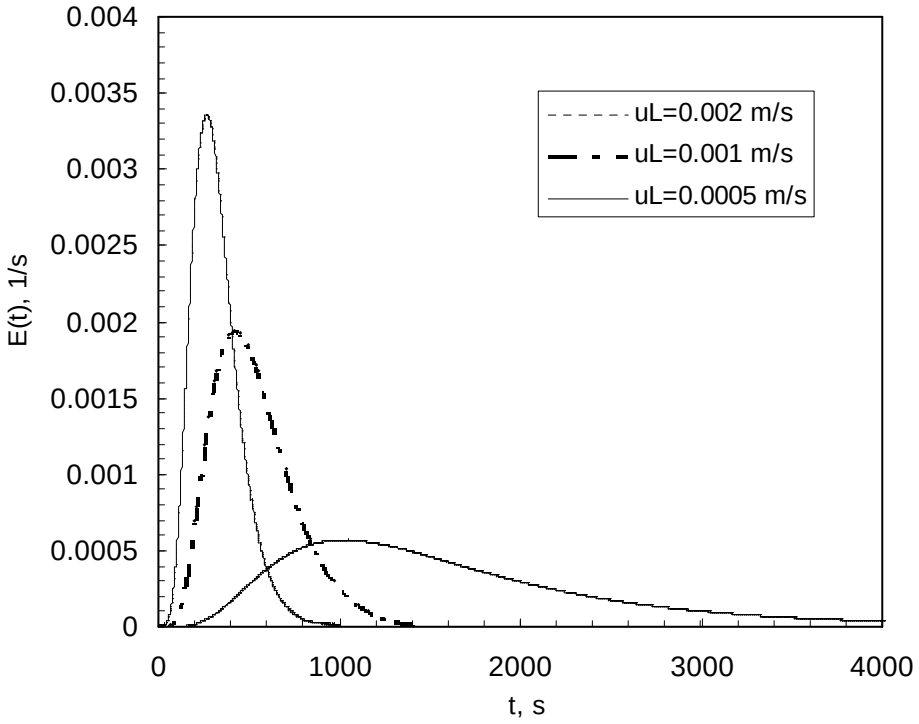

Figure 4. 5 Typical residence time distribution curves (50% sugar solution, N=12 rps and u_G=0 m/s)

It is shown in Figure 4.5 that with an increase in liquid flow rate, the residence time decreases as expected and the spread of residence time distribution decreases, indicating that liquid backmixing decreases. The normalized variance of RTD curves are 0.17, 0.19 and 0.25 for liquid velocity u_L=0.002, 0.001 and 0.0005 m/s, respectively. A higher normalized variance indicates a lower number of theoretical stages when using n CSTRs in series to model the reactor. As a result, lower stage efficiency is obtained,

which is undesirable in application. Various RTD curves can be obtained by varying operation conditions, such as stirring speed, gas flow rate and liquid properties, etc.

4.3.3 Model Discrimination

In the previous chapter, it has been shown that the CTB model fits the experimental RTD curves in air-water system. An attempt was also made to examine the suitability of the above models and was studied via a comparison of experimental RTD curves with theoretical curves predicted using the above models. The axial dispersion coefficient, De, in the AD model is evaluated from Equation 3.15 at a given normalized variance. The results are shown in Figure 4.6.

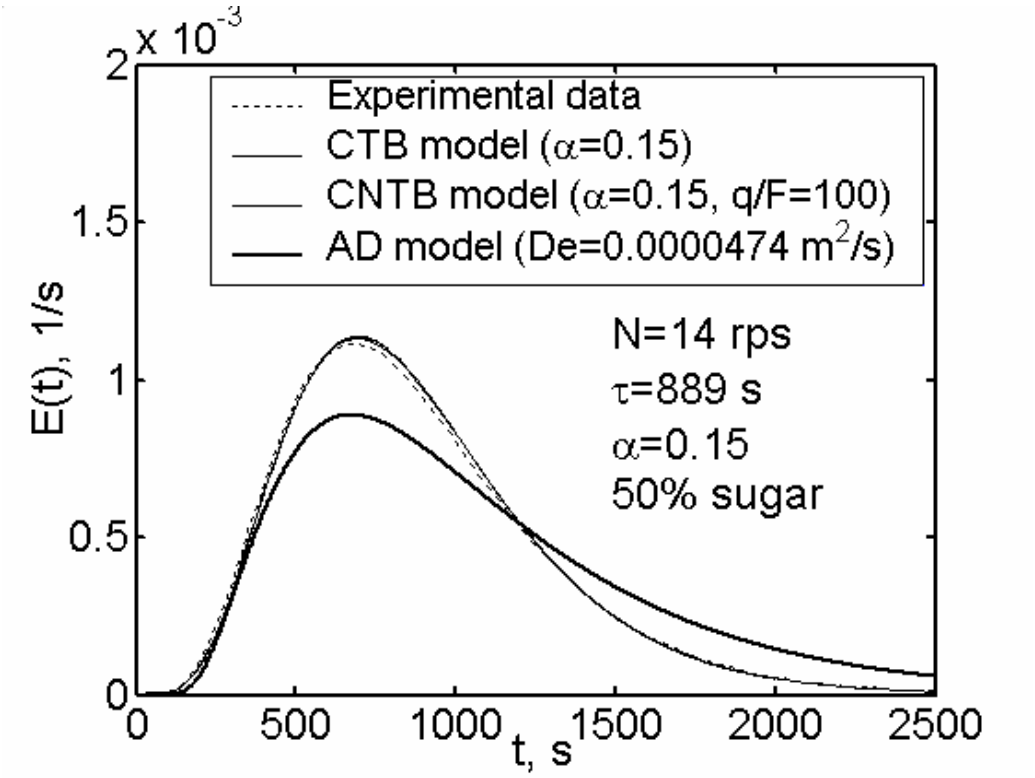

Figure 4. 6 Model discrimination (AD model with close-close boundary, CTB model and CNTB model)

Figure 4.6 shows that the CTB model fits the curve better since the AD model is more suitable for a MAC with a large number of stages and the axial dispersion parameter *De* has less physical meaning for a low number of stages. When the CNTB model is applied to fit the experimental curves, the performance

approaches that of the CTB model when the intra-stage back flow ratio, *q/F*, is larger than 100. According to previous studies (Vasconcelos et al., 1995, 1996), *q/F* is generally more than 100 in the present study. When a two-phase system is considered, the CTB model still satisfactorily fits the curve as shown in Figure 4.7.

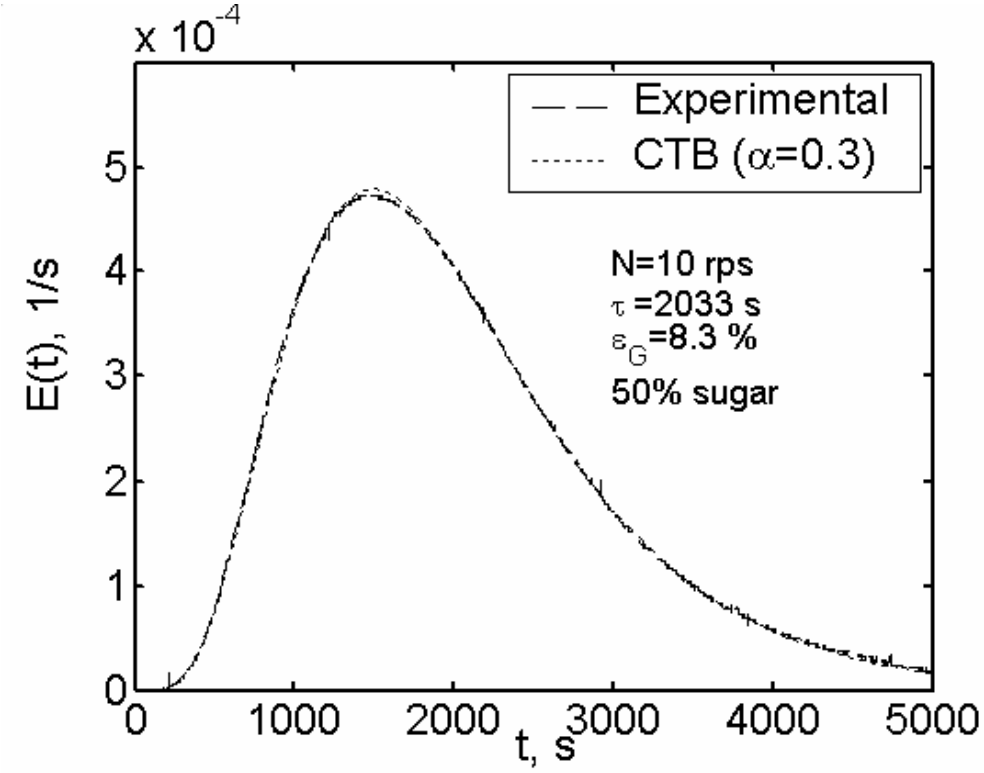

Figure 4. 7 A comparison of experimental RTD results with theoretical prediction in a two-phase system (D=0.1 m and u_G=0.018 m/s)

Therefore, the CTB model was used to describe liquid phase mixing behavior in viscous systems. From the resulting variances, the back flow ratios can be evaluated by the similar method detailed in our studies (Zhang et al., 2005a, 2005b).

4.3.4 Backmixing versus Operational Conditions

Figure 4.8 indicates that the effect of stirring speed on back flow ratio for different liquid systems. With an increase in stirring speed, backmixing increases as anticipated due to the intensified turbulence; in particular, velocity fluctuations.

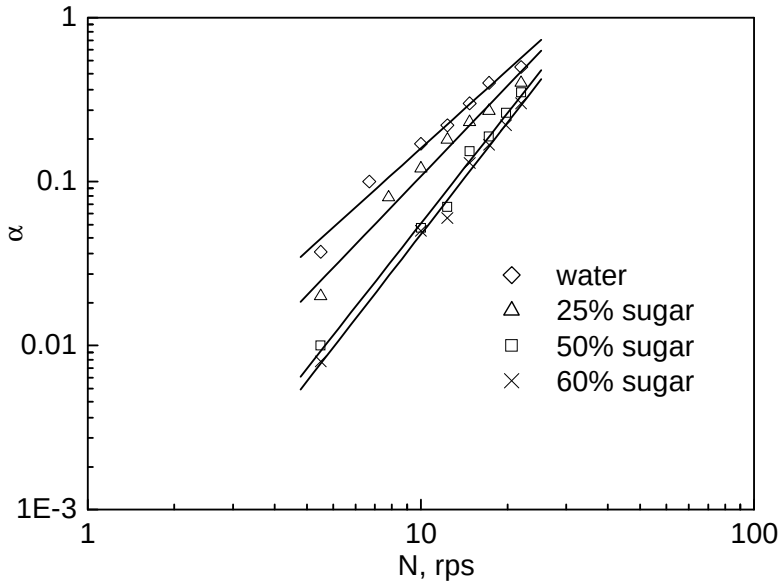

Figure 4. 8 Effect of stirring speed on backmixing in various Newtonian fluids

(D=0.1 m, u_G=0 m/s and u_L=0.001 m/s)

The phenomena agree with many reported studies (Haug, 1971; Magelli et al., 1982; Breman et al., 1996b; Takriff et al., 1998; Xu et al., 2005). In Figure 4.8, it is also shown that the viscosity has a negative impact on the backmixing, which is consistent with the findings of Vidaurri and Sherk (1985) and Xu et al. (2005) for MACs and Vasconcelos et al. (1996) for a non-standard vessel with multiple impellers. However, the phenomena conflicts with the findings of Breman et al. (1996b). The backmixing between consecutive stages is determined by the local level of turbulence nearby the opening. From a hydrodynamic point of view, the backmixing is directly related to the pumping capacity of the impeller. It is well known that when the Reynolds number decreases from turbulent flow regimes to transitional and laminar flow regimes, pumping capacity decreases. As a result, the back flow rate decreases.

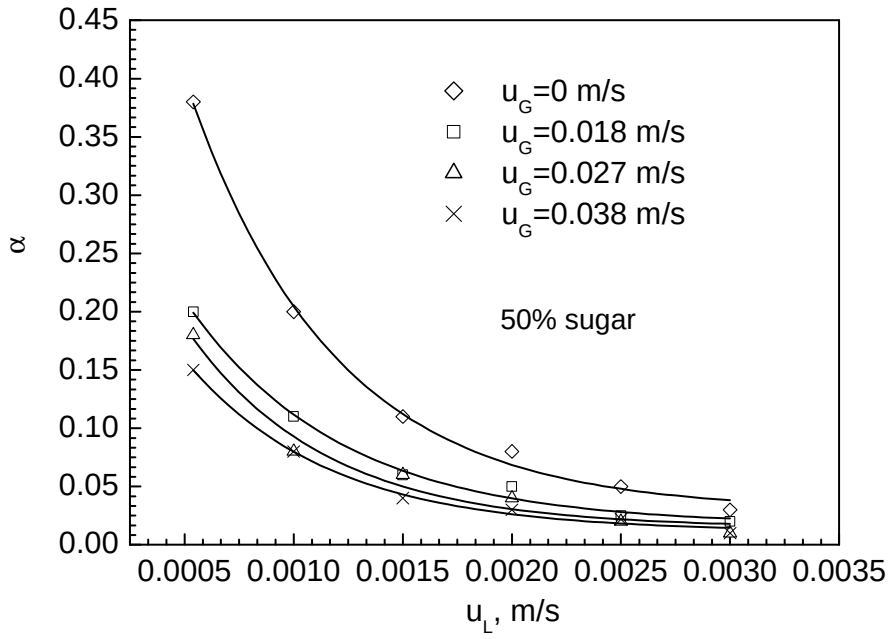

Figure 4. 9 Effect of liquid velocity on backmixing (D=0.1 m and N=15 rps)

The negative influence of main flow on back flow between stages is shown in Figure 4.9. It is observed that the liquid flow rate does not follow a linear relationship with back flow ratio while it plays a more significant role on it. Xu et al. (2005) observed that liquid forward flow rate considerably reduces backmixing between stages in a two-stage MAC of D= 0.2427 m and H=0.2413 m. Haug (1971) reported that back flow ratio is proportional to $u_L^{-1.24}$ in a water system in Oldshue-Rushton columns with diameters of 0.15 m, 1.20 m, and 2.40 m and six-stages, and a zero back flow ratio was observed at low Reynolds numbers. The data from Breman et al. (1996b) was not compared here since a non-flow technique was employed in their studies and the effect of liquid flow rate was not taken into account. The present work shows that increasing liquid flow rate considerably reduces the back flow ratio. However, increasing liquid flow rate is not always a practical way for suppressing the back mixing as the liquid flow rate is given by the required productivity of the apparatus. Addition of a draft tube around central opening could be an effective approach to reduce backmixing (Ingham, 1972; Vidaurri and Sherk, 1985; Xu et al., 2005). In addition, the figures also indicate that the presence of the gas phase helps in the reduction of

backmixing due to its straightening effect on liquid velocity. Similar phenomena are also shown in Figure 4.10.

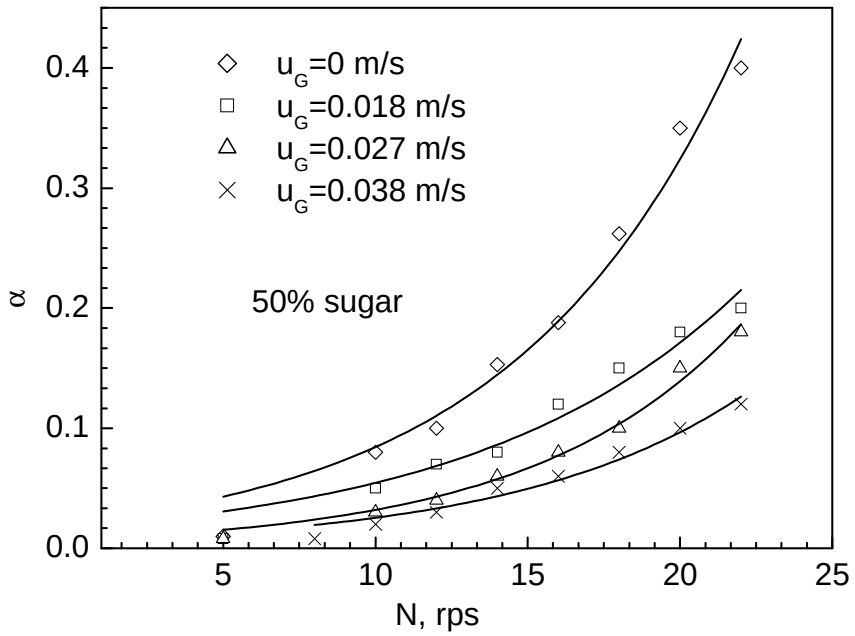

Figure 4. 10 Effect of stirring speed under gas velocities (u_L=0.001 m/s and D=0.1 m)

It is shown in Figure 4.10 that with an increase in gas velocity, the backmixing decreases for the two liquids employed. The influence of the gas phase on the back flow could be profound ($\propto (1-\varepsilon_G)^3$) as reported by Breman et al. (1996b) in a MAC with nine-stages of D=0.09 m and H=0.09 m. Under aerated conditions, the gas affects the hydrodynamics in a complicated way. The presence of the gas phase straightens the superficial liquid velocity by reducing liquid hold-up which in turn reduces the back flow and the entrainment effects of gas bubbles in a co-current manner which leads to a lower back flow rate. Consequently, as indicated in the above figures, at a low gas flow rate, the effect of stirring speed is more significant than that at high gas flow rate due to the fact that increasing the stirring speed increases turbulence, however, on the other hand, the liquid hold-up decreases. A similar trend was observed in a liquid-liquid extraction column (Ingham, 1972) and a MAC (Takriff et al., 1998).

4.3.5 Correlation for Liquid Backmixing in Viscous Systems

In the literature, there are diverse forms of correlating back flow rates with operating variables. Under turbulent conditions, a new correlation was proposed from the power input point of view (Zhang et al., 2005b). However, when a viscous liquid is involved, the dampening effect of the viscosity on the turbulence should be taken into account. In view of this, two Reynolds numbers are employed to characterize the flow behavior in the contactor. Re_1 is taken with respect to impeller, $\frac{\rho_L N d_I^{\ 2}}{\mu_L}$, while Re_2 is based on reactor column, $\frac{\rho_L u_L D}{\mu_L}$.

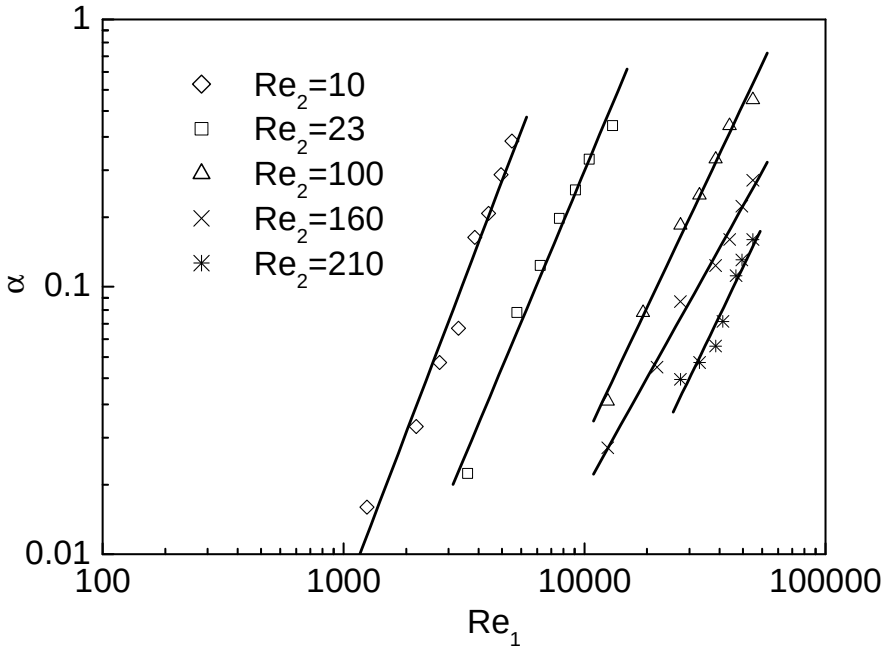

Figure 4. 11 Back flow ratio as a function of Reynolds number

Figure 4.11 shows a diagram for the back flow ratio under different operating regions. In the literature, a complex form to correlate back flow rate with Reynolds number was developed by Lelli et al. (1972) under two different regimes (Re_1>5000 and Re_1<5000) based on three different set-ups with the same central opening ratio (11%). Obviously, the effect of opening area was not considered. Magelli et al.

(1982) varied the central opening to establish a more general relationship. However, the central openings in their study are generally larger than 11%. An attempt is made to generalize a simple correlation to characterize back flow ratio as follows:

$$\alpha = p_1 \, \mathrm{Re}_1^{\,p_2} \, \mathrm{Re}_{2'}^{\,p_3} \qquad \textbf{Equation 4. 4}$$

In order to account for the effect of the central opening, $Re_{2'}$ was calculated from the liquid velocity passing through the central opening instead of the superficial liquid velocity based cross area of the column. Nonlinear least-square fitting gave p_1= (3.69±0.56) $\times 10^{-4}$, p_2=1.8 ±0.15, and p_3=-1.4±0.14 with a confidence interval of 95%. A comparison of experimental data in the present study with theoretical prediction is shown in Figure 4.12 and the values predicted from the correlations proposed by Magelli et al. (1982) and Xu et al. (2005) were also compared in this figure.

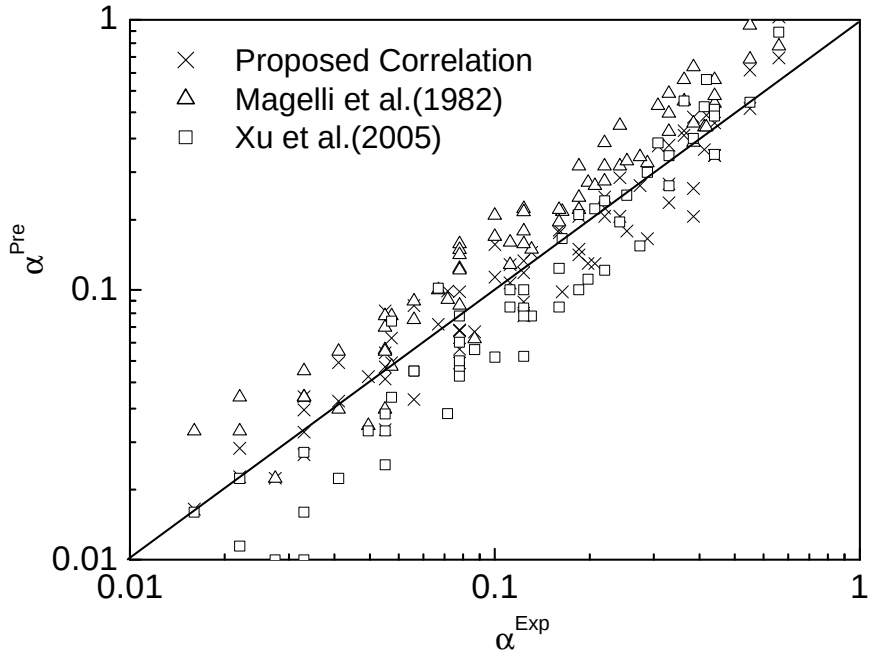

Figure 4. 12 A comparison of experimental data with theoretical prediction in single phase systems

The data from Haug (1971) are not compared here since only a water system was considered in his study. The data predicted using the relation provided by Magelli et al. (1982) is generally 30 % higher than the current work since the central opening ratio in the present study is only 1.5%. When the central opening becomes small, the effect of diameter of the shaft should be taken into account. In contrast, the correlations reported by Xu et al. (2005) provide a relatively good agreement with our experimental data (the deviation is within 25%) due to that the effect of central opening on backmixing has been reflected by the effect of liquid forward flow rate through the opening in their correlation. The higher scatter from the correlation is also observed at low back flow ratio owing to the difficulties of achieving accurate results at very low level of backmixing.

From the experimental analysis, the presence of the gas phase reduces the backmixing. Following our previous work in an air-water system (Zhang et al., 2005a, 2005b), a similar form is used to describe liquid backmixing in an air-viscous system is proposed as follows:

$$\alpha_{GL} = p_4 \alpha\ (1-\varepsilon_G)^{p_5} d_B{}^{p_6} \qquad \textbf{Equation 4. 5}$$

where p_4 is the coefficient in Equation 4.4, m^{-P6}. p_5 and p_6 are the exponents with respect to phase holdup and bubble size. Similar to water systems, d_B is the bubble size, m, and can be predicted by the relation proposed by Bhavaraju et al.(1978). Nonlinear fitting gives p_4=0.26±0.34, p_5=2.2±0.71, and p_6=-0.22±0.24 with a confidence interval of 95%. A MARR of 15% is obtained by comparing the predicted values with the experimental data. Compared to our previous study in a MAC with D=0.15 m (Zhang et al., 2005a), this p_4 is smaller (the previous p_4 is 0.34) possibly due to the different impeller positions used in the two correlations. In the present study, the impeller is positioned at 1/2 distance of one stage while it is located at 1/3 distance of one stage in the previous study (Zhang et al., 2005a). A comparison between the model prediction and experimental data was carried out and the results are shown in Figure 4.13.

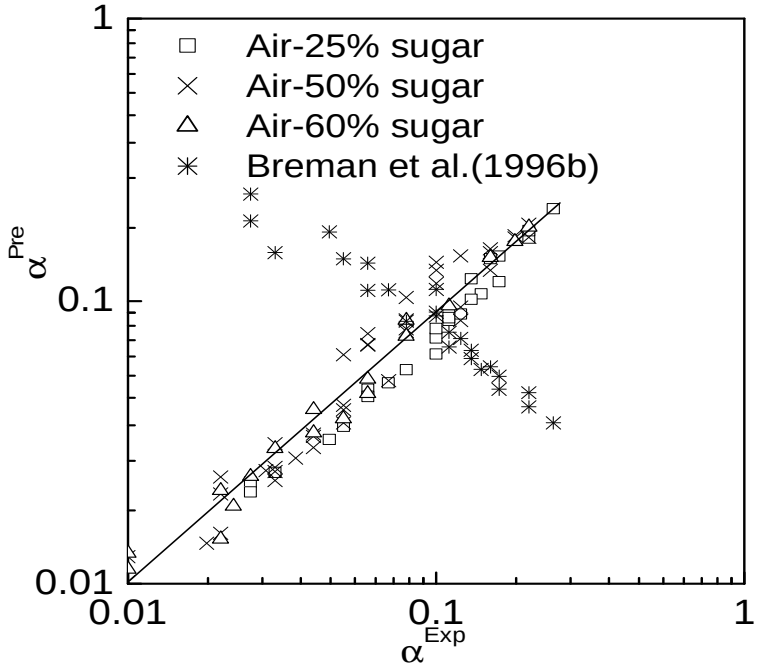

Figure 4. 13 Comparison of theoretical prediction and experimental data in two-phase system

The data from Breman et al. (1996 b) are also compared by correcting liquid flow rate and central opening area (19.5 % in their study) in order to obtain the back flow ratio. It is found that the back flow ratio is proportional to $(A_{hb}/A)^{0.62}$ (Haug, 1971). The back flow ratio from their study is estimated as follows:

$$\alpha = \frac{f^{Pre}}{\frac{\pi}{4}D^2 u_L}\left(\frac{0.195}{0.015}\right)^{0.62} \qquad \textbf{Equation 4. 6}$$

A good prediction is not expected for the data from Breman et al. (1996b) as shown in Figure 4.13 since the effect of liquid flow rate on back flow ratio is not taken into account in their study. From the comparison, it can be concluded that without a consideration of the influence of the liquid flow on back flow rate, it is not suitable to apply the backmixing data from non-flow conditions to a two-phase flow system.

4.4 Concluding Remarks

In Chapter 4, liquid phase backmixing in a MAC with gas liquid upflow was explored in Newtonian liquids (up to 0.02 Pa.s) through residence time distribution investigation. The CTB model is still suitable to describe the behavior of liquid flow within the MAC in liquids with medium viscosity. The back flow ratio for the first time was reported for a two phase flow system in viscous media. From the experimental study, it is found that the viscosity helps in reducing backmixing due to the resulting lower level of turbulence. The presence of the gas phase also reduces backmixing by a straightening effect and entrainment effect as discussed in air-water system in Chapter 3. The gas hold-up in viscous media is comparable to previously reported literature data. A new correlation was proposed to predict backmixing by taking into account the influence of the gas phase and the resulting bubble size.

Chapter 5 RTD Prediction by CFD Simulation in Single Phase Systems

5.1 Introduction

Computational Fluid Dynamics (CFD) has emerged as a powerful tool to conduct reactor design and reactor diagnosis and provide detailed information prevailing in the reactors, such as velocity field, concentration distribution, temperature profile, power consumption and phase hold-up distribution, etc. The encouraging achievements of the utilization of CFD tools in stirred vessels have been progressively published, such as flow behaviour characterization (Wu and Patterson, 1989; Ranade et al., 1990; Patwardhan, 2001a) mixing time prediction (Sahu et al., 1999; Bujalski et al., 2002; Montante et al., 2005), power consumption (Patwardhan, 2001a) and residence time distribution (Patwardhan, 2001b; Choi et al., 2004). With the aid of CFD, the flow patterns as well as their influences on mixing performance can be revealed. To the best of our knowledge, the application of CFD simulation to predict mixing behavior in MACs is not available in the literature although many successful examples on single stage baffled/unbaffled contactors or reactors with multiple impellers have been published. The unique feature of MAC to other stirred vessels is the utilization of horizontal baffles which separates the whole column into several stages. The function of horizontal baffles is already known for reducing backmixing between consecutive stages. The geometric similarity between MAC and stirred vessels with multiple impellers shows a promise of using CFD to predict flow field as well as mixing behavior in the designed reactor. Regarding the effect of viscosity on liquid backmixing, it is found that the viscosity shows a dampening effect on backmixing in our previous experimental work. However, contradictory conclusions have been drawn by other researchers (Miyauchi et al., 1966; Breman et al., 1996b) and it was interpreted that with an increase in viscosity the power input under the same stirring speed increases, which leads to an increase in turbulence accounting for the liquid backmixing between stages. The existing contradiction could be resolved by solving the transport equations in a MAC through CFD techniques, by which the flow and turbulence fields can be predicted in order to determine the mixing performance in the reactor.

The objective of this chapter was to investigate the mixing behaviour in a MAC using an available commercial CFD package by predicting liquid residence time distribution. The resulting residence time distribution was also compared to experimental data to demonstrate the feasibility of using CFD technique to assist reactor design. The stirring speed, liquid flow rate, and reactor geometries, all could have a

profound impact on the flow patterns in the stirred vessel which, in turn, affects the liquid mixing behaviour of a MAC.

5.2 Simulations

Similar to other stirred vessels, a challenging issue when using CFD to analyze a MAC is to model rotating impellers. In the literature, various approaches have been employed to model rotating impellers, namely, (1) black box approach, (2) multiple frames of reference approach (MFR), (3) inner-outer approach (IO) and (4) sliding mesh approach (SM) (Ranade et al., 1991; Brucato et al., 1998; Patwardhan, 1999; Montante et al., 2001, 2005). The black box approach requires impeller boundary conditions as input, which needs to be determined experimentally, although it is successful in prediction of the bulk flow. The sliding mesh approach is introduced by Luo et al. (1993), where transient simulations are conducted step after step for each relative position of the stirrer and baffles. However, this approach is very computation-intensive. Both IO and MFR approaches simplify the simulation by assuming suitable steady state conditions for the flow field simulation, resulting in substantial computational savings of computational demand compared to SM. In this work, an MFR approach is adopted. Due to the unsymmetrical fluid input, the whole 2π azimuthal extent of the MAC was considered in this work. The meshes employed for the simulations consisted of 300,000 cells for the reactor of two stages and up to 1,800,000 cells for six stages. In a multiple frames of reference approach, the tank bulk is set to a stationary domain while the impeller is embedded in a rotating domain as shown in Figure 5.1. The interface between the rotating domain and stationary domain was set to half way of the distance between the impeller tip and the tank wall. In the present study, the meshes used were unstructured. Additional mesh refinements near the walls of the vessel and near the stirrer were furnished so that the accuracy in the zone of high velocity gradients was improved. The impeller domain contained a mesh scheme of around 100,000 to 600,000 cells while the tank domain consisted of a mesh scheme of around 200,000 to 1,200,000 cells in the contactors with different stages.

A suitable turbulence model is required to take into account the turbulence prevailing in a stirred vessel. In general, a standard k-ε model was used for dealing with turbulence prevailing in the reactors.

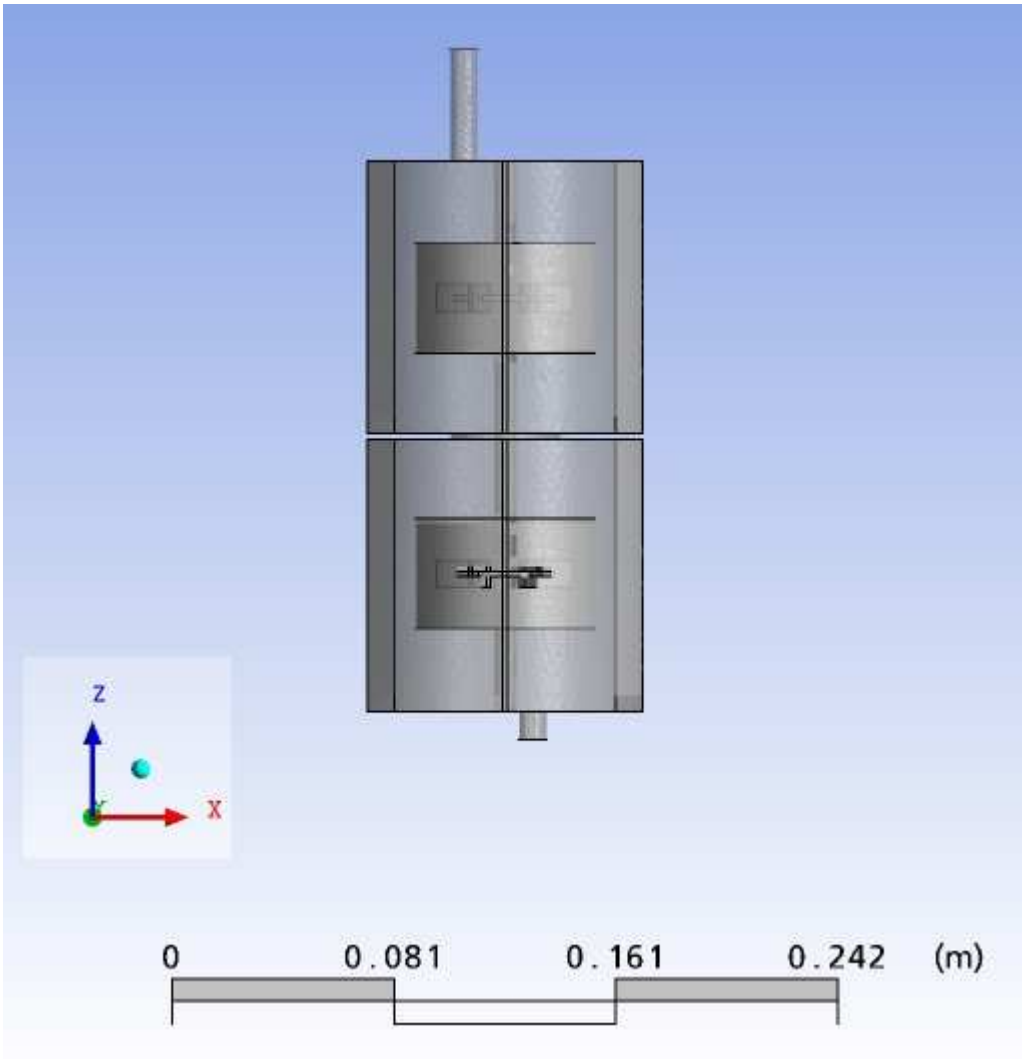

Figure 5. 1 Multiple frames of reference (MFR) model in a contactor of two stages

A commercial package CFX 5.7.1 was used for modeling and simulations in this work. The standard k-ε model was used for dealing with fully turbulent regions while a low Reynolds number turbulent model, RNG k-ε was also investigated for early turbulent regions for the purposes of comparison. The conservation of mass and momentum were determined using the Reynolds averaged Navier-Stokes Equation 5.1 and Equation 5.2 (ANSYS, 2005).

$$\frac{\partial \rho_L}{\partial t} + \nabla \cdot (\rho_L U) = 0 \qquad \textbf{Equation 5. 1}$$

$$\frac{\partial}{\partial t}\rho_L U + \nabla \cdot (\rho_L U \otimes U) = -\nabla p' + \nabla \cdot (\mu_{eff}(\nabla U + (\nabla U)^T)) + M \qquad \textbf{Equation 5. 2}$$

where ρ is the liquid density, kg/m^3, M is the sum of body forces, N, and **U** is mean velocity vector. In Equation 5.2, μ_{eff} is the effective viscosity, Pa.s, and evaluated in the following equation.

$$\mu_{eff} = \mu_L + \mu_t \qquad \textbf{Equation 5. 3}$$

The turbulent viscosity, μ_t, is given by

$$\mu_t = C_\mu \rho_L \frac{k}{\varepsilon} \qquad \textbf{Equation 5. 4}$$

where the model constant C_μ is set to 0.09, k is the kinetic energy, J/kg, and is a measure of velocity fluctuation. ε is the eddy energy dissipation, J/kg.

The equations of continuity and motion were solved first to attain velocity profiles, kinetic energy, eddy energy and eddy diffusivity. Subsequently, the information of the flow field and turbulent field obtained was used to solve a non-reacting scalar transport equation, based on the assumption that the tracer is dispersed in the vessel by convection and diffusion as follows:

$$\frac{\partial \rho_L \Phi}{\partial t} + \nabla \rho_L U \Phi = \nabla(\rho_L D_L \nabla \Phi + \frac{\mu_t}{\sigma_t} \nabla \Phi) \qquad \textbf{Equation 5. 5}$$

where Φ is the tracer concentration, kg/m^3, D_L is the molecular diffusivity, m^2/s and σ_t is the turbulent Schmidt number, indicating the difference between the rate of momentum transportation and passive scalars. The molecular diffusivity was assumed to be equal to 10^{-9} m^2/s, a typical value for liquids.

The required boundary conditions for the system are complex. In the stationary domain, the tank walls, vertical baffles and horizontal baffles were assumed as standard wall boundary conditions with no-slip flow while the shaft was set to a rotating wall with a speed of 5 rps to 20 rps. The velocity at the inlet was set uniform with a value reflecting a superficial liquid velocity from 0.0005 m/s to 0.002 m/s under investigation whereas at the outlet, pressure was set as being uniform across the outlet area. In the rotating

domain, its rotating speed was set to the same as that of the impeller and blades were set to wall boundary conditions.

At a given instant, the tracer concentration at the outlet could be obtained by taking the value of Φ at the same location from the transient results.

$$C(t) = \Phi_{outlet}(t) \qquad \textbf{Equation 5. 6}$$

$\Phi_{outlet}(t)$ is the concentration at the outlet at time t, kg/m^3.

The residence time distribution is evaluated from the concentration evolution at the outlet as follows:

$$E(t) = \frac{dC(t)}{C_0 dt} \qquad \textbf{Equation 5. 7}$$

where C_0 is the inlet concentration, kg/m^3. The parameters characterizing residence time distribution were evaluated according to the same approach detailed in Chapter 3.

5.3 Results and Discussion

5.3.1 CFD Simulations

The quality of meshes is essential for CFD simulations and the size of meshes should be optimized in order to obtain accurate results within a reasonable calculation time. In this work, the meshes used are unstructured. Additional mesh refinements near the walls of the vessel and near the stirrer were furnished so that the accuracy in the zone of high velocity gradients was improved. The maximum residue (MAX) < 10^{-4} was chosen to ensure a tight convergence of all the variables to be solved. The velocity is not measured in this work, and the power number evaluated from the torque exerting on the blades and the shaft is used as a criterion to determine the mesh quality, which is a common approach largely adopted in the literature (Ranade et al., 1991; Ranade, 1999; Letellier et al., 2002; Bujalski et al., 2002). The power number was evaluated from the torque exerted on the blades and the shaft from the simulations as follows:

$$N_P = \frac{P_0}{\rho_L N^3 {d_I}^5} = \frac{2\pi\psi N}{\rho_L N^3 {d_I}^5} \qquad \textbf{Equation 5. 8}$$

where P_0 is the power input, W, and ψ is the total torque exerting on blades and the shaft, N.m. The effect of the size of meshes on the power number is shown in Table 5.1

Table 5. 1 Effect of mesh size on simulation (u_L=0.001 m/s and N=10 rps in water system; Re=2.5×10^4)

Contactor scale	Two Stages		Four stages		Six Stages	
Number of cells	296,113	631,936	592,245	1,032,987	888,657	1,807,809
Power number, N_p	4.30	4.33	4.30	4.31	4.31	4.33
Deviation, %	±0.35		±0.12		±0.23	

In Table 5.1, it can be seen that when the size of meshes increases approximately three fold, the predicted power number only changes within about 0.4 %. Therefore, it can be concluded that the effect of the mesh size is not significant over this range of the mesh sizes. In addition, the predicted power number is in fairly good agreement with the value of Np=4.2 predicted by the equation proposed by Bujalski et al. (1987), which relates the power number to the minor dimensions of the impeller such as the blade thickness as well as the scale of reactors for Reynolds numbers $\geq 2\times10^4$. The slight difference exists due to the position of impeller and the continuous operation manner adopted in this work. The impeller is 1/2 of the diameter of that of the reactor and is positioned at the center of each stage and the deviation from the standard reactor combination possibly causes the slightly higher power number. Therefore, the simulated results are reasonably accurate.

Typical flow patterns are shown in Figure 5.2 and it can be seen that the velocity profile around each impeller is similar, where the liquid is pumped outward from the impeller and pushed back when approaching the tank wall. Therefore, two circulation loops are formed above and underneath the impeller, which is consistent with the experimental observation from other researchers (Nienow et al., 1968). The flow patterns could vary significantly with varying geometric structures. One circulation would occur when the position of the impeller is very close to the bottom of the tank (Montante et al., 2001). Due to the application of horizontal baffles and a relatively long distance between each impeller, the velocity field can be considered to be developed independently.

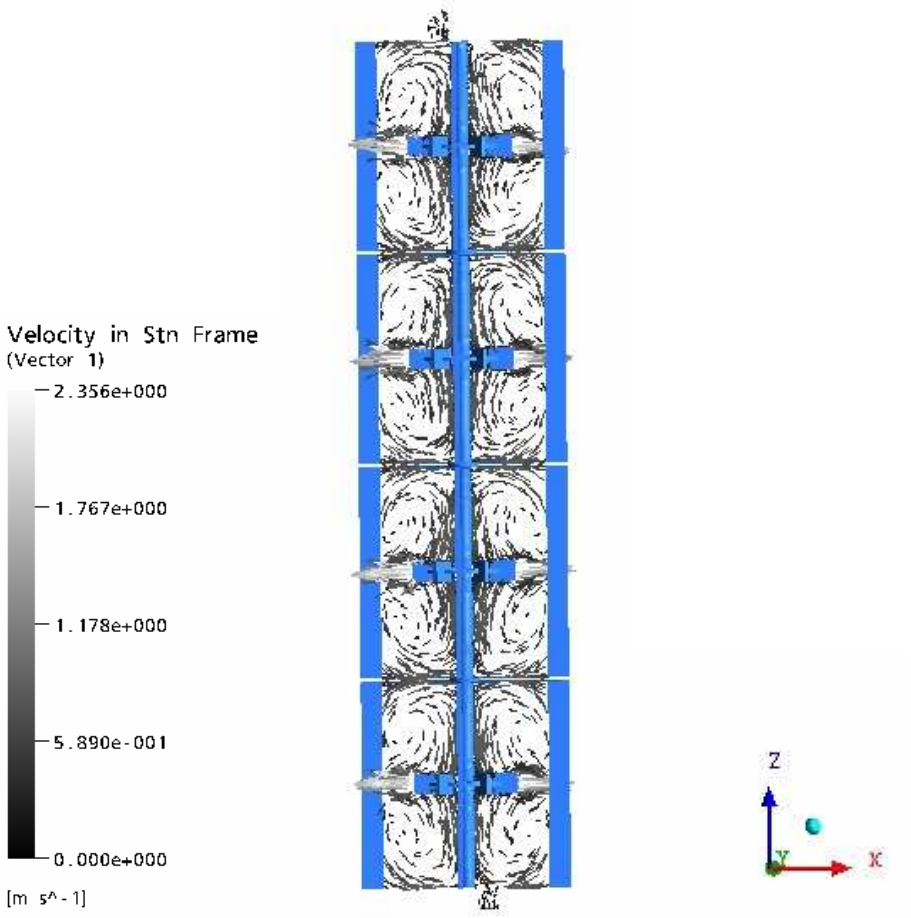

Figure 5. 2 Typical flow patterns in a four-stage reactor with water system

(N=15 rps and u_L=0.001 m/s; Re=3.75×10^4)

After the achievement of a steady state velocity field and turbulence field, the transportation equation of the tracer concentration was solved. The time evolution of the tracer concentration can be acquired by setting up a suitable time interval. A typical tracer profile captured at the outlet of the reactor is shown in Figure 5.3.

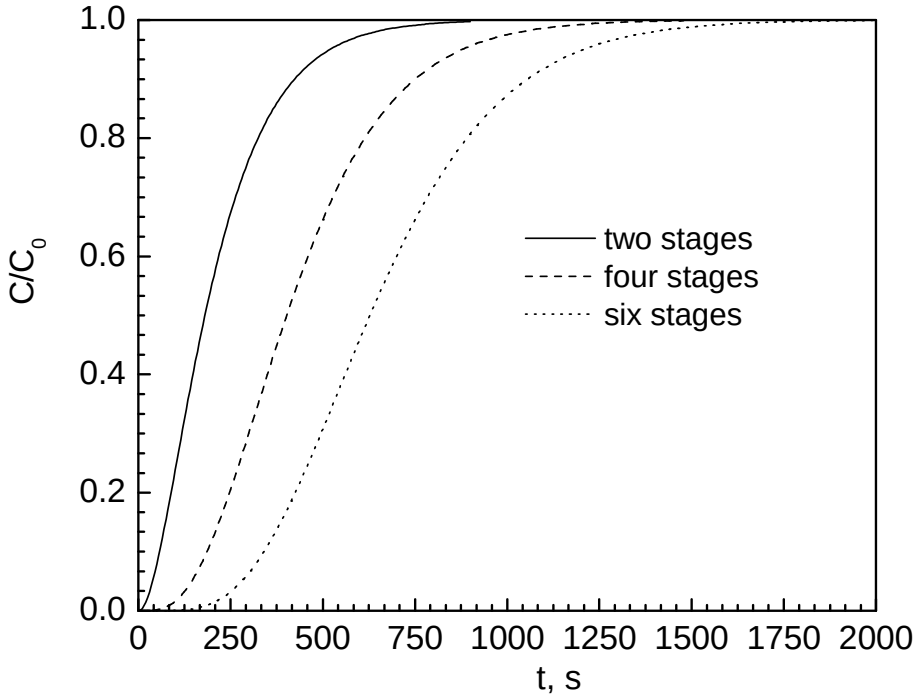

Figure 5. 3 Typical tracer concentration profile collected at the outlet

(u_L=0.001 m/s and N=10 rps)

Figure 5.3 shows a typical concentration profile at the outlet of the three reactors under investigation. It is obvious that the tracer concentration at the outlet approaches the unity faster in a reactor with a smaller number stages due to that the reactor volume is smaller. The residence time distribution can be determined using Equation 5.7 and the results are shown in Figure 5.4.

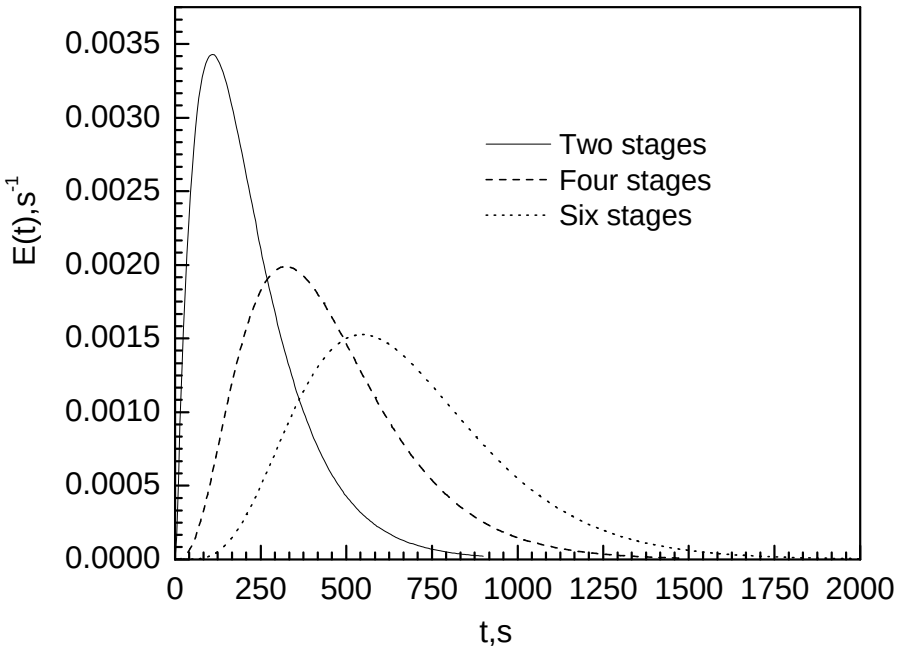

Figure 5. 4 Typical liquid RTD via CFD simulation in MACs with different stages

In Equation 5.5, different turbulent Schmidt number values have been adopted by the various authors, ranging from 1 to 0.1 ((Ranade et al., 1991; He, et al., 1999; Patwardhan, 2001; Montante et al., 2005), and different recommendations have been given depending on applications (Yimer et al., 2002). Montante et al. (2005) suggested a value of 0.1-0.2 for the forecasts of mixing time in stirred vessels with 6-pitched blades. In this work, the default value of 0.9 has been used down to 0.1 in order to examine the influence of turbulent Schmidt number on RTD prediction. Another critical factor considered in the present work is the time interval adopted. The standard time interval, t_0, is 5 seconds which is small enough compared to the average residence time studied (the latter is usually at least several hundred seconds) and its effect on RTD was explored by performing additional simulations with a time step of either one order of magnitude larger or smaller than the standard time interval.

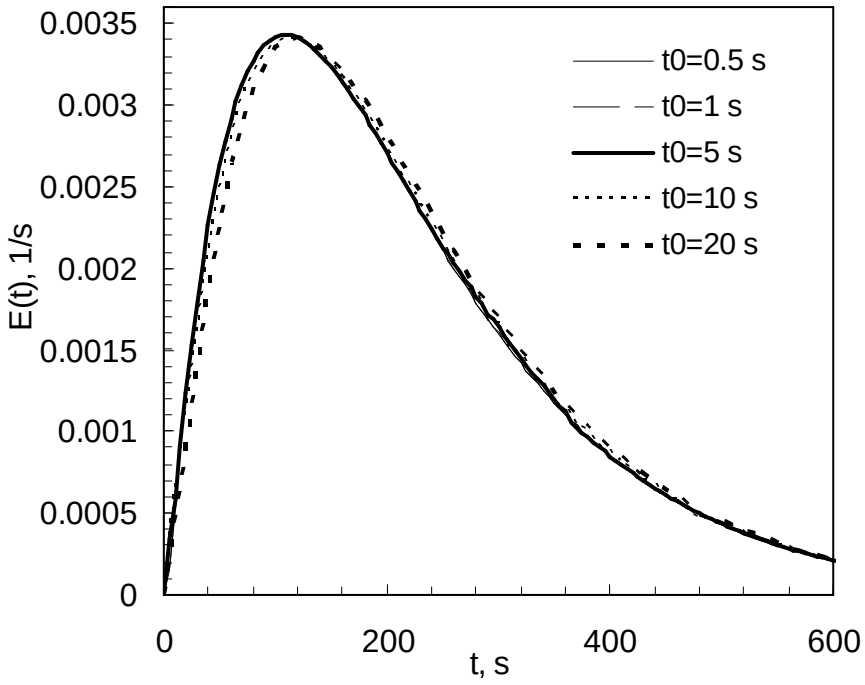

Figure 5. 5 Dependence of RTD on time interval selected in a two-stage contactor

(Turbulent Schmidt number=0.9, N=10 rps, Re=2.5×10^4 and u_L=0.001 m/s)

It can be seen from Figure 5.5 that when the time step was reduced to 5 seconds no further improvement is observed. Therefore, a time interval of 5 seconds was used in this work.

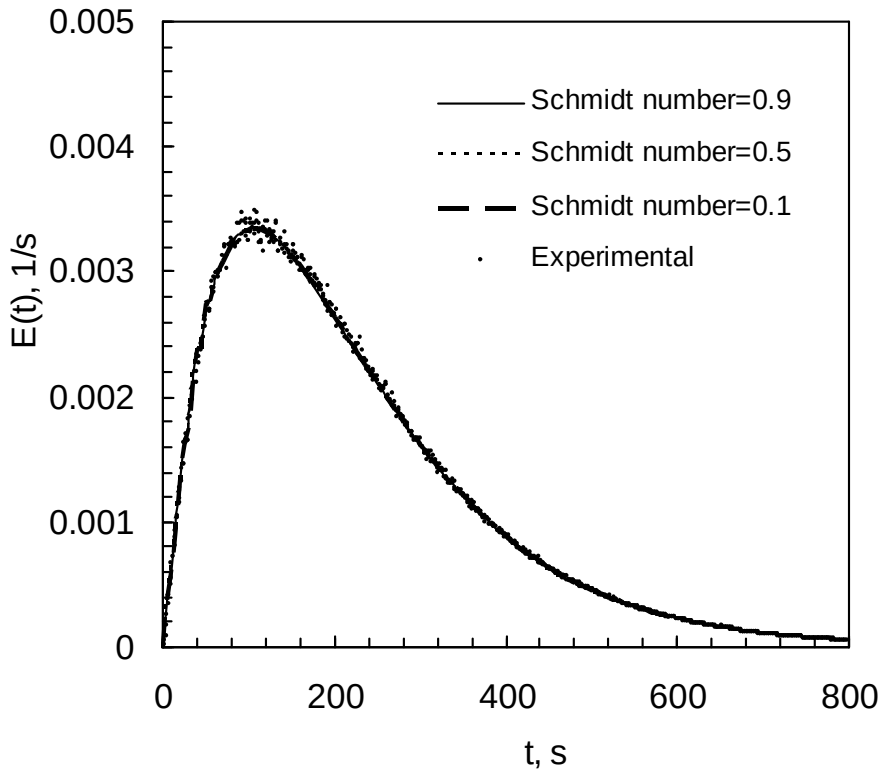

Figure 5. 6 Effect of the value of turbulent Schmidt number on RTD in a two-stage contactor (N=10 rps and u_L=0.001 m/s; Re=2.5×10^5)

As discussed earlier, different values for the Schmidt number have been selected by various authors, ranging from 1 to 0.1. However, in the present work, it is found that the Schmidt number has no significant impact on RTD predictions as shown in Figure 5.6 when the Schmidt number varies from 0.9 to 0.1. This is not consistent with the effect of the turbulent Schmidt number on homogenization curves and the mixing time in stirred vessels with multiple turbines reported by Montante et al. (2005). The independent behavior of the RTD simulations on the Schmidt number in the present work is presumably due to the fact that the mixing performance is completely dominated by the convection flow and each stage has reached the maximal mixing, which can be validated by the experimental phenomena that the mixing time (usually around 3 seconds) is fairly small compared to the mean residence time (hundreds seconds) for the MACs studied in this work. Therefore, the default value of 0.9 is used in all simulations later on. In Figure 5.6, the mean residence time and normalized variance predicted are 216 seconds and 0.53 respectively while the corresponding experimental values are 222 seconds and 0.55. The space time

under the same operating conditions, i.e., the reactor volume over liquid flow rate, is 217 seconds. The relatively small deviation (~3%) indicates that the RTD curve in the reactor can be satisfactorily predicted by the CFD simulation and the liquid mixing behavior can be understood by the CFD technique.

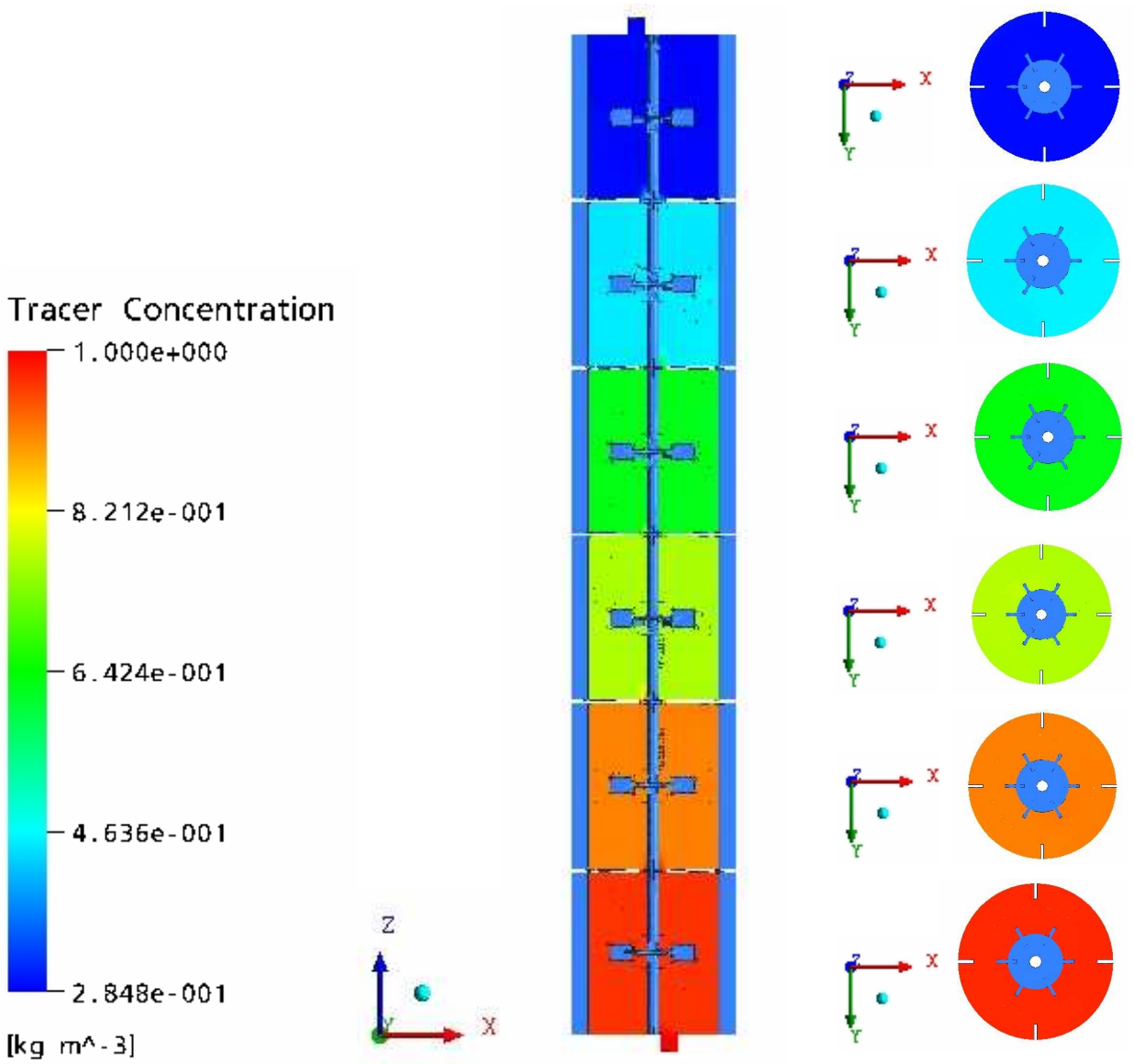

Figure 5. 7 Typical transient tracer concentrations at different stages in a six-stage contactor

(t=250 s, N=10 rps, u_L=0.001 m/s, Re=2.5×10^4)

In the simulations, the transient concentration profile can be obtained and a typical concentration distribution at a given instant is shown in Figure 5.7. In addition, a concentration profile for each stage is also presented on the right column.

Figure 5.7 shows that there is no concentration gradient observed within one stage, indicating that each stage is perfectly mixed, which further confirms the above analysis regarding the effect of the Schmidt number. It's already known that the AD model and the CTB model are commonly used to describe the flow behavior in the MACs. However, with a small number of stages, the CTB model is more suitable than the AD model since there is less physical meaning of the AD model in a MAC at a relatively low number of stages. Hence, the simulation results provide a line of evidence that the AD model is not suitable to describe the flow behavior in MACs with few stages.

5.3.2 Simulation Results and Discussion

5.3.2.1 Effect of Stirring Speed on RTD

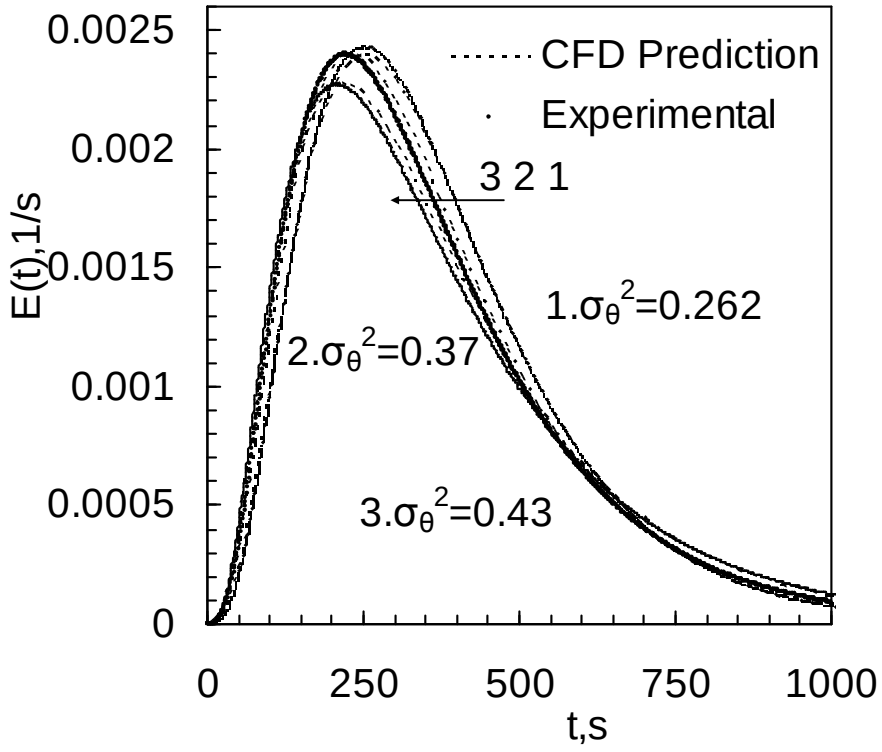

Figure 5. 8 Effect of stirring speed on residence time distribution in a four-stage contactor (u_L=0.001 m/s and water system:1. N=10 rps; 2.N=15 rps; 3.N=20 rps)

Figure 5.8 illustrates the effect of stirring speed on the normalized variance of the RTD (σ_θ^2) predicted by CFD. With an increase in stirring speed, the spread of residence time distribution increases as reflected in an increase in the σ_θ^2 values. Increasing stirring speed results in more back flow between stages and as a consequence, the distribution becomes broader. This observation is consistent with many other previous studies (Haug, 1971; Vidaurri and Sherk, 1985; Breman et al., 1996b; Xu et al., 2005; Zhang et al., 2005 a). In addition, the peaks on the RTD curves occur earlier at a higher stirring speed. The peak appears at 206 seconds when N=20 rps while it happens at 254 seconds when N=10 rps. Since high stirring speeds lead to earlier occurrence of the RTD peaks and a broader distribution, to employ high agitation intensity is not preferred if the purpose is to suppress the backmixing.

5.3.2.2 Effect of Liquid Flow Rates on RTD Curves

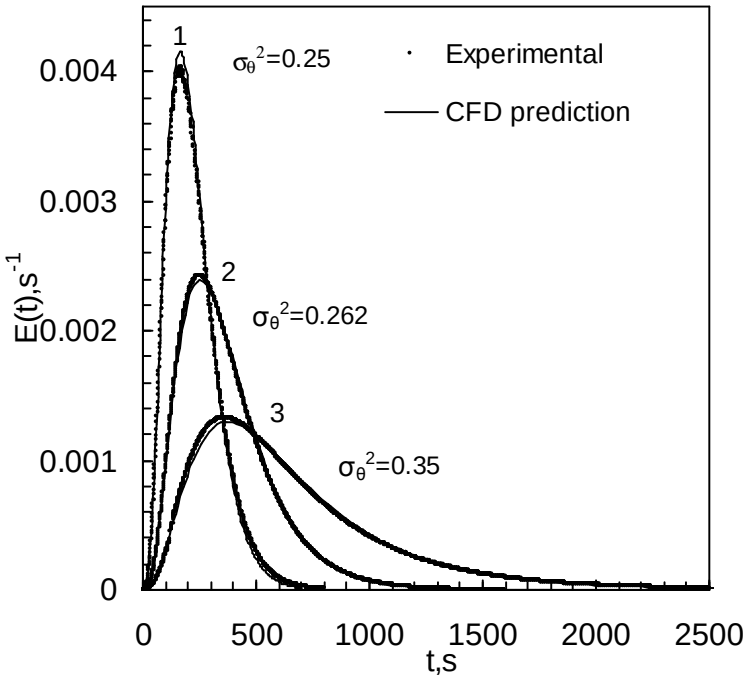

Figure 5. 9 Effect of liquid flow rate on RTD curves in a four-stage contactor (N=10 rps: 1. u_L=0.002 m/s; 2. u_L=0.001 m/s; 3. u_L=0.0005 m/s; water system)

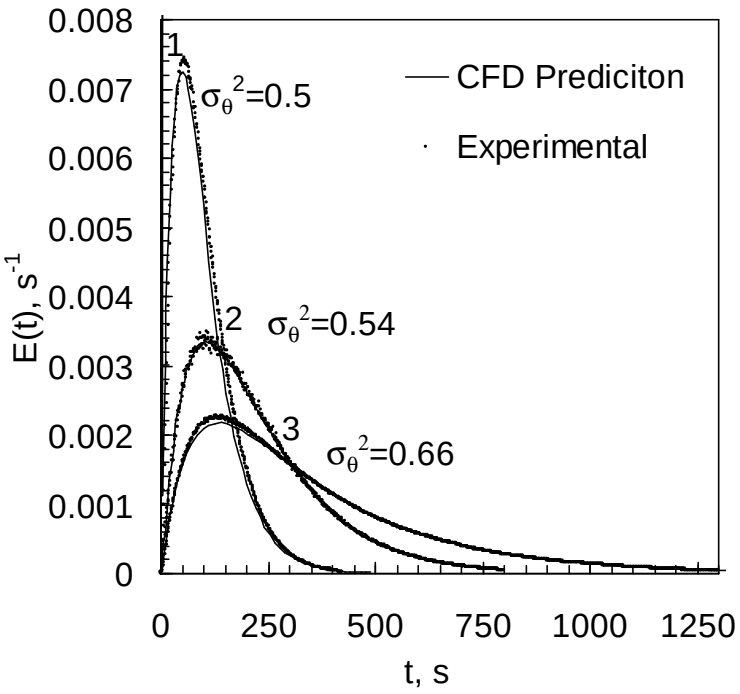

Figure 5. 10 Effect of liquid flow rate on RTD curves in a two-stage contactor

(N=10 rps: 1.u_L=0.002 m/s; 2.u_L=0.001 m/s; 3. u_L=0.0005 m/s; water system)

It is shown in Figures 5.9 and 5.10 that increasing liquid flow rate decreases the average residence time as expected. In addition, the spread of the RTD becomes narrower as indicated from the normalized variances when increasing liquid flow rates. In a four-stage contactor, the corresponding experimental variances are 0.25, 0.30 and 0.39 for liquid flow rates of 0.002 m/s, 0.001 m/s and 0.0005 m/s, respectively. In a two-stage contactor, the corresponding experimental variances are 0.50, 0.58 and 0.69, respectively. Compared to the values from the CFD simulation, the simulated results with the experimental data are in a reasonably good agreement. At a lower liquid flow rate, a higher normalized variance value is obtained, namely, a lower stage efficiency resulted. At u_L=0.0005 m/s, the performance of a four-stage contactor is equivalent to 2.8 CSTRs and the performance of a two-stage contactor is equivalent to 1.5 CSTRs under the same operating conditions. The stage efficiency reduces to as low as 72%, indicating that decreasing the liquid flow rate to achieve a longer residence time is not desirable.

5.3.2.3 Effect of Horizontal Baffles on the RTD Curves

It is known that the application of horizontal baffles is helpful in reducing back flow between consecutive stages. The influence of the opening area on the residence time distribution is predicted as shown in Figure 5.11 and Figure 5.12.

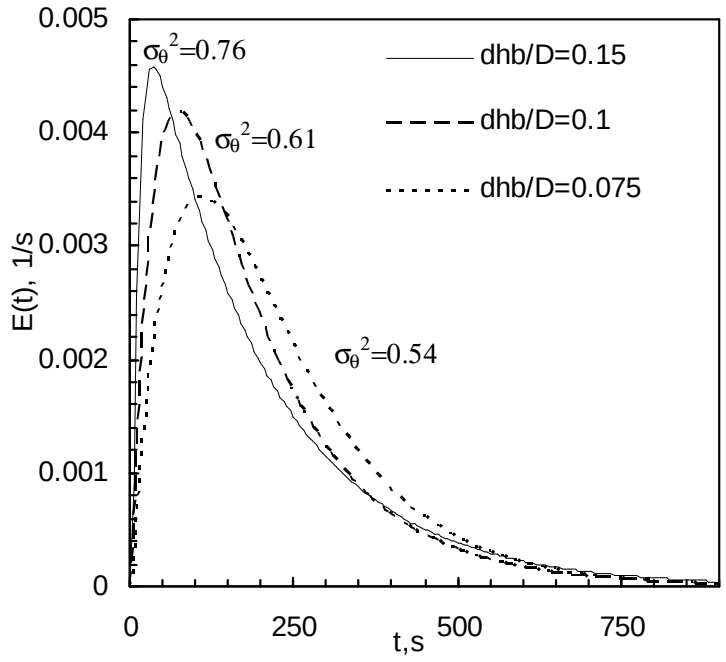

Figure 5. 11 Effect of horizontal baffles on RTD curves predicted via CFD simulation in a two-stage contactor (N=10 rps and u_L=0.001 m/s)

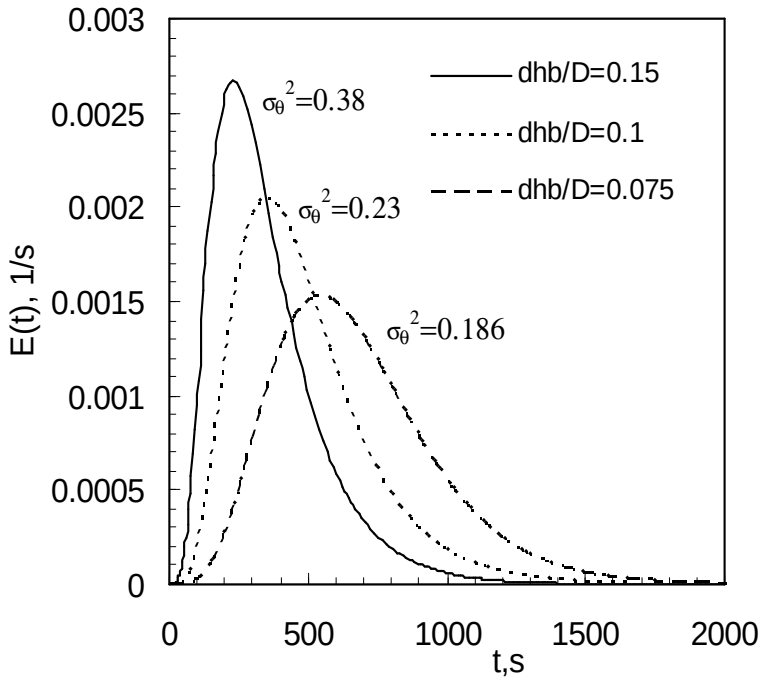

Figure 5. 12 Effect of horizontal baffles on RTD curves in a six-stage contactor

(N=10 rps and u_L=0.001 m/s)

In the above two figures, it can be seen that the horizontal baffles profoundly change the RTD curves. The peak of the RTD curve appears earlier and the tail of RTD is becoming longer when the central opening is larger. For instance, it appears at 200s, 400s and 600s in a MAC of six stages for three openings, respectively, as illustrated in Figure 5.12. Theoretically, it will occur at a time of zero when the back flow between stages approaches infinity and the overall performance of the whole reactor is equal to one CSTR with the same volume, where the RTD curve exponentially decays at t=0 second. In addition, the resulting variances show that the stage efficiency decreases from 90% to 45% in a six-stage contactor while it decreases from 91% to 66% in a two-stage contactor when the central opening area to cross section of the column ratio increases from 0.0161 to 0.0836. A larger central opening allows more back flow between stages, which is confirmed by many experimental findings (Haug, 1971; Vidaurri and Sherk, 1985; Xu et al., 2005).

5.3.2.4 Effect of Liquid Viscosity on RTD

CFD simulations were also performed in sugar solutions with different concentrations in order to investigate the effect of liquid viscosity on RTD curves. When dealing with viscous system, the Reynolds number with respect to the impeller falls into early turbulent regions (2,000<Re<10,000). Therefore, dependence of RTD predictions on different turbulent models was investigated. The utilization of the standard k-ε model and RNG k-ε model was investigated at Re=9,167 and Re= 2,600. There is no significant difference between the predictions by two models at two cases as shown in Figure 5.13. The RNG k-ε model predicts a power number of about 5 % higher than that obtained from the standard k-ε model at Re=9,167. The values of τ for k-ε and RNG k-ε models are 191.8 and 192.0 seconds, respectively and their corresponding σ_θ^2 are 0.779 and 0.781. Similarly, the RNG k-ε model estimates a 4.5% higher power number than that from the k-ε model at Re=2,600. The values of τ for the k-ε and the RNG k-ε models are 192.7 and 192.8 seconds, respectively. Compared to Re=9,167, lower normalized variances at Re=2600 are obtained, 0.75 for the standard k-ε models and 0.755 for the RNG k-ε models, indicating that backmixing is less at a lower Reynolds number. From the comparison, it can be seen that the choice of either model does not considerably affect the prediction of RTD curves at early turbulent regions (2,600< Re< 10,000).

Therefore, all simulations in sugar solutions were performed with the standard k-ε model otherwise stated differently. A comparison of simulation with experimental data in a MAC of six stages was conducted and the results are shown in Figure 5.14. The mean residence time and variance of RTD from the CFD simulation in this case are 634 seconds and 0.200 respectively while the corresponding experimental values are 618 seconds and 0.215 under the same operating conditions. Deviations of 2.5% and 7.5% for the mean residence time and normalized variance respectively are obtained, indicating that the RTD curve for a viscous system also can be predicted by the current approach.

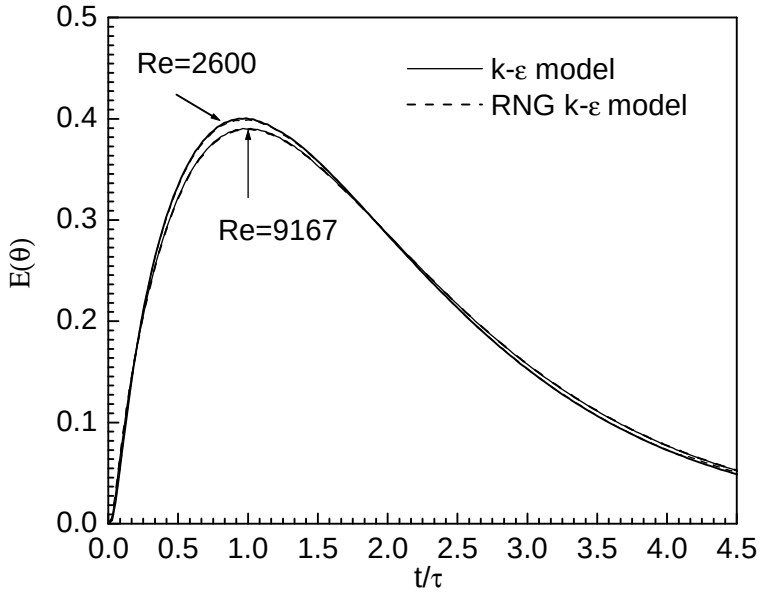

Figure 5. 13 Effect of two different turbulent models on RTD curves in a two stage MAC (25% sugar solution, N=15 rps, u_L=0.001 m/s and Re=9167; 50% sugar solution, N=10 rps, u_L=0.001 m/s, Re=2600)

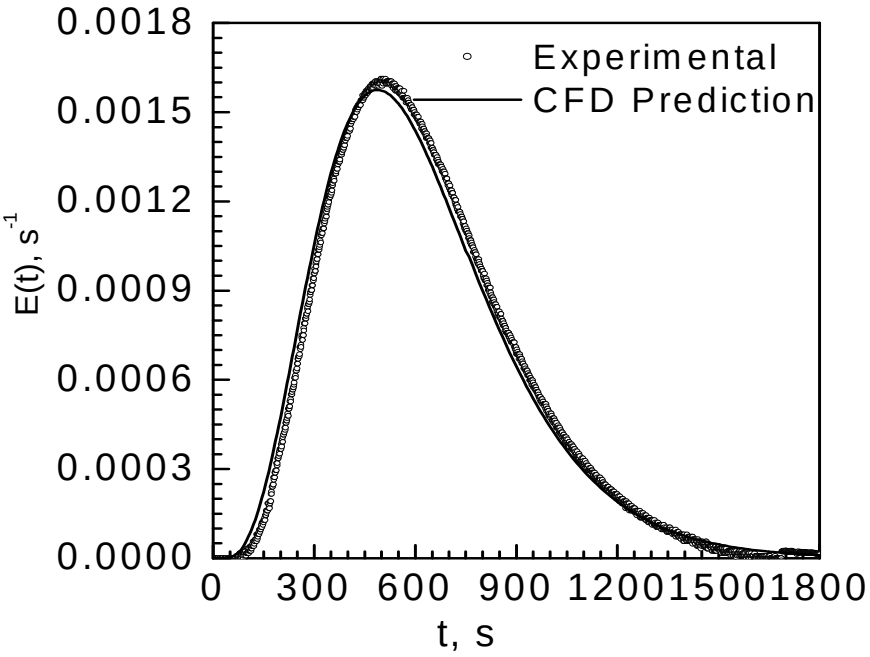

Figure 5. 14 Comparison of RTD prediction by CFD simulation with experimental data in a six-stage contactor with 50% sugar solution (N=15 rps, u_L=0.001 m/s and Re=3000)

RTD curves in various sugar solutions are shown in Figure 5.15. It is shown in Figure 5.15 that with an increase in sugar concentration, σ_θ^2 decreases from 0.23 to 0.20, indicating that the back flow between stages in a more viscous system becomes less at the same operating conditions. The observation is in good agreement with the previous studies (Magelli et al., 1982; Xu et al., 2005). The peaks of the RTD curves appear slightly earlier for a less viscous system. In a water system ($Re=3.7\times10^4$), it occurs at 350 seconds while it appears at 365 seconds and 375 seconds for 25% ($Re=9.4\times10^3$) and 50% sugar ($Re=3.0\times10^3$) solutions, respectively.

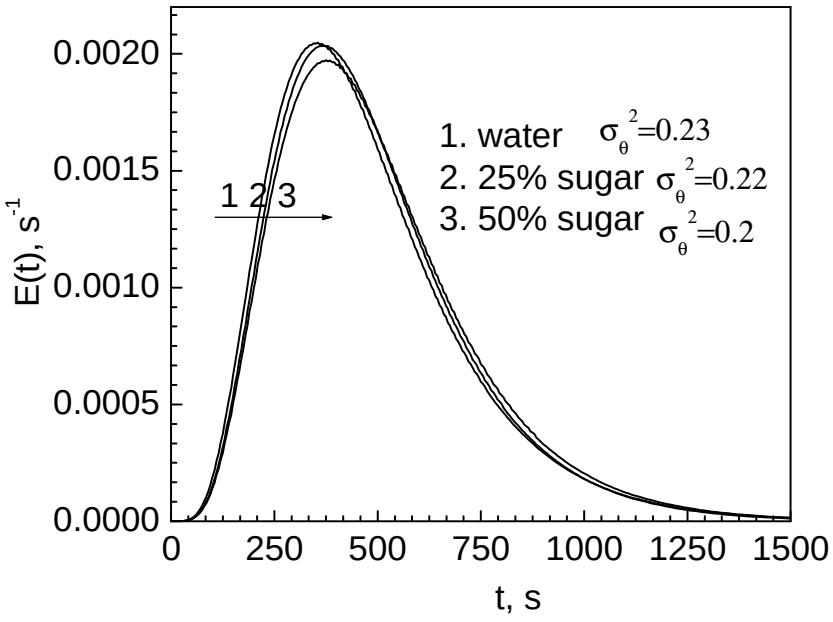

Figure 5. 15 The effect of liquid viscosity on RTD curves in a six-stage contactor (N=15 rps and u_L=0.001 m/s)

5.3.3 Backmixing Characterization

As demonstrated earlier, the CTB model is more suitable to describe the flow behavior of MACs. As discussed in Chapter 3 and Chapter 4, a back flow ratio is employed to characterize the backmixing extent between consecutive stages. From the resulting normalized variance, a back flow ratio could be evaluated using the method reported in previous studies (Vidaurri and Sherik, 1985; Zhang et al., 2005a, 2006). A comparison of the back flow ratio from the CFD simulation with experimental values was also conducted as shown in Table 5.2. In addition, the values predicted from the correlations proposed by Magelli et al. (1982) and Xu et al. (2005) were only compared in a six-stage reactor as shown in this table since the number of stages are assumed to play a marginal role on the back flow ratio between stages in their correlations.

From Table 5.2, it is shown that the back flow ratio from the CFD simulations generally is lower than the corresponding experimental value with a deviation of less than 20%. A relatively large deviation usually occurs at low back flow ratio level since it is difficult to get accurate experimental values. It is

already understood that the back flow between stages is caused by turbulence prevailing in the reactors, which is directly associated with the pumping capacity of the impellers. The inherent deficiency of the k-ε model to accurately predict turbulence could possibly account for the underestimation of backmixing besides the experimental error. In different reactors with different stages, either the back flow ratio from the CFD simulation or the experimental values are almost the same at the same stirring speed and liquid velocity, which is consistent with the theoretical foundation of the CTB model. With respect to the effect of viscosity on the back flow ratio, both the simulation and the experimental work show the same trend that viscosity has a negative role on back flow, which agrees with previous studies (Megalli et al., 1982; Vidaurri and Sherik, 1985; Xu et al., 2005). The data predicted using the relation provided by Magelli et al. (1982) is generally 30 % higher than that provided in the current work probably due to the fact that the central opening area over the cross sectional area is only 1.5% in the present work while the correlations were generated based on reactors with large central openings (greater than 11%). In contrast, the correlations reported by Xu et al. (2005) are in a relatively good agreement with the present study since the effect of central opening on backmixing has been reflected by the effect of liquid forward velocities through the opening adopted in their work.

Table 5. 2 Comparison of back flow ratio predicted from CFD simulation with experimental data

Reactors	N, rps	u_L, m/s	Back flow ratio, CFD prediction	Experimental	Magelli et al., 1982	Xu et al., 2005
6	10	0.001	0.12	0.17	0.198	0.1
6	15	0.001	0.25	0.35	0.35	0.24
6	20	0.001	0.45	0.5	0.71	0.495
6	10	0.002	0.03	0.04	0.031	0.03
6	10	0.0005	0.33	0.4	0.45	0.47
4	10	0.001	0.11	0.14	-	-
4	15	0.001	0.23	0.29	-	-
4	20	0.001	0.5	0.55	-	-
4	10	0.002	0	0.05	-	-
4	10	0.0005	0.5	0.6	-	-
2	10	0.001	0.087	0.12	-	-
2	15	0.001	0.25	0.28	-	-
2	20	0.001	0.49	0.53	-	-
2	10	0.002	0	0.04	-	-
2	10	0.0005	0.47	0.6	-	-
6*	10	0.001	0.08	0.12	0.2	0.09
6*	15	0.001	0.19	0.24	0.3	0.22
6*	20	0.001	0.35	0.4	0.6	0.46
6*	15	0.0021	0.04	0.05	0.06	0.034
6^+	10	0.001	0.05	0.07	0.14	0.05
6^+	15	0.001	0.12	0.19	0.22	0.17
6^+	20	0.001	0.3	0.35	0.41	0.4

* 25% sugar system; + 50% sugar system; others for water system.

5.4 Concluding Remarks

The CFD technique was employed to predict residence time distribution (RTD) curves for MACs with Newtonian liquids. The CFD modeling work was implemented using a commercial CFD package CFX5.7.1. The resulting RTD curves have been compared with experimental data obtained by a

conductivity meter. The observed power numbers from the simulation show good agreement with the literature. The observed mean residence time and normalized variance are in a reasonably good agreement with the experimental data. The concentration profile obtained from simulations provides a line of evidence that the CTB model is more suitable to describe the flow behavior in MACs. Both simulation and experimental work show that the viscosity helps in reducing backmixing by its dampening effect. Therefore, the mixing behavior of MACs can be understood by CFD simulation and CFD simulation can facilitate reactor design.

The slight underestimation of back flow ratio from CFD prediction is presumably attributed to the inherent deficiency of standard turbulence model in describing turbulence at low Reynolds numbers. It is expected that further improvement can be achieved by considering more advanced turbulence models.

Chapter 6 Development of a Continuous HNBR Process

6.1 Introduction

In previous chapters, a thorough hydrodynamic study of the MAC proposed for hydrogenation of NBR was carried out. Based on the hydrodynamic understanding, a bench scale continuous process will be designed and established to demonstrate hydrogenation behavior to realize the ultimate objective of this research project. Before fabricating a MAC to perform the hydrogenation process, a preview of the hydrogenation performance in the proposed reactor has been attained through a numerical analysis of an established mathematical model (Zhang et al., 2005c). The numerical studies also have revealed that the dynamic behavior of hydrogenation performance in a MAC is controlled by the following parameters: catalyst loading, back flow ratio, C=C loading level, phase hold-up and the residence time parameter. Among those parameters, back flow ratio, gas holdup and the residence time parameter have been well understood in the previous chapters, providing fundamental knowledge of designing a continuous setup for hydrogenation of NBR. From the previous numerical study, it is demonstrated that a MAC can satisfactorily produce a desired hydrogenation conversion and exhibit operation flexibility. Hence, in order to explore hydrogenation behavior in the MAC and provide more fundamental data for industrial application, a bench-scale prototype was designed and a continuous set-up for hydrogenation of NBR was established. The objective of this chapter was to illustrate a novel continuous process for hydrogenation of NBR by using a MAC. Based on the knowledge of hydrodynamic behavior achieved in the previous chapters, a MAC with a volume of 1liter was designed and a continuous setup for hydrogenation of NBR was established. Hydrogenation efficiency furnished by the developed unit is discussed and a comprehensive mathematical reactor model is also provided for the hydrogenation dynamic prediction. In addition, a simple correlation is proposed to estimate hydrogenation degree at steady state.

6.2 Basic Rational for the Process Design

After a complete understanding of hydrodynamic performance of MACs at various operating conditions, one is able to design a continuous setup involving a MAC for hydrogenation of NBR. Prior to designing and establishing such a gas liquid reactor, the following considerations are to be taken into account from the perspective of hydrogenation. A minimum hydrogenation degree of 95% is required in the final HNBR product, which ensures a significant improvement of physical properties. Since the hydrogenation behavior follows a first order reaction with respect to the concentration of carbon carbon double bonds, a

residence time of 10 minutes to 40 minutes is required to achieve the desired conversion (over 95%) based on the kinetic rate constants provided by Parent et al. (1998). In principle, the residence time of the liquid phase is determined by the liquid flow rate and reactor volume as well as the liquid holdup. Therefore, there could be a variety of combinations of a reactor volume and a liquid flow rate which could provide the residence time requirement. However, when the practical operation of such a reactor is concerned, a suitable reactor volume is desired. From the previous experimental observation, it is found that it takes at least 2-3 times of a residence time for the flow system to approach steady state. In view of this, a reactor with a volume of around 1 liter is pursued to perform the continuous process. When the reactor volume is fixed, a variety of combinations of the reactor diameter and the number of stages also arises. A larger reactor diameter would result in a smaller number of stages, leading to a lower hydrogenation conversion under the same reactor volume according to our previous numerical simulations (Zhang et al, 2005c). The previous numerical study shows that a MAC with a larger number of stages could achieve a higher conversion under the same reactor volume. However, the capital cost will significantly increase to fabricate a very long MAC. Hence, a MAC with a suitable number of stages is preferentially adopted. The hydrodynamic studies in previous chapters show that liquid residence time, gas holdup and mass transfer can be well predicted based on the developed correlations and literature values available. In addition, the preview of the hydrogenation performance was achieved through numerical simulation. Therefore, the comprehensive knowledge obtained with respect to this particular reactor enables us to design a MAC with any dimensions at a high level of confidence.

A MAC of six stages was designed for the hydrogenation process due to its capability of achieving the desired hydrogenation conversion of over 95% under industrial conditions predicted from the simulation. In addition, it also possesses the operation convenience at a lab scale compared to a MAC with a very large number of stages. Within the reactor, vertical baffles were not installed in order to make reactor internal structures simpler since the absence of those baffles would not compromise its mixing effect when the reactor size is relatively small and vibrant agitation is provided (Nagata, 1975). A Rushton turbine was used as an impeller due to that it can provide sufficient liquid mixing as well as gas dispersion. The cooling coil was present in the first stage in order to remove the heat released from the hydrogenation if necessary. The horizontal baffles separate the whole column into six stages and present a central opening of 5% over the whole area of the column. The schematic representation of the designed reactor is provided in Appendix A. The detailed geometric information is given in Table 6.1.

Based on hydrodynamic understanding of a MAC, a co-current upflow is employed since it offers the capacity of minimizing backmixing between stages and reducing pressure drop during the flow. Therefore, both polymer solution and hydrogen are introduced from the bottom of the reactor.

Table 6. 1 Reactor dimension

Reactor parameter	Stage diameter, m	Stage height, m	Impeller diameter, m	Number of stages	Central opening, m
	0.06	0.06	0.03	6	0.015

After the reactor geometry is fixed, the hydrodynamic performance of the designed reactor can be predicted from the correlations developed in Chapter 3 and Chapter 4. The stirring speed employed in the continuous unit ranges from 10 rps to 20 rps to maintain the same power input level with that in our previous hydrodynamic studies. In order to achieve a liquid residence time of 10 to 40 minutes, a liquid flow rate ranging from 20 ml/min to 90 ml/min is required. As a consequence, the resultant back flow ratio is generally less than 0.2 from the previous hydrodynamic results, indicating a stage efficiency of above 83%. Accordingly, the gas holdup is ranging from 0.1 to 0.3 at the same operating conditions. In addition, volumetric mass transfer coefficient, $k_L a$, is in the range of 10^{-2} s^{-1}. At the above operating conditions, the preview of the established set up shows that the desired hydrogenation degree of over 95% could be achieved. Therefore, further experimental efforts are required to demonstrate hydrogenation behavior and to provide fundamental data for industrial application design.

6.3 Experimental

A bench-scale prototype was designed and constructed to demonstrate principles of utilizing a MAC to perform the continuous process for hydrogenation of NBR. Capable of handling pressures up to 100 bars and temperatures between 110 °C and 200 °C, the system can be used to study NBR hydrogenation at industrial operating conditions. Detailed in this section are the process components and the procedures developed for its operation.

6.3.1 Apparatus

A schematic of the prototype is provided in Figure 6.1 while the list of the component models and part numbers are provided in Appendix B. Solution of NBR in chlorobenzene are prepared and stored in a 10 liter, polyethylene carboy (A) under the continuous flow of oxygen-free N_2, a high pressure pump (B) meters a precise flow of the polymer solution to a 2 liter Parr autoclave (C) where it is preheated or

contacted with the hydrogen stream if necessary. Hydrogen is supplied via a Brooks mass flow controller (D). A high agitation rate is used while pre-heating the polymer solution about 20 °C above that in the MAC (I).

Solutions of catalyst are prepared and stored in a 1 liter stainless steel bomb (H) under a N_2 atmosphere. The bomb is pressurized to 10 bars with hydrogen to accommodate the volume created as the solution is discharged into the MAC (I) by a second, high pressure pump (G).

The catalyst solution contacts the hydrogen and NBR mixtures at the entrance of the reactor. From the MAC the reactants pass through a water-cooled heat exchanger (J) before reaching the distributing valve. Two 500 ml, high pressure sight glass (K) are operated in parallel to separate gas liquid phases, while the hydrogenated polymer solution is retained in the sight glass, hydrogen proceeds through a check valve (M). The parallel system allows for collection in one unit while draining the other into a 10 L carboy container (L).

The system pressure is maintained by the back pressure regulator (O) and measured by a gauge (N). On the low pressure side of the regulator is a second stage (P) which protects the gas rotameter (Q) in the event of a process upset. The hydrogen is vented to the walk-in fume hood output ducts.

Steam is supplied at 40 psig to the top of the MAC jacket by a pressure regulating valve. Condensate expulsion from the bottom of the steam jacket is actuated by a thermostatic steam trap. The NBR solution and catalyst pumps provide an output of 5-40 ml/min and 30-200 ml/min with +/- 5% precision, respectively. Hydrogen is supplied by the mass flow controller (D) up to 6 SLPM (standard liter per minute) after which the flow must be manually adjusted.

The MAC is a 0.36 m long six-stage column having a 0.06 m internal diameter. The height of each stage is equal to 0.06 m and one impeller is provided in each stage with a diameter of ½ of the column diameter. The central opening is 5% of the cross sectional area of the column.

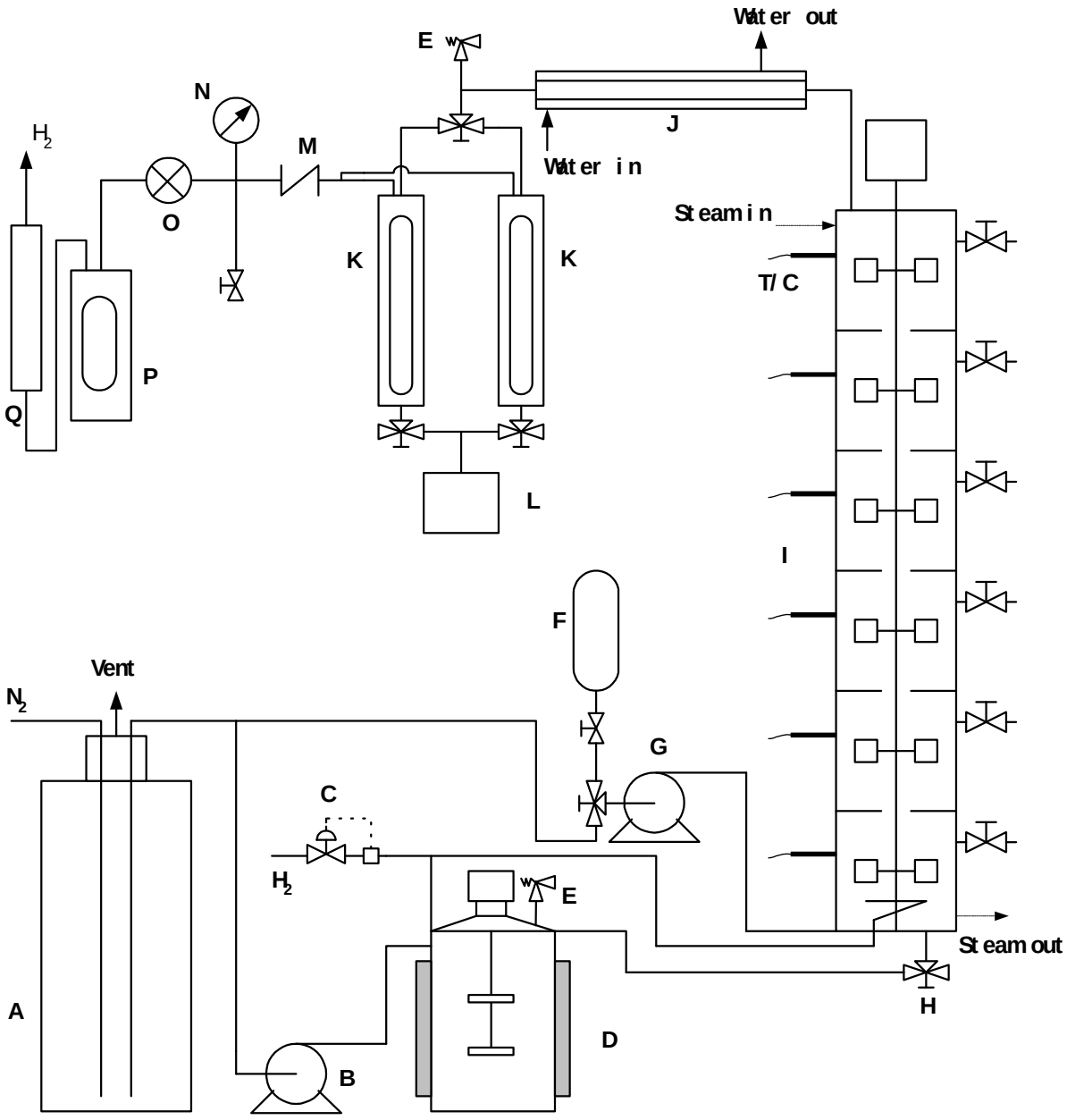

A-10L carboy B-Metering pump C-Mass flow controller D-Preheater E-Relief valve F-1L catalyst bomb G-Metering pump H-Three way valve I-MAC J-Heater exchanger K-Gas liquid separator L-Collection container M-Check valve N-Bourdon gauge O-Back pressure regulator P-Low pressure separator Q-Gas rotameter

Figure 6. 1 Schematic of the continuous process prototype

Continuous pumping of the liquid into a closed system may over-pressurize the system, this may occur when the system is blocked. Therefore, a relief valve set at 1500 psig has been installed following the heat exchanger and another relief valve of 1500 psig has been placed on the preheater. The entire set-up is positioned within a continuously purged, walk-in enclosure to vent hydrogen and solvent fumes. A hydrostatic test of the equipment at 1000 psig and 130 °C was undertaken before the experimental work was commenced.

6.3.2 General Operation Procedures

The unsaturated NBR studied was (Krynac 38.50 from LANXESS) contained 62% butadiene by weight which was distributed as 80% trans, 15% cis, 5% vinyl olefin distribution and possessed an Mn=70,000 and a polydispersity of 3.6. The solvent employed was monochlorobenzene (MCB) used as received from Fisher Chemicals. Solutions of NBR in MCB were prepared in a 20 liter carboy and purged of atmospheric gases by bubbling with 99.9% nitrogen (Praxair) for two days. A steady stream of nitrogen through the carboy was maintained during hydrogenation experiments to retain an inert atmosphere. Catalyst solutions were prepared under N_2 using degassed chlorobenzene. A technique has been developed to charge the catalyst solution to the catalyst bomb. After the preparation of the catalyst solution in a 1 L flask under N_2 atmosphere, the catalyst bomb was put under vacuum for 20 minutes. A positive pressure was maintained in the flask where the catalyst solution was retained. Therefore, the pressure difference between the flask and the catalyst bomb transferred the catalyst solution into the bomb where it was subsequently pressurized to about 10 bars with hydrogen gas.

With the NBR and catalyst solution vessels in place the pumps were primed and the entire reactor system degassed by successive pressurization and venting of 20 bars H_2 (Praxair) for a total of three cycles. The steam was supplied with a pressure of 40 psig to ensure a temperature of 140 °C within the reactor. The steam pressure can be adjusted according to the desired temperature required in the MAC. The hydrogen was charged to the system and regulated by the mass flow controller. The system pressure was maintained at any desired value by the back pressure regulator. The polymer metering pump delivered NBR solutions through the whole period of operation time. The other metering pump started to charge catalyst solution into the reactor after the temperature and the pressure of the reactor were stabilized. Subsequently, the transient behavior of the reactor was monitored by sampling NBR solutions at various stages every 10 minutes. The system is usually considered to approach its steady state after three times of

the liquid residence time. Therefore, an operation period of two to three hours was generally adopted under investigated conditions. The hydrogenation degree of NBR solution was monitored using a widely accepted FTIR approach.

6.4 Experimental Results and Discussion

6.4.1 Catalyst Reactivity

An efficient osmium catalyst precursor, $OsHCl(CO)(O_2)(PCy_3)_2$, was used for selective hydrogenation of NBR in the designed continuous process. The catalyst was prepared according to the method employed by Parent et al. and reference therein (1998). In order to confirm the same catalyst entity presently synthesized, the osmium catalyst reactivity was investigated in a batch reactor before embarking on hydrogenation performance investigation using the continuous set-up. The catalyst reactivity was investigated in a Parr reactor at similar operating conditions to those explored by Parent et al. (1998). Two temperatures were primarily chosen, 130 °C and 140 °C. A stirring speed of 600 rpm was used. The catalyst concentration was 80 µM and the pressure of the system was 350 psig. Two independent experimental runs were conducted for two sets of conditions. The hydrogenation saturation was measured using FTIR. The conversion was calculated according to the following equation, which is developed by Bruck (Kehl, 1998).

$$\%conversion = \frac{\frac{A(730)}{k(730)}}{[A(2250) + \frac{A(970)}{k(970)} + \frac{A(730)}{k(730)}](1 - ACN)} \qquad \textbf{Equation 6. 1}$$

where A(x) is the absorbance height at a characteristics wavenumber, x cm^{-1}, and ACN is the acrylnitrile content in the rubber. For the NBR rubber Krynac 38.5, the weight ratio of ACN to butadienene is 38:62. k(x) is the FTIR constant. The values for k(730) and k(970) used are 0.255 and 2.3, respectively (Kehl, 1998).

The characteristics peak heights used here were the 2250 cm^{-1} peak resulting from cyano group, the 970 cm^{-1} peak measuring the level of unsaturated trans olefin by the proton vibration on the C=C-H, and a modified peak at 730 cm^{-1} which resulted from the oscillating H attached to measured backbone, $-CH_2-$

CH_2-. The typical infrared spectra were captured during the process of hydrogenation as shown in Figure 6.2.

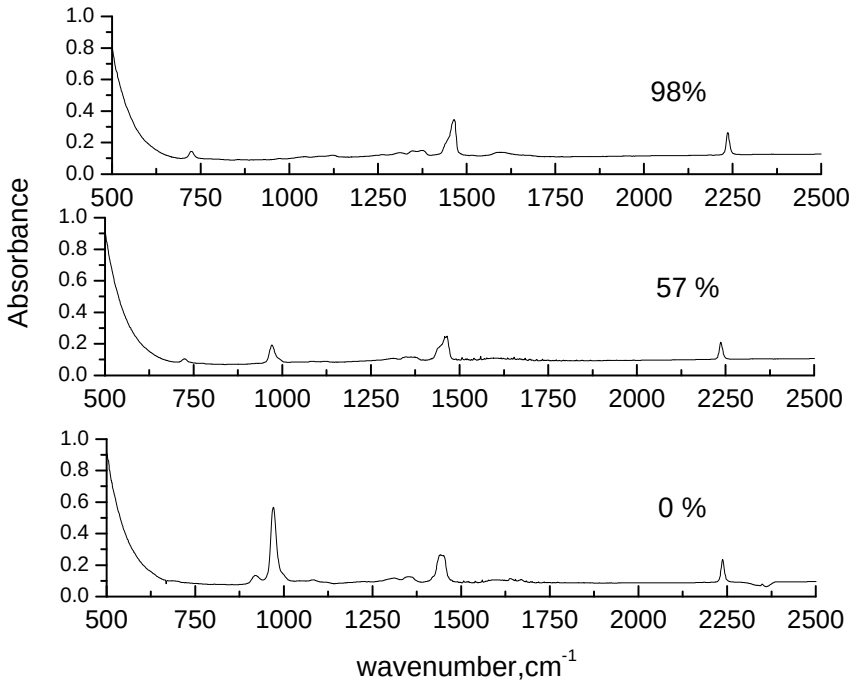

Figure 6. 2 FTIR spectra during hydrogenation process

It is shown that the height of 970 cm^{-1} peak diminishes with an increase in the level of NBR saturation while the height of 2250 cm^{-1} peak remains the same, indicating that the hydrogenation is taking place on -C=C- entity without affecting –CN group which is the source of oil resistance and hardness in the rubber product.

The hydrogenation results from the batch studies are shown in Figure 6.3. It is clearly indicated in this figure that the hydrogenation reaction rate is faster at a higher temperature as expected. A good reproducibility is also confirmed in this figure and the maximum experimental deviation from two different runs is less than 10%. The influence of temperature on hydrogenation behavior also indicates that the hydrogenation behavior at the present operating conditions might not be limited by mass transfer. The previous studies show that hydrogenation rate follows a first order behavior with respect to carbon carbon

double bond concentration. Therefore, a plot of ln (1-HD) versus time was made in order to obtain kinetic constant and the results are shown in Figure 6.4.

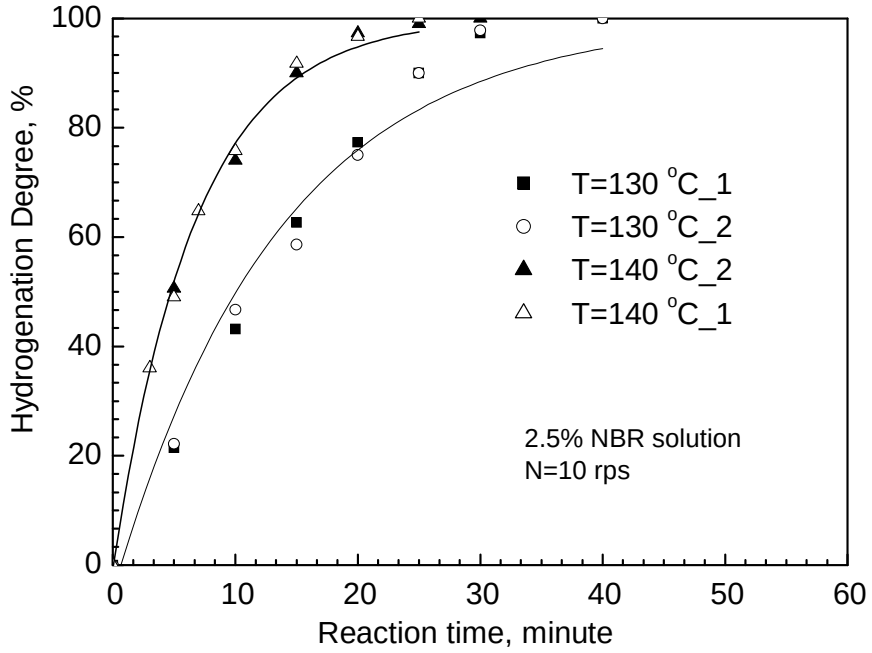

Figure 6. 3 Hydrogenation degree at two different temperatures ([Os]=80 µM and P=350 psig)

From Figure 6.4, it can be seen that the hydrogenation reaction does not follow the first order reaction with the same kinetic constant during the whole period of the reaction. The initial period shows a slower reaction activity presumably due to that the cold liquid catalyst feed brings down the system temperature. Usually several degrees (3 to 5 degrees) were observed immediately after the catalyst was charged into the reaction system. Another possible reason is that it takes sometime for catalyst to contact hydrogen to form active complexes. This observation is not consistent with that found by Parent et al. (1998) using a gas uptake system. In contrast, an initially rapid hydrogenation was observed in their study due to that cis and vinyl isomers are preferentially saturated over trans entity. The phenomenon was shielded by the cold catalyst feed since it only takes place within several minutes after the hydrogenation starts. The small amount of catalyst solid does not influence the temperature of the system. In addition, the catalyst has been contacted with hydrogen gas before entering the reaction system in the solid addition approach. Theretofore, in the continuous experimental procedure, the catalyst solution should be exposed to

hydrogen before it is added to the system. Based on the hydrogenation profile obtained using the solution addition manner, a kinetic constant can not be achieved through the whole period of reaction. However, the last three or four experimental data points which fall in a linear relationship still can be used to get a rate constant by a linear fitting to carry out a comparison with previous study and to provide fundamental data for reactor modeling later on. The resultant kinetic constants, k'(s^{-1}), from a linear regression at a confidence level of 95% are shown in Table 6.2 and a comparison to the data from Parent et al. (1998) is also given.

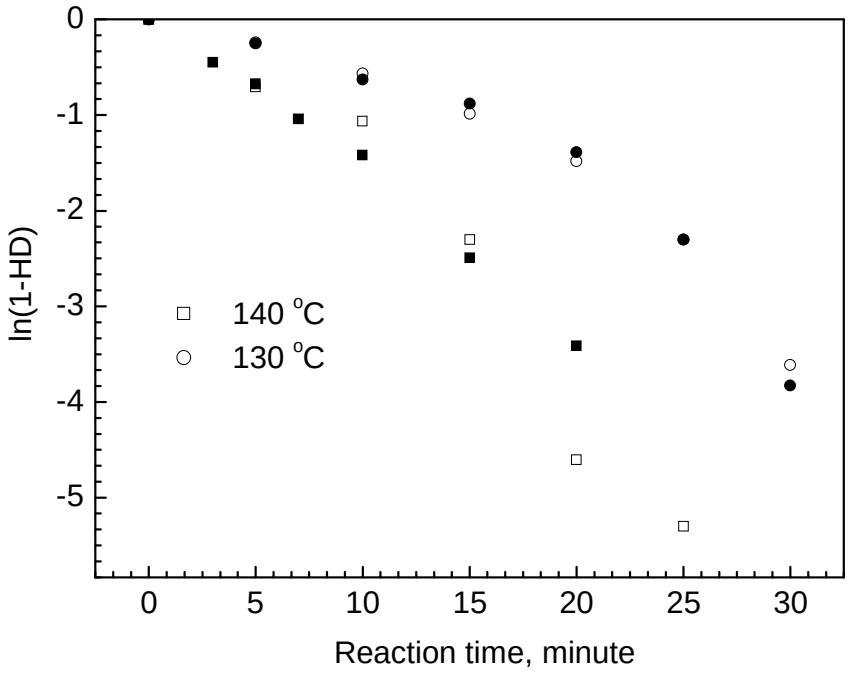

Figure 6. 4 ln(1-HD) versus time

Table 6. 2 Kinetics data

Experimental Run	k', s^{-1}, present study	k', s^{-1}, Parent et al. (1998)
130 °C	$(3.1\pm0.7)\times10^{-3}$	3.57×10^{-3}
140 °C	$(4.6\pm2.1)\times10^{-3}$	----

From the comparison, it can be seen that the reaction activity of the present catalyst is about 88% of that obtained by Parent et al. (1998) in a gas uptake system. If a continuous process is performed at the same conditions(T=130 °C, 80 μM and P= 350 psig), a minimum residence time or reaction time of 16 minutes will be required to achieve a hydrogenation degree of 95% when using the above kinetic constant. However, based on the observed kinetic behavior using the solution addition approach, it takes about 30 minutes to approach the same saturation level. Consequently, without any loss of catalyst activity, a residence time of about 30 minutes should be secured in the continuous runs under the same operating conditions. It can be concluded that the resulting kinetic data provides the foundation of experimental design for the continuous set-up and fundamental data for reactor modeling. According to our numerical study, polymer solution saturated with hydrogen before entering the reactor helps in increasing hydrogenation degree (Zhang et al., 2005c). Therefore, NBR solution should be contacted with hydrogen gas in the pre-heater before it is charged into the reactor.

6.4.2 Hydrogenation Performance Investigation

Using the same batch of catalyst, hydrogenation performance of the designed setup can be examined according to the above-described procedure. Dynamics hydrogenation profile in the MAC can be achieved by periodically monitoring hydrogenation degrees in different stages. A series of experiments were conducted and the system conditions are given in Table 6.3. The hydrogenation degree at the final stage and the gas holdup are also given in this table. The gas holdup was measured by draining polymer products after an experiment. The gas flow rate was set twice of that of liquid flow rate at operating conditions in order to achieve a desirable gas holdup. A mass flow controller was installed to monitor the gas flow rate and the setting was adjusted according to different operating conditions.

In the current experiments, polymer samples were taken every 10 minutes from each stage. Therefore, dynamic profiles of hydrogenation performance at various stages could be obtained. Indicated in Figure 6.5 are the experimental results for Run #1. It is revealed in this figure that hydrogenation degrees increase and approach steady state as the operation proceeds. A maximum hydrogenation conversion of 91% is achieved in the 6^{th} stage. It also should be noted that at the beginning period of the hydrogenation process, a lower hydrogenation degree in later stages compared to the earlier stage is also observed due to that no catalyst is initially deposited in the reactor before the reaction starts and the catalyst concentration in the whole reactor is established gradually from the first stage to the 6^{th} stage.

Table 6. 3 Operation conditions and experimental results

Run #	Liquid flow rate, ml/min	Gas flow rate, ml/min	Os loading, μM	Stirring speed, rpm	T, °C	P, psig	Maximum hydrogenation degree	Gas holdup
1	24	48	80	600	140	350	0.91	0.12
2	24	48	27	750	140	350	0.61	0.12
3	24	48	80	750	140	500	0.98	0.15
4	48	48	30	750	140	500	0.46	0.11
5	48	48	100	750	140	500	0.95	0.14
6*	24	48	140	750	140	500	0.99	0.086
7*	24	48	95	750	140	500	0.85	0.088
8*	48	48	127	750	140	500	0.98	0.085

- 5% NBR solution is used for those runs.

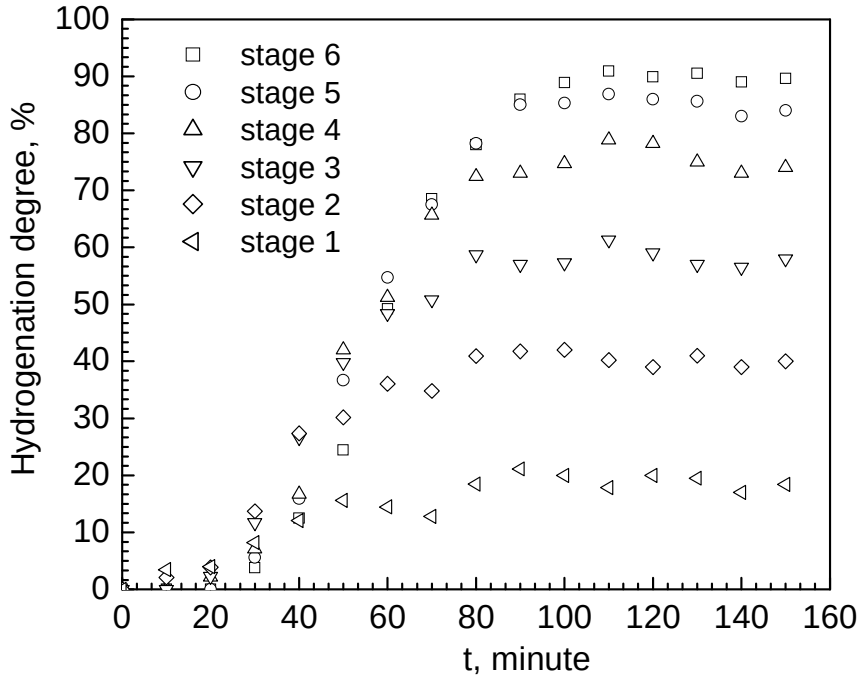

Figure 6. 5 Hydrogenation degree profile in a MAC (Run #1: N=10 rps, T=140 °C, [Os]=80 μM and [C=C]=275 mM, P=350 psig, τ=40 minutes)

From hydrogenation of NBR in a batch reactor as shown in Figure 6.3, the hydrogenation degree could reach 99% after 30 minutes under the same operating conditions. However, the hydrogenation degree at the 6th stage which has a residence time of 40 minutes is about 91%. The lower hydrogenation conversion could be explained that hydrogenation performance in the continuous process is not solely dependent on intrinsic kinetics. Flow behavior of the reactor could also play an important role on the hydrogenation performance of the designed process. For instance, the variation of hydrogen concentrations in different stages which doesn't appear in a batch system could lead to different hydrogenation rates in the continuous process. The temperature gradient through the whole reactor column also could occur because different amounts of heat could be released in different stages. Another possible factor causing the loss of the catalyst activity could be impurity within polymer bulk. The deactivation of the catalyst will be discussed in later section.

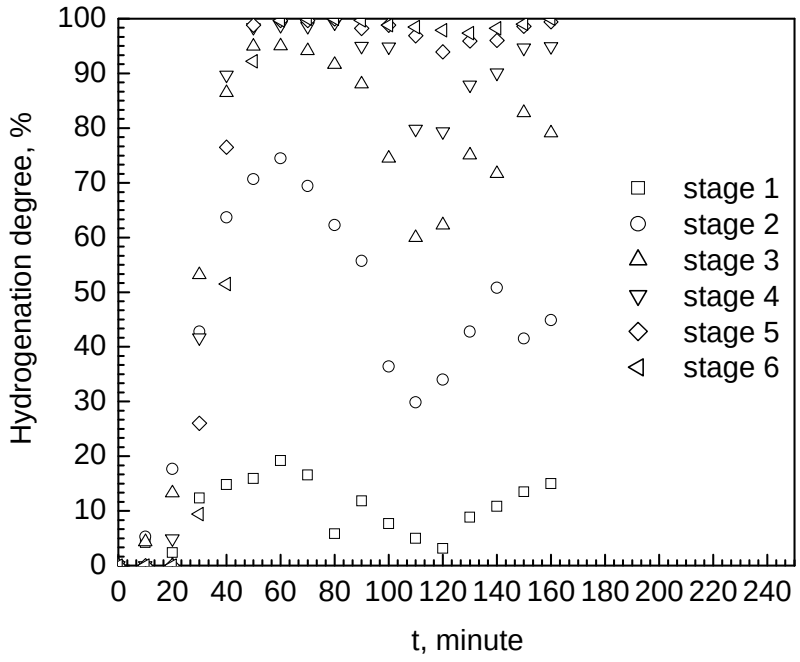

Figure 6. 6 Dynamic hydrogenation degree profile in a MAC (Run#3: N=12.5 rps, T=140 °C, [Os]=80 μM and [C=C]=275 mM, P=500 psig, τ=40 minutes)

As the targeted hydrogenation conversion is 95%, the operation parameters can be adjusted to increase hydrogenation conversion. For example, when the pressure is increased from 350 psig to 500 psig and the stirring speed is increased from 10 rps to 12.5 rps, with other operating parameters being the same as in the previous run, the hydrogenation degree increases to 99% at the 6th stage as shown in Figure 6.6. It can be seen in this figure that the maximum hydrogenation degree at the 6th stage is about 99% at steady state. From this run, the hydrogenation degree reaches 95% even at the 4th stage. Under this circumstance, it is apparent that the last two stages, stage 5 and stage 6, are not necessarily required if a hydrogenation conversion of 95% is only desired. However, under a lower catalyst loading level, a MAC of six stages may not suffice to achieve a high hydrogenation conversion. For instance, in Run #2, when the catalyst loading level decreases to 27 μM with other operating conditions the same as in the previous run, the hydrogenation degree at the 6th stage is only about 60 % as shown in Figure 6.7. In addition, it is found that the gas holdup in Run #2 is 12% while a gas holdup of 15% was obtained in Run# 3. A slight decrease in gas holdup is believed to be caused by a decrease in the system pressure from 500 psig to 350 psig. A higher pressure results in a higher gas density, which favors an increase in gas holdup.

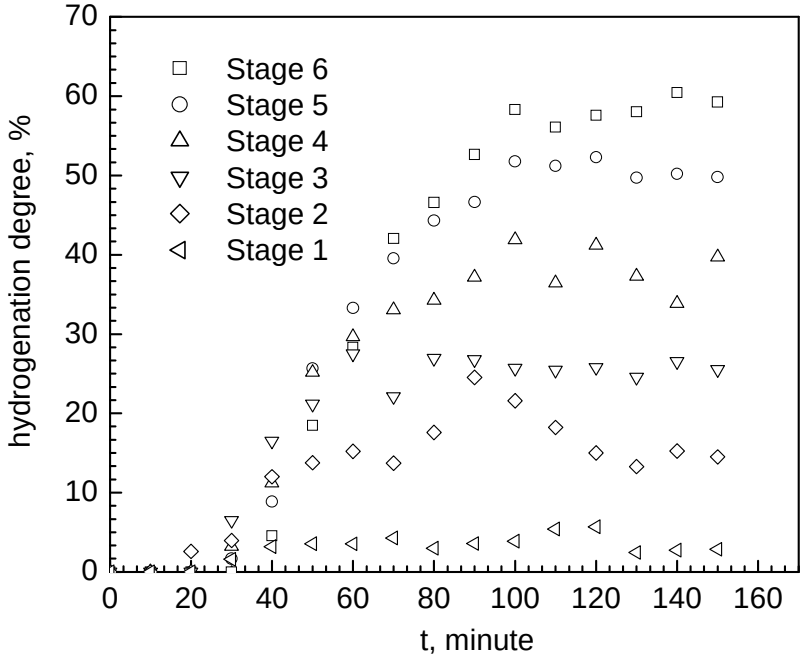

Figure 6. 7 Hydrogenation degree profile in a MAC (Run #2: F=24 ml/min, N=12.5 rps, T=140 °C, [Os]=27 μM and [C=C]=275 mM, P=350 psig, τ=40 minutes)

From both Figure 6.6 and Figure 6.7, some fluctuation is observed due to that the pressure in the system fluctuates during sampling polymer solutions and draining polymer products from the gas liquid separators. However, the phenomena are not observed in later stages and a stable hydrogenation trend still can be obtained.

Another important factor considered here is the liquid flow rate which determines the productivity of the designed process. A higher liquid flow rate is always desirable if the targeted hydrogenation conversion (95%) can be met. In Run #5 as shown in Figure 6.8, a liquid flow rate of 48 ml/min was employed while the gas flow rate still remained the same since the gas holdup is predominately determined by the stirring speed in stirred vessels. Therefore, a residence time of 20.3 minutes resulted. In order to achieve the desired conversion, a higher catalyst loading (100 μM) was also used.

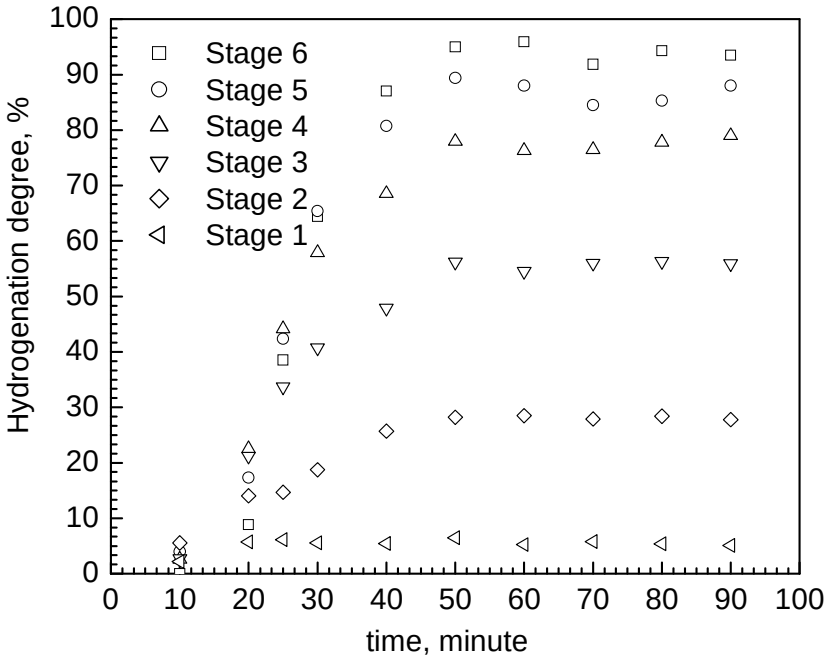

Figure 6. 8 Hydrogenation degree profile in a MAC (Run #5: F=48 ml/min, N=12.5 rps, T=140 °C, [Os]=100 μM and [C=C]=275 mM, P=500 psig, τ=20.3 minutes)

For this experimental run, the maximum conversion at the 6th stage is 95% as demonstrated in Figure 6.8. The steady state is approached at around 50 minutes which is above twice of the residence time and similarly it takes 100 minutes to achieve steady state at a lower liquid flow rate (24 ml/min) indicated in the previous figures.

The capability of handling a polymer solution with a higher concentration in the designed process was also investigated since the productivity of the continuous process not only depends on the liquid flow rate but also the polymer concentration. It has been found that the hydrogenation activity of the osmium catalyst is inversely influenced by the polymer concentration because that the nitrile group remaining within the polymer is reversibly coordinating to the osmium catalyst to form a catalytically inactive complex (Parent et al., 1998). Therefore, when using a higher polymer concentration in a continuous process, a higher catalyst load is required to achieve the desired hydrogenation saturation. In Run #6, 5% NBR in MCB solution and a catalyst concentration of 140 µM was used in order to investigate the reactor performance under higher polymer concentrations. In this case, nitrile concentration increases from 172 mM to 344 mM. The results are shown in Figure 6.9.

The hydrogenation conversion achieved in the sixth stage at steady state is 99% and a conversion degree of 98% is achieved in the fifth stages. At the current operating conditions, a MAC with five stages can realize the desired conversion. Similar to previous runs, it takes 100 minutes (more than two times of a residence time) to reach steady state. A gas holdup of 8.6% is obtained since 5% NBR has a higher viscosity which usually shows a negative effect on gas holdup as discussed in Chapter 4. Another factor attributing to the decrease in gas holdup is that a higher polymer solution consumes more hydrogen gas, leading to less hydrogen accumulated in gas phase under the same gas flow rate. When the catalyst loading decreases from 140 µM to 95 µM with the other conditions being the same to Run# 6, the hydrogenation degree in the 6th stage drops to 85% as indicated in Table 6.3. Similar to 2.5% NBR system, when a higher flow rate (48 ml/min) is used, a higher catalyst loading is required as indicated in Run#8 in order to achieve the desired conversion.

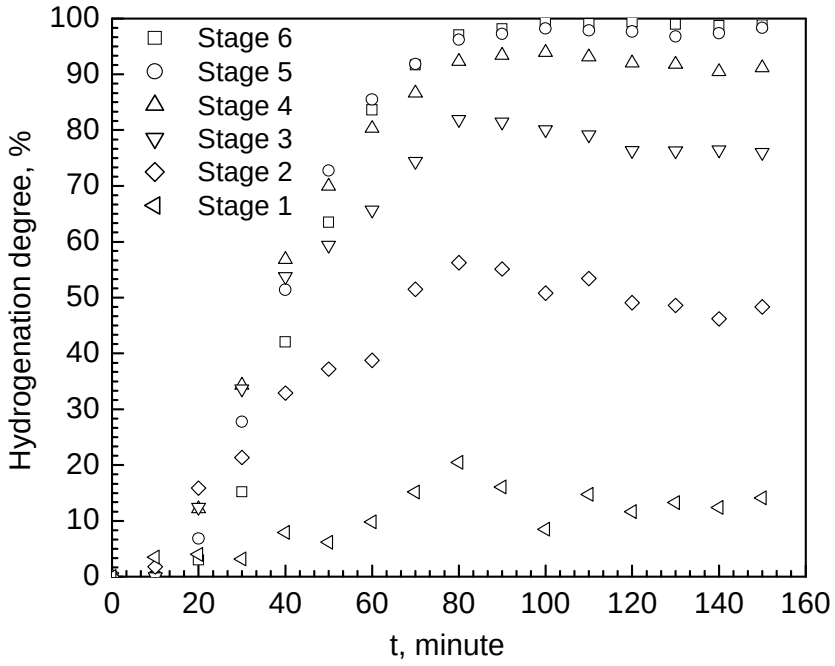

Figure 6. 9 Hydrogenation degree profile in a MAC (Run #6: F=24 ml/min, N=12.5 rps, T=140 °C, [Os]=140 μM and [C=C]=550 mM, P=500 psig, τ=40 minutes)

The primary hydrogenation results have demonstrated that the desired hydrogenation conversion of over 95% can be successfully achieved in the current set-up and operation flexibility also has been exhibited by varying operating parameters. It is apparent that in order to efficiently utilize a MAC to hydrogenate NBR rubber, further work on optimization of operating variables is still required. As demonstrated in experimental results, those influential parameters to be considered include liquid flow rate, gas flow rate, stirring speed, temperature, system pressure as well as the number of stages. The optimization work could wholly reply on an experimental approach. However, intensive experimental loads are sometimes time-consuming and very costly. Therefore, process modeling and numerical simulation will be a cheaper alternative. For this purpose, a comprehensive model is sought to describe the hydrogenation behavior. The development of a reactor model as well as numerical studies will be detailed in the following section.

6.4.3 Reactor Modeling and Numerical Study

In this section, an attempt is made to establish a comprehensive model to predict hydrogenation performance in the designed reactor. In previous chapters, it is evidently shown that the CTB model is more suitable than the AD model to describe the flow behavior in MACs. Thus, the CTB model is employed to characterize the flow behavior in the presence of hydrogenation. Before developing a comprehensive reactor model, the mathematical formulation is based on some assumptions and prior knowledge of intrinsic kinetics. In the liquid phase, three components are considered, NBR polymer, simply represented by [C=C] for carbon carbon double bonds in the liquid phase, mM, [H_2] for hydrogen molecules dissolved in MCB, mM, and osmium catalyst concentration, [Os], μM. In the gas phase, only hydrogen gas is involved. The small amount of MCB vapour in the gas phase is assumed to show a negligible effect on the hydrogenation only taking place in the liquid phase.

When $OsHCl(CO)(O_2)(PCy_3)_2$ is used to hydrogenate NBR, a second order response of kinetic constant, k', to hydrogen concentration and a first order relationship between k' and catalyst loading have been demonstrated by Parent et al. (1998) with the pressure of the system being below 41 bar. Therefore, it can be concluded that the relation of $k' \propto [Os][H_2]^2$ holds at mild operating conditions. The rate of reduction of double bond concentration is proportional to its concentration when the hydrogen pressure is not exceeding 51 bar. In general, at the mild operation conditions, the intrinsic hydrogenation behavior of NBR in the osmium catalyst system can be expressed by the following equation:

$$-r' = \frac{d[C=C]}{dt} = k_1[Os][H_2]^2[C=C] \qquad \textbf{Equation 6. 2}$$

where k_1 is the rate constant, $(M)^{-3}\ s^{-1}$.

Further assumptions have been made in order to describe gas flow behavior.

1. The gas phase is assumed to follow plug flow behaviour between stages since only pure hydrogen is involved and excess amount of hydrogen gas is supplied during the process.
2. Pressure gradient within one stage is very small compared to the system pressure. Therefore, both gas and liquid share the same pressure.
3. Ideal gas law applies at present mild operating conditions (T <140 °C and P< 500 psig).

4. The interfacial mass transfer is described by a thin-film model, which could equivalently describe mass transfer between phases compared other models, such as penetration model and surface renewal model.
5. No spatial distribution of liquid concentration and temperature occurs within one stage under ideally mixed conditions.

Therefore, a schematic description of reactive gas liquid flow in the designed MAC could be illustrated as follows:

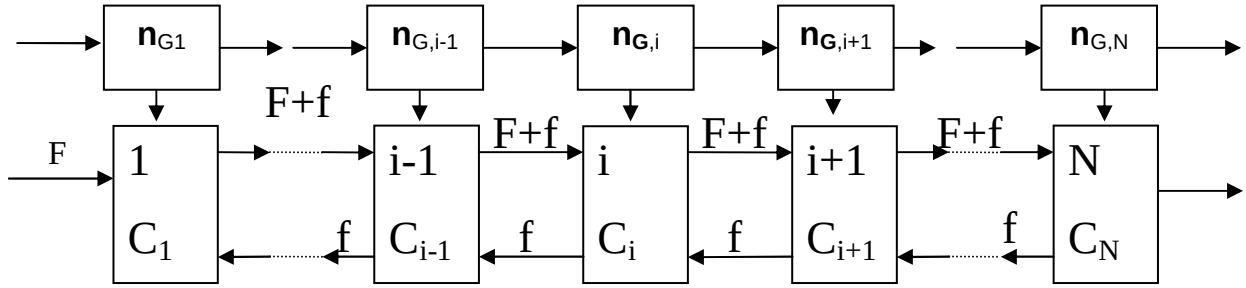

Figure 6. 10 Reactor model

In the schematic description of the reactor model, the volumetric forward liquid flow, F, m^3/s, and back flow rate, f, m^3/s, are assumed to be constant since the liquid density does not vary with change in the saturation degree of polymer. For the i^{th} stage, the mass conservation of [C=C] in the liquid phase can be expressed as follows:

$$\frac{d(\varepsilon_{L,i}V[C=C]_i)}{dt} = (F+f)([C=C]_{i-1} - [C=C]_i) + f([C=C]_{i+1} - [C=C]_i) \quad - r'\varepsilon_{L,i}V$$

Equation 6. 3

and conservation of the hydrogenation concentration in the liquid phase can be expressed as:

$$\frac{d(\varepsilon_{L,i}V\,[H_2]_i)}{dt} =$$
$$(F+f)([H_2]_{i-1} - [H_2]_i) + f([H_2]_{i+1} - [H_2]_i) \quad - r'\varepsilon_{L,i}V + k_L a\varepsilon_{L,i}V([H_2]^* - [H_2]_i)$$

Equation 6. 4

The mass conservation for the gas phase is:

$$\frac{dn_{G,i}}{dt} = -k_L a([H_2]^* - [H_2]_i) + \frac{F(n_{G,i-1} - n_{G,i})}{\varepsilon_{L,i} V} \qquad \textbf{Equation 6. 5}$$

where n_{Gi} is the number of moles of hydrogen in the unit liquid volume of the i^{th} stage, mole/liter liquid volume. $[H_2]^*$ is the equailibrium hydrogenation concentration, mM. It is assumed that the ideal gas law can be applied to the gas phase, a mean bubble diameter is used to characterize the bubble size, and the pressure change inside the bubble can be neglected. The interfacial surface area can be evaluated by the following equation.

$$a = \frac{6\varepsilon_G}{d_B} = \frac{6(1-\varepsilon_L)}{d_B} \qquad \textbf{Equation 6. 6}$$

where d_B is the diameter of hydrogen bubble, m. Then, the above equation can be rewritten as follows.

$$\frac{d(\varepsilon_{L,i}[H_2]_i)}{dt} =$$

$$\frac{(F+f)}{V}([H_2]_{i-1} - [H_2]_i) + \frac{f}{V}([H_2]_{i+1} - [H_2]_i) \; - r'\varepsilon_{L,i} + k_L \frac{6(1-\varepsilon_{L,i})\varepsilon_{L,i}}{d_B}([H_2]^* - [H_2]_i)$$

Equation 6. 7

Mass conservation of catalyst concentration in the i^{th} stage can be given by

$$\frac{d(\varepsilon_{L,i}[Os]_i)}{dt} = \frac{(F+f)}{V}([Os]_{i-1} - [Os]_i) + \frac{f}{V}([Os]_{i+1} - [Os]_i) \qquad \textbf{Equation 6. 8}$$

When the ideal gas law is applied, Equation 6.4 can be expressed as

$$\frac{d\varepsilon_{L,i}}{dt} = k_L \frac{6P\varepsilon_{L,i}(1-\varepsilon_{L,i})}{d_B RT}([H_2]^* - [H_2]_i) + \frac{F(\varepsilon_{L,i-1} - \varepsilon_{L,i})}{V} \qquad \textbf{Equation 6. 9}$$

The dynamic performance of the designed reactor is determined by the above set of ordinary differential equations (ODEs) with given initial conditions. The established equations can be solved by a fourth order Runge-Kutta method implemented in MATLAB. Before solving these equations, the parameters involved should be identified according to the experimental conditions. The values of those parameters are

indicated in Table 6.4. Some unknown parameters are estimated from corresponding empirical correlations. The bubble size was not measured in the present study. However, it can be predicted by the approach described in Chapter 3 and Chapter 4. Another parameter to be determined is liquid mass transfer coefficient, k_L, m/s. The following equation can be used to predict mass transfer coefficient (Calderbank, 1958).

$$k_L = 0.42\left(\frac{\mu g}{\rho_L}\right)^{1/3}\left(\frac{D_L \rho_L}{\mu}\right)^{0.5} \qquad \textbf{Equation 6. 10}$$

where D_L is the molecular diffusivity, m^2/s and $D_L=2\times10^{-8}$ m^2/s was a typical value for gas molecules. All other polymer physical properties can be estimated from the correlations proposed by Pan and Rempel (2004).

When using the established model to predict hydrogenation behavior in a 5% NBR solution, the rate constant should be adjusted according to the inverse effect of nitrile group on catalytic activity. Based on the kinetic data presented by Parent et al. (1998), the hydrogenation rate constant is proportional to $[CN]^{-1.4}$. Therefore, the corresponding factor is taken into account when simulating a higher polymer concentration.

For the numerical simulation, a MATLAB program is provided in Appendix F. When using the original experimental osmium loading, it is found that the CTB model generally overestimates the hydrogenation conversion as shown in Figure 6.11.

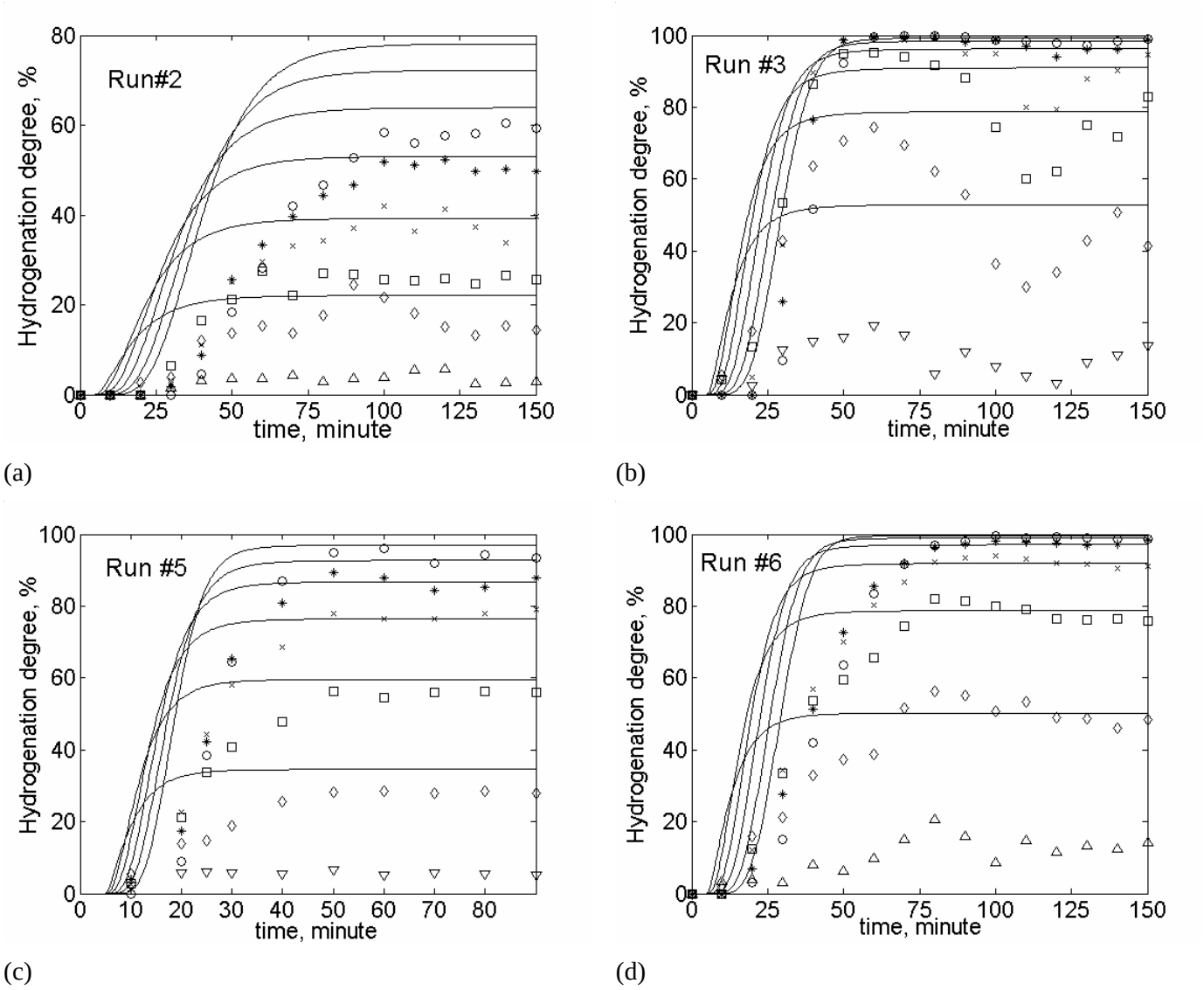

Figure 6. 11 Prediction of the CTB model without catalyst adjustment (solid line: model prediction; symbol: experimental data)

In particular, it overestimates the hydrogenation behavior in the earlier stages, which is partly due to a lower temperature in the earlier stages, especially, the first stage. In general, a temperature of 5 to 10 degrees lower in the first stage was observed during the hydrogenation process. A representative temperature profile is provided in Appendix G. Another reason can be the catalyst deactivation. In the previous setup, it has been found that almost half of the osmium catalyst was sacrificed because of oxygen contamination (Kehl, 1998). Therefore, in order to improve prediction, the effect of temperature gradient

on the hydrogenation rate is taken into account and an equivalent amount of osmium catalyst is used in the model instead of the original osmium concentration. The equivalent amount of osmium catalyst in all experimental runs is also given in Table 6.4.

Table 6. 4 Parameters involved in the simulations

Experimental Run #1	Experimental Os loading, μM	$[H_2]$, mM	Back flow rate, ml/min	Mass transfer, k_L, m/s	Equivalent Os loading, μM
1	80	110	6.8	0.001	52
2	27	110	6.8	0.001	16
3	80	140	6.8	0.001	56
4	30	140	3.8	0.001	15
5	100	140	3.8	0.001	78
6	145	140	4.8	0.0008	110
7	95	140	4.8	0.0008	56
8	127	140	2.5	0.0008	100

After the catalyst adjustment, the prediction of hydrogenation profile by the CTB model is improved as can be seen in shown in Figure 6.12. The dynamic trend under various operating conditions can be captured by the established model with consideration of temperature fluctuation and catalyst activity loss due to impurity within the rubber bulk and oxygen contamination. The model prediction also shows that the earlier stages approach steady state earlier than the later stages.

The osmium catalyst loss in a continuous fixed bed was discussed by Kehl (1998). From the same rubber concentration, the percentage of catalyst deactivated varies. At a higher catalyst loading level, the effective percentage of the catalyst is higher. For instance, in Run#1 and Run#3, the osmium concentration is 80 μM. The percentages of catalyst loss for Run #1 and Run #3 are 35% and 30%, respectively. It seems that a high pressure system protects the catalyst activity. However, a further conclusion can be only drawn from a large amount of experimental data. In experiments Run #2 and Run #4, the percentages of the catalyst loss for those runs are 40.7% and 50%. The observation is reasonable if the amount of catalyst sacrificed for impurities with a certain polymer concentration level is fixed. However, the exact amount of catalyst loss due to impurity can not be evaluated from the current experimental data. In a 5% NBR solution, the amount of osmium lost is higher when compared to 2.5% NBR solution. For example, in Run

#5 and Run #7, a similar catalyst loading level is used with different polymer concentrations. The percentage of 22% and 41% catalyst loss is observed for Run#5 and Run #7, respectively.

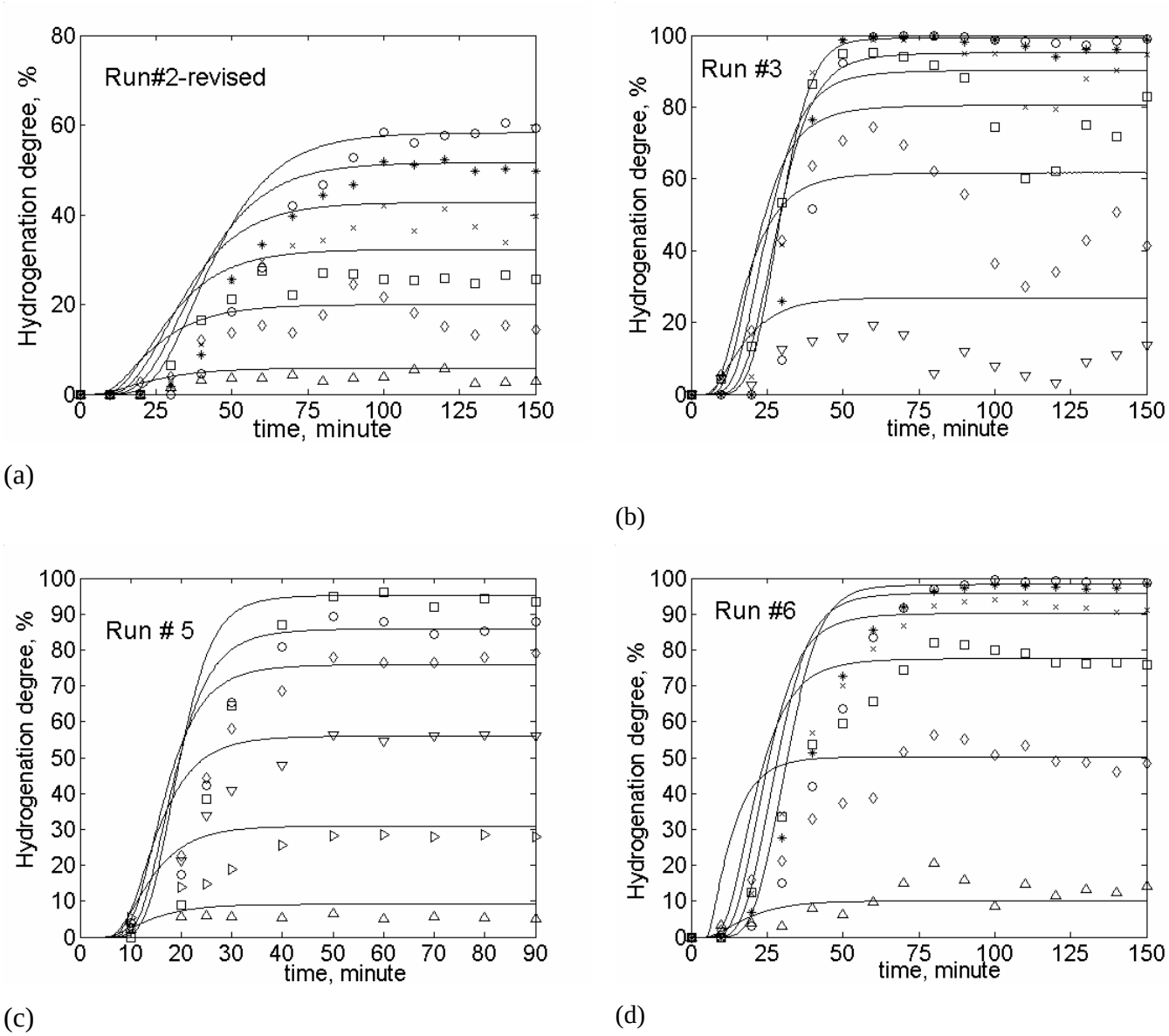

Figure 6. 12 Comparison of hydrogenation degree predicted by the CTB model with experimental data with catalyst adjustment (solid line: model prediction; symbol: experimental data)

More impurities are expected to exist in a solution with a higher polymer concentration. A threshold of the catalyst concentration has not been observed in the current operation. However, even at a low catalyst loading level (30 µM), the catalyst still shows a reasonable activity (hydrogenation conversion of 61% is obtained) while in the fixed bed a threshold catalyst level was as high as 30 µM (Kehl, 1998). The improvement in the present set up can be due to a better oxygen-stripping technique applied. In the current operation procedure, the polymer solution is prepared in a stirred vessel under aeration of nitrogen gas. Less amount of oxygen remains in the polymer solution. Therefore, efforts are still required to reduce oxygen residues within the rubber solution to improve catalyst activity and the contribution of impurities to catalyst loss should be singled out by an experimental approach. Nevertheless, it can be recommended that 20% to 50% percentage more catalyst will be added to the system in order to achieve a desired hydrogenation level based on the deactivation analysis.

From the established model, the liquid phase holdup profile could be predicted and a typical holdup distribution in various stages at Run#1 conditions is given in Figure 6.13.

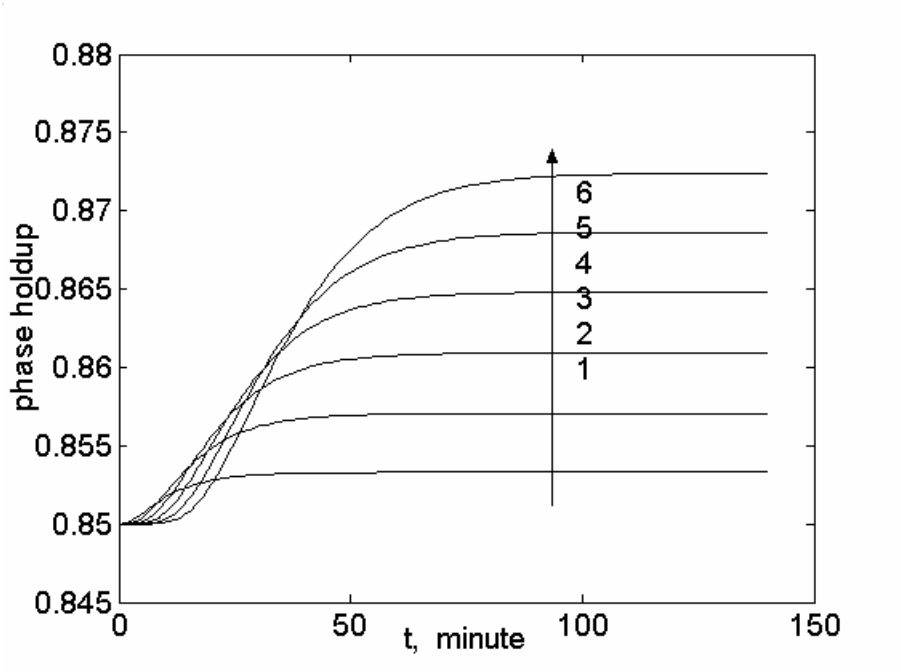

Figure 6. 13 Liquid holdup profile predicted by the model

(Run#1: [C=C]=275 mM, [Os]=80 µM, P=350 psig and T=140 °C)

It is indicated in Figure 6.13 that at steady state the liquid phase holdup is higher in later stages due to that more and more hydrogen gas is consumed along with the progress of the hydrogenation process. It can be predicted that hydrogen concentration is higher in later stages as shown in Figure 6.14 since less hydrogen is consumed owing to a slower hydrogenation rate.

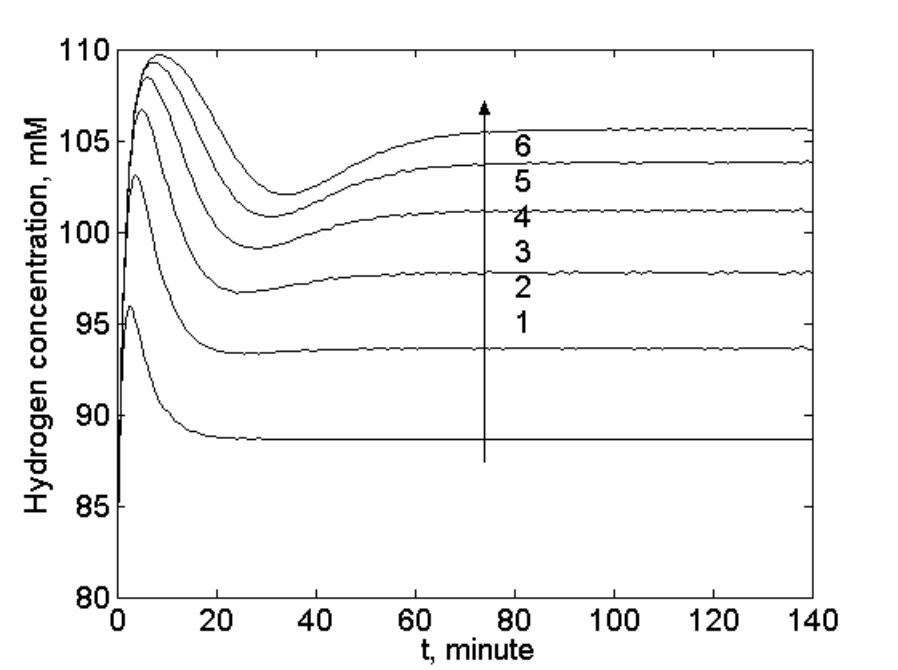

Figure 6. 14 Hydrogen concentration profile predicted by the established model

(Run #1: [C=C]=275 mM, [Os]=80 μM, P=350 psig and T=140 °C)

Since osmium catalyst is not charged in the reactor before the process, the dynamic catalyst concentration can be viewed in Figure 6.15. The osmium concentrations in different stages are gradually built up and approach the same level since it is assumed that the catalyst is neither produced nor consumed by the reaction.

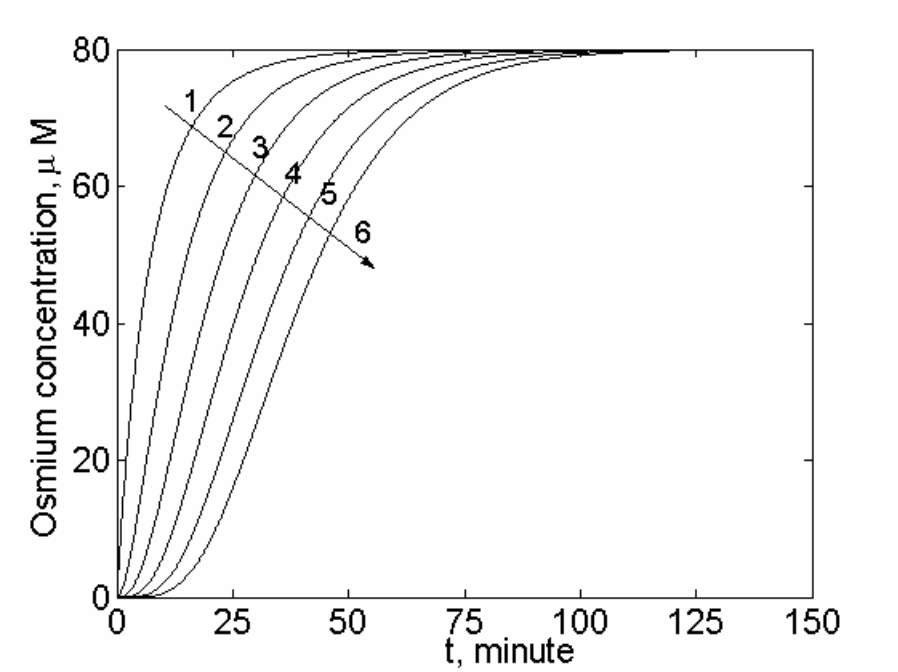

Figure 6. 15 Osmium catalyst in various stages predicted by the established model

(Run #1: [C=C]=275 mM, [Os]=80 μM, P=350 psig and T=140 °C)

The numerical simulations have been conducted without consideration of a possible enhancement effect of hydrogenation reaction on gas liquid mass transfer. Using a thin-film theory, the hydrogenation could solely take place within the liquid bulk or liquid film, depending on the reaction regimes the process falls in. Hatta number is usually employed to characterize the reaction regime (Danckwerts, 1970). The expression for Hatta number varies according to different reaction system. When the hydrogenation process in the present study is considered, the reaction rate possesses a second order reaction with respect to hydrogen concentration. Therefore, a modified Hatta number could be used as follows:

$$Ha = \frac{\sqrt{k_1[Os][H_2][C=C]D_L}}{k_L} \qquad \textbf{Equation 6. 11}$$

when Hatta >3, the hydrogenation rate is termed as a fast reaction with respect to mass transfer rate of hydrogen while the reaction rate is termed as a slow reaction with respect to mass transfer rate when Hatta<0.3 (Dankwerts, 1970). It also can be seen that the value of Hatta number varied during the hydrogenation process in a dynamic process. Hence, under the operating condition (T=140 °C, P=500 psig,

[C=C]=275 mM, [Os]=80 μM, $D_L=2.0\times10^{-8}$ m^2/s and $k_L=0.001$ m/s), a dynamic profile of Hatta number could be obtained through numerical simulation. The results are shown in Figure 6.16.

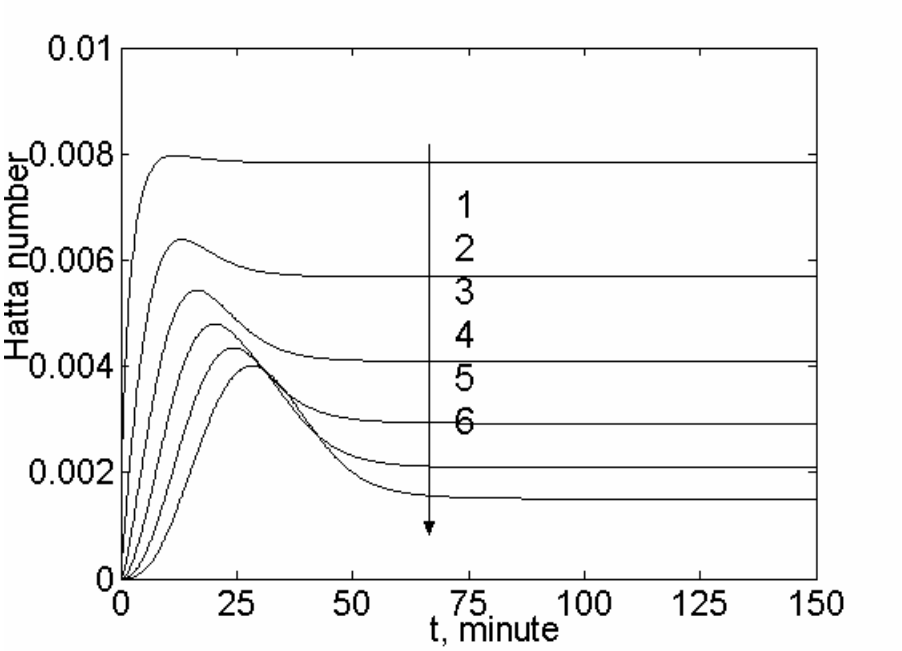

Figure 6. 16 Dynamic profile of Hatta number during the hydrogenation process in the MAC ([C=C]=275 mM, [Os]=80 μM, P=350 psig and T=140 °C)

From Figure 6.16, it can be seen that Hatta number is always less than 0.01 under the investigated conditions, indicating that the process is taking place in the liquid bulk. Hatta number increases from zero since no catalyst is initially charged to the system and no hydrogenation occurs at t=0. The values of Hatta number gradually increases due to that both $[H_2]$ and [Os] increase when the hydrogenation process proceeds as indicated in Figure 6.14 and Figure 6.15. The values of Hatta number at the later stages are smaller than the earlier stages because the amount of unsaturated carbon carbon double bonds available for hydrogenation decreases, resulting in a slower hydrogenation rate. When a limiting case is considered, a polymer concentration is increased three folds and a low pressure is used. Meanwhile, a residence time decreases from 40 minutes to 20 minutes. The dynamic profile for Hatta number is shown in Figure 6.17. The values of Hatta number at various stages are still less than 0.3, indicating that the hydrogenation reaction rate is slow compared to mass transfer rate from the gas phase to the liquid phase. Therefore, at the current operating conditions, the process is most likely under slow reaction regime and the mass

transfer rate is not enhanced by the hydrogenation rate. The mass transfer component in Equation 6.4 could be used without considering enhancement effect of hydrogenation on mass transfer.

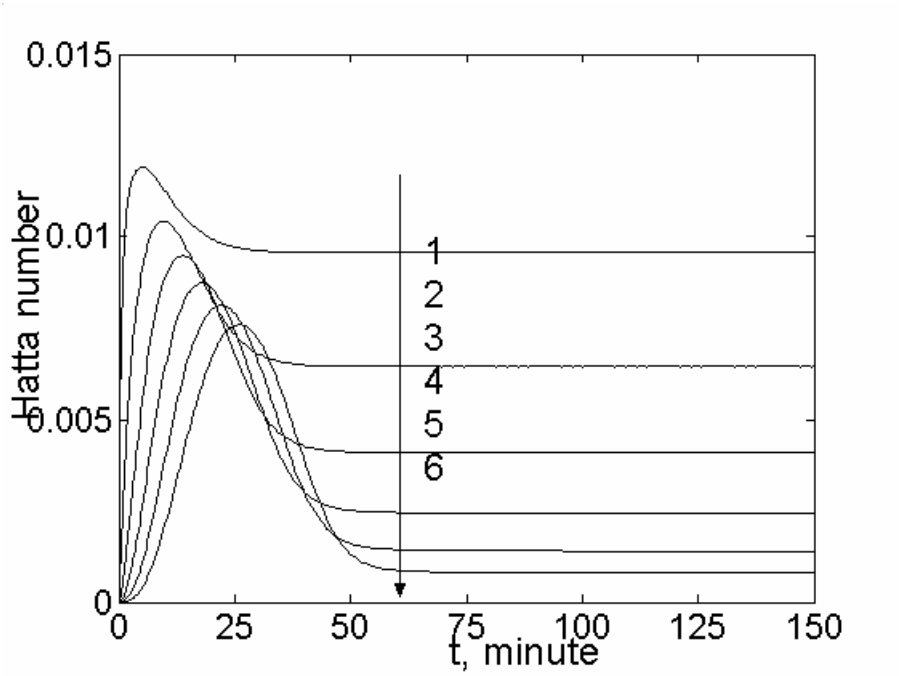

Figure 6. 17 Dynamic profile of Hatta number during the hydrogenation process in the MAC ([C=C]=750 mM, [Os]=180 μM, τ=20 minutes, P=350 psig and T=140 °C)

6.4.4 Hydrogenation Performance Analysis

Based on the established model, the effects of operating variables on hydrogenation performance can be appreciated based on the established model. Dimensionless parameters are usually informative and those dimensionless parameters include polymer loading level, β, back flow ratio, α, mass transfer coefficient, ξ, and dimensionless residence time, θ_τ.

$$\beta = \frac{[C=C]_0}{[H_2]^*} \qquad \textbf{Equation 6. 12}$$

$$\theta_\tau = k_1[Os][H_2]^{*2}\tau \qquad \textbf{Equation 6. 13}$$

$$\xi = \frac{k_L a}{k_1[Os][H_2]^*[C=C]_0}$$ **Equation 6. 14**

where τ is the residence time in the reactor, second. The effects of operating parameters on hydrogenation behavior could be appreciated through the numerical simulations from the established model as shown in Figure 6.18.

From Figure 6.18(a), it can be seen that the hydrogenation conversion is considerably influenced by the residence time as expected. The dimensionless residence time, θ_τ, should be about 6 when a hydrogenation conversion of 95% is desired. According to the intrinsic kinetic behavior (a 1st order rate with respect to [C=C]), it is reasonable to observe that polymer loading level shows a marginal impact on the hydrogenation conversion after considering the coordinating effect of nitrile group to the active metal center as indicated in this figure. All simulation data points appear to overlap each other even at different polymer loading levels in Figure 6.18 (a). The similar phenomena can be found from Figure 6.18(c) which shows effects of mass transfer at various polymer loading levels. The mass transfer favors to increase hydrogenation conversion since a sufficient amount of hydrogen is provided, leading to a higher hydrogenation rate. However, a further increase in mass transfer doesn't help to increase hydrogenation saturation any more because the process is totally under reaction control. The negative influence of liquid backmixing on hydrogenation conversion is shown in Figure 6.18(b). A high level of liquid backmixing tends to reduce the reactor efficiency. Theoretically, the performance of a MAC will approach that of a CSTR with the same reactor volume when the liquid backmixing between consecutive stages becomes infinity. On the contrary, the hydrogenation performance of a MAC will be the same as that of six CSTRs in series when the liquid backmixing between stages is zero, which is expected to be the best scenario of usage of MACs. The effect of MACs with different numbers of stages is show in Figure 6.18(d). It is clearly indicated in this figure that a MAC with a larger number of stages provided a higher hydrogenation degree under the same operation conditions. However, a further increase in the number of stages does not provide a further improvement in terms of hydrogenation conversion. For example, a hydrogenation degree increases from 0.90 at a MAC of 6 stages to 0.93 in a MAC of 9 stages while the hydrogenation conversion is only 0.66 in a MAC of 3 stages.

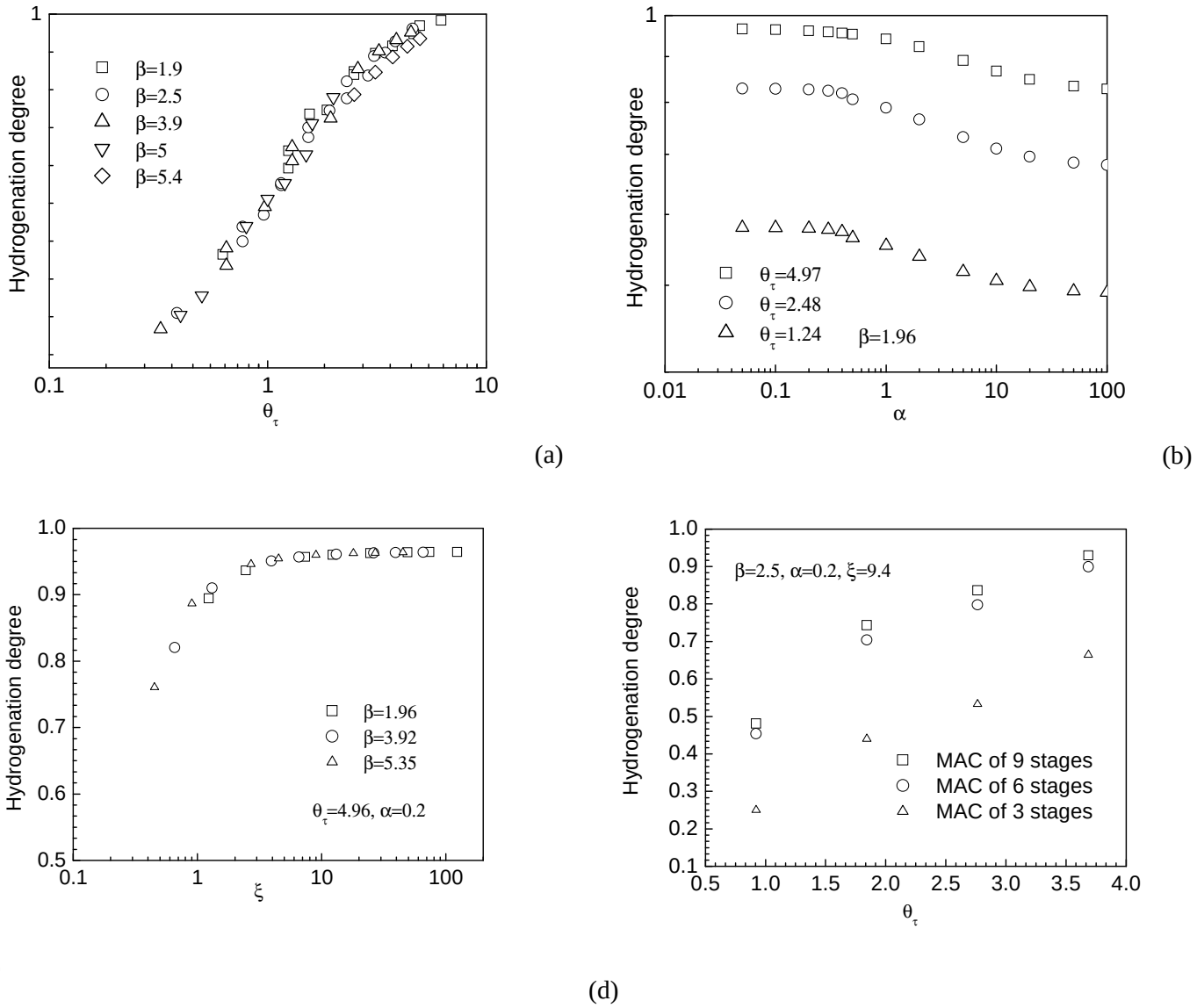

Figure 6. 18 Effects of operation parameters on hydrogenation performance ((a): effect of residence time; (b): effect of backmixing; (c): effect of mass transfer ;(d): effect of MACs with different stages)

From the above analysis, it can be concluded that the hydrogenation performance in a MAC is determined by dimensionless residence time, mass transfer and backmixing whereas dimensionless polymer loading does not play a role since the hydrogenation process possesses a first order with respect to polymer concentration. Although a comprehensive model has been established to predict the dynamic

hydrogenation profile, a convenient way of prediction hydrogenation performance in MACs is still required. In view of this, an attempt is made to identify a relation between operating parameters and hydrogenation performance at steady state. Previous studies on liquid backmixing in Chapter 3 and Chapter 4 show that when a back flow ratio increase, the stage efficiency decreases. In other words, the equivalent number of CSTRs decreases with an increase in the back flow ratio if n CSTRs-in-series model is applied. The direct link between a back flow ratio and stage efficiency can be determined by Equation 3.18. In addition, the equivalent number of CSTRs can be evaluated by the following equation if a normalized variance, σ_θ^2, is given.

$$n = \frac{1}{\sigma_\theta^{\,2}} \qquad \textbf{Equation 6. 15}$$

where n is the equivalent number of CSTRs. Therefore, the expression of hydrogenation conversion can be derived according to n CSTRs-in-series model without mass transfer limitation.

$$1 - HD = \frac{1}{(1 + \frac{\theta_\tau}{n})^n} \qquad \textbf{Equation 6. 16}$$

where HD represents hydrogenation degree. The above equation is only valid to a condition that there is no mass transfer resistance between two phases. As demonstrated in Figure 6.18(c), mass transfer can considerably influence the hydrogenation conversion. Hence, Equation 6.16 has to be modified before it is applied to situations where there is mass transfer resistance between the gas phase and the liquid phase. A revised equation is proposed to predict hydrogenation conversion as follows:

$$1 - HD = \frac{1}{(1 + (\frac{\xi}{1+\xi})\frac{\theta_\tau}{n})^n} \qquad \textbf{Equation 6. 17}$$

The factor, $\frac{\xi}{1+\xi}$, is introduced to account for mass transfer effect. It can be seen that if there is no mass transfer, HD will be zero and when ξ approaches infinity, the maximum hydrogenation conversion will the same as indicated in Equation 6.16.

A comparison of the prediction of the proposed model and the simulation results is conducted and the results are shown in Figure 6.19. In this figure, a comparison of the model prediction with experimental data is also presented. A resulting small MARR of about 3% indicates that the prediction from the proposed model agrees well with the results from the comprehensive model. The comparison of experimental data is also conducted as shown in this figure. It can be seen that the proposed approach is convenient for prediction of the hydrogenation conversion and equivalently accurate to the comprehensive model at steady state. Another advantage compared to the comprehensive model is that the number of stages is built in Equation 3.18. However, the dynamic feature of the designed reactor can only be captured by the comprehensive model. The dynamic information is very important for the process start up.

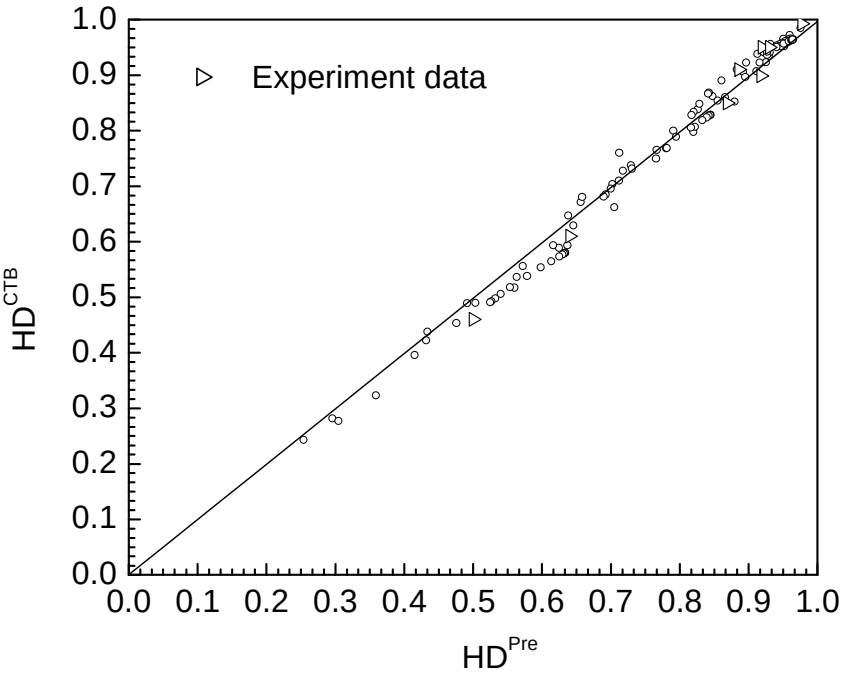

Figure 6. 19 Comparison of hydrogenation conversion predicted from the proposed model

From the experimental study and the numerical simulations, a thorough knowledge of hydrogenation performance of this reactor has been achieved, which enables us to design and operate such a promising reactor with any scale totally under a high level of confidence. A design of a continuous process at a pilot scale can be readily carried out and the more detailed information will be presented in Chapter 7.

6.5 Concluding Remarks

In this chapter, development of a continuous process for hydrogenating nitrile butadiene rubber is illustrated. Hydrogenation in a batch reactor demonstrated a different behavior from the previous studies due to that a solution addition method was utilized rather than charging the catalyst in solid form. A hydrogenation degree above 95% in two different polymer solutions, 2.5% and 5% NBR solutions, can be successfully obtained at a suitable set of operation conditions. In a 2.5% NBR solution, a minimum of 80 μM osmium loading is required in order to achieve a desired hydrogenation conversion over 95% at a residence time of 40 minutes. On the contrary, a minimum of 100 μM osmium is needed for a residence time of 20 minutes. In a 5% NBR solution, a minimum of 100 μM osmium is required for a residence time of 40 minutes while a minimum of 120 μM is sought for a residence time of 20 minutes at the same pressure and temperature conditions. The designed system also exhibits operation flexibility when varying operating conditions. A higher pressure system and higher [Os] helped in increasing hydrogenation degree as well as higher loading level of osmium catalysts. The catalyst loss in the continuous set up was discussed based on the current experimental data. It is recommended that 30% to 50% more catalyst than the designed level is required to achieve the same hydrogenation efficiency. A comprehensive model is established by coupling the reactor flow behavior and intrinsic hydrogenation reaction. The hydrogenation conversion predicted by the established model agrees quite well with the experimental data by taking into account the catalyst loss due to impurities within the rubber bulk and oxygen contamination. A revised model of n CSTRs in series is proposed to predict hydrogenation conversion at steady state. A good agreement has been obtained when comparing the hydrogenation degree predicted from the proposed model to experimental data.

Chapter 7 Pilot Design of a Continuous Process for Hydrogenation of NBR

In Chapter 6, hydrogenation efficiency has been investigated on the designed continuous unit. The primary hydrogenation results indicate that the designed process can successfully achieve the desired hydrogenation saturation. However, in order to scale up the present process for industrial application, studies on a pilot scale are necessary. Therefore, a pilot design of a continuous process for hydrogenation of NBR is presented in this chapter.

A pilot scale design has to meet the following requirements. The primary requirement of the pilot scale process is similar to that in the bench scale unit. A hydrogenation degree of 95% in the final products must be provided, which ensures the physical properties desired for their final applications. Secondly, a process with a productivity of 50 tons/year is targeted for a pilot scale set up. Lastly, an optimal gas liquid reactor with superior mass transfer and heat transfer and high stage efficiency is preferred.

Regarding a mandatory hydrogenation degree of 95% for a pilot scale process, generally a residence time of 20 to 40 minutes for liquid reactants depending on catalyst loading level and mass transfer capability should be maintained based on the previous studies on the bench scale setup. The polymer solution concentration can vary from 2.5% to 20% depending on operating variables applied such as temperature, pressure and catalyst loading level. However, a polymer solution with a low polymer concentration is preferred due to the significant power input for high viscosity solutions during material transportation and mechanical agitation inside the stirred vessel.

7.1 Reactor Design for a Pilot Scale Set-up

A polymer solution flow rate can be estimated from the productivity required. Assuming that the designed process is operating 2/3 (usually 300-330 days) of a whole year period, the daily productivity is about 180 kg HNBR/ day. It has been demonstrated that a residence time of 40 minutes for liquid reactants is required to provide a hydrogenation degree over 95% in chapter 6. When a polymer solution of 5% is considered, a gas liquid reactor with a minimal volume of 120 liters is sought to accomplish the targeted productivity. Such a reactor could have various numbers of stages based on the diameter of the reactor. According to the previous simulation, a MAC with a large number of stages presents a higher hydrogenation degree. However, when the number of stages is exceeding 9, no further benefit has been observed in terms of hydrogenation performance (Zhang et al., 2005c). Therefore, a MAC of 9 stages would suffice to provide such a production capacity. If a MAC of 9 stages is applied, a diameter of 0.257

m is required to present a reactor volume of 120 L when the height of each stage is equal to its diameter. Similarly, a diameter of an impeller is equal to half of the diameter of the reactor. The impeller will be located at center of each stage. The horizontal baffles are still required to mitigate backmixing between stages in order to obtain high reactor stage efficiency. The central access between consecutive stages remains 5% of the cross sectional area to maintain low back flow rate and high stage efficiency.

7.2 Process Conditions at a Pilot Scale

Based on the designed reactor, a 5% polymer solution flow rate will be 3L/minute in order to attain a residence time of 40 minutes in the designed reactor at a temperature of 140 ^{0}C and a pressure of 500 psig. The gas flow rate/polymer solution flow rate ratio is usually maintained at 1 to 5 according to the previous studies. Therefore, hydrogen gas flow rate can vary from 3L/minute to 15L/minute, depending on other operating parameters such as temperature, pressure and stirring speed. A suitable stirring speed should be applied to provide superior mass transfer and heat transfer. When carrying out scale-up process, many approaches have been applied such as geometry similarity, the same Reynolds number and the same unit power input, etc. Amongst those approaches, the same unit power input has been mostly employed since the power input usually determines mass transfer, heat transfer and mixing characteristics in stirring vessels. Therefore, the operating conditions at a pilot scale could be determined from the results from the bench scale set-up. As illustrated in chapter 3 and chapter 4, the power input under aeration conditions could be evaluated from the empirical correlations although a direct measurement of power input is not available in this work. The power input per unit volume in the bench scale is ranging from 40W/m^3 to 200 W/m^3 under the investigated conditions. Therefore, the desired stirring speed at a pilot scale will be from 5 to 10 rps.

7.3 Hydrogenation Estimation at a Pilot Scale

The hydrogenation behavior of the designed pilot scale set-up could be previewed based on the established CTB model. According to the above proposed operating conditions, the hydrogenation dynamics performance at the designed pilot scale is shown in Figure 7.1. The estimated maximum hydrogenation degree at the 9th stage is 95.5%, which is a desired conversion for the final products.

Table 7. 1 Operation conditions for a pilot scale process

Liquid flow rate, L/min	3
Gas flow rate, L/min	6
Stirring speed, rps	8
Catalyst loading *, μM	104
Polymer solution, mM	550
Temperature, ^{o}C	140
Pressure, psig	500

* Desired active catalyst loading level is 80 μM, 30% more added to account for deactivation.

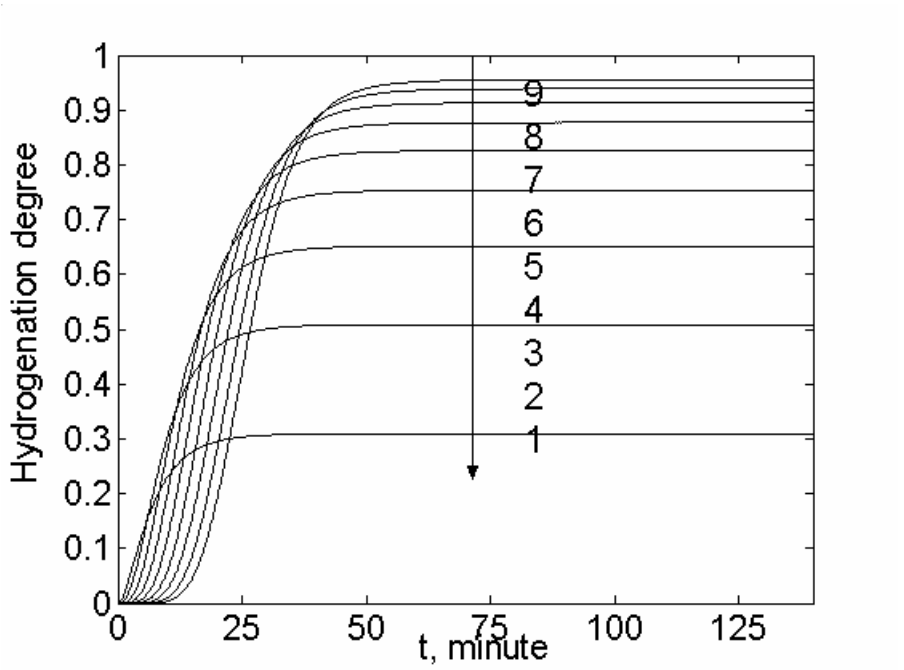

Figure 7. 1 Hydrogenation profile in a MAC of nine stages at a pilot scale

(T=140 °C, [C=C]=550 mM, P=500 psig, [H_2]=140 mM, [Os] =104 μM)

For the comparison purposes, hydrogenation performance in a MAC of six stages with the same reactor volume is also given in Figure 7.2. The operation conditions in this reactor are identical to those used in

Table 7.1. The maximum hydrogenation conversion at the 6th stage is only 87.7%. It is clear shown that hydrogenation degree at a MAC of a larger number of stages is higher due to that a MAC with more stages approaches a PFR which benefits in increasing hydrogenation degree. However, as discussed in design considerations, a MAC with a very large number of stages is not always desirable when considering reactor fabrication and operation costs.

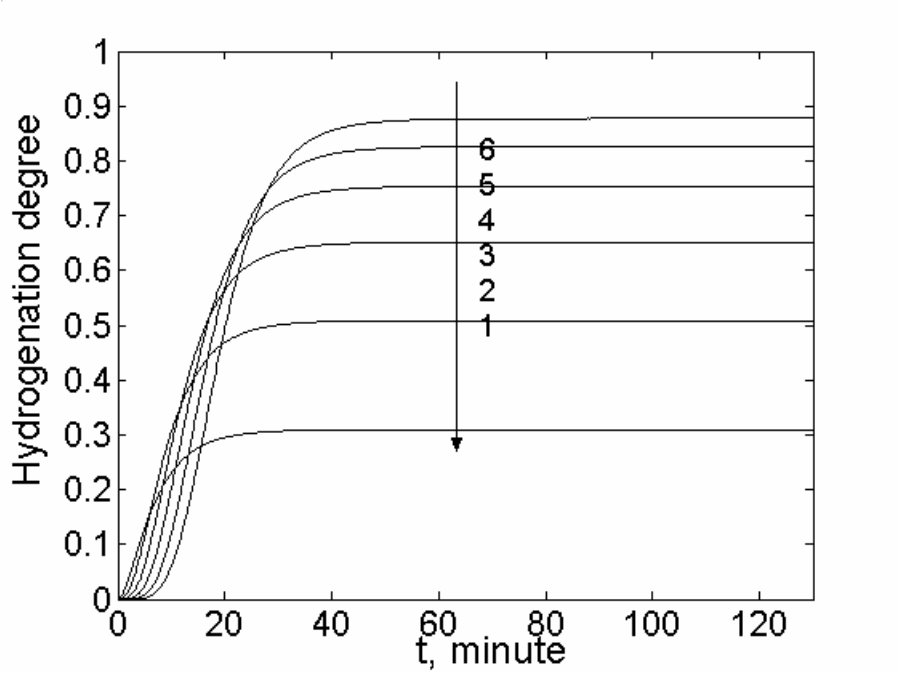

Figure 7. 2 Hydrogenation profile in a MAC of six stages at a pilot scale

(T=140 °C , [C=C]=550 mM, P=500 psig, [H_2]=140 mM, [Os] =104 µM)

It can be seen from the results predicted from that the designed pilot scale can satisfactorily meet the hydrogenation degree required for the final products at industrial operation conditions.

7.4 Heat Transfer Consideration at a Pilot Scale

It is well known that hydrogenation reaction is usually exothermic. A considerable amount of heat will be released during the hydrogenation process. To promptly remove the heat generated, sufficient heat transfer capability is required. In a bench scale setup, heat transfer area is relatively large compared to a reactor with a large scale. Therefore, it is crucial to estimate the heat transfer capability during the scale up. The

reaction heat is evaluated by the difference of enthalpy between reactants and products. The heat of formation for hydrogen is available from literature whereas the enthalpy of nitrile rubber and hydrogenation nitrile rubber can be determined by group contribution (Hougen et al., 1960). The following equation can be used to calculate the enthalpy change or the reaction heat at a given reaction temperature.

$$\Delta H = \Delta H_0 + \Delta w_1 T + (1/2)\Delta w_2 T^2 + (1/3)\Delta w_3 T^3 \qquad \textbf{Equation 7. 1}$$

The coefficients, w_1, w_2 and w_3 are coefficients for hydrogen, nitrile and hydrogenated nitrile presented by Bhattacharjee et al. (1991). Table 7.2 summarizes all parameters for estimation of the reaction heat.

Table 7. 2 Parameters for heat release estimation

	ΔH_0 (298K)(kJ mol^{-1})	w_1, kJ mol^{-1} K^{-1}	$10^2 w_2$, kJ mol^{-1} K^{-2}	$10^3 w_3$, kJ mol^{-1} K^{-3}
NBR(38.5 %ACN)	-36657.07	578.90	13593.02	-818.03
H_2	8.46	6.42	0.10	-781×10^{-4}
HNBR(38.5 %ACN)	-96993.84	2055.53	14653.92	-858.16

At T=413 K, the heat released based on the polymer concentration is 59,800 kJ/mol while it is 76.8 kJ/mol according to a [C=C] base.

It can be seen that a significant amount of heat released in the earlier several stages due to the high hydrogenation rates occurring in those stages. A relatively low level of heat is released from the later stages. In the first stage, about 680 W is generated while only 40 W is observed in the 9th stage due to their significant difference in [C=C] available for hydrogenation. Therefore, the ability of heat removal is examined in the first stage.

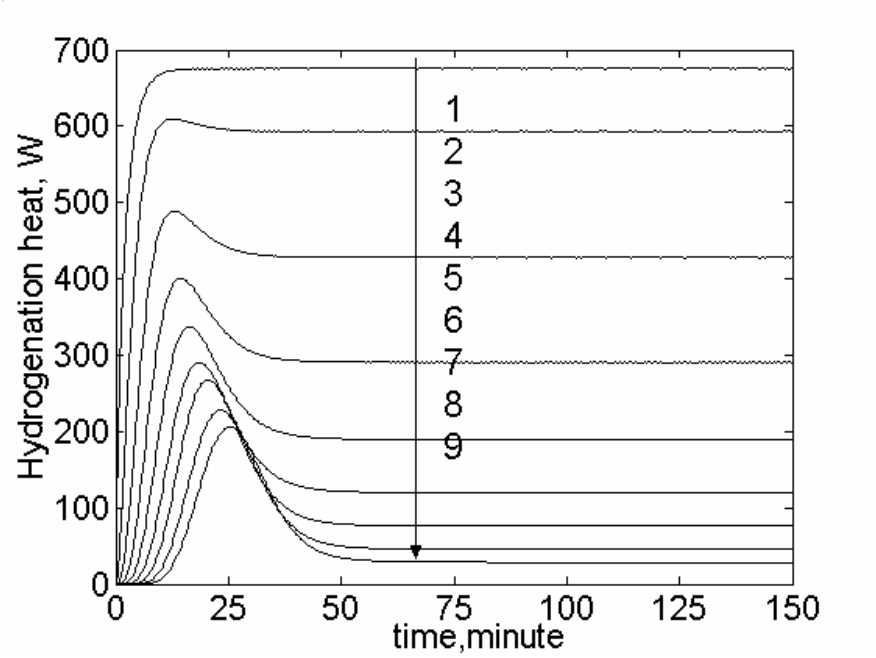

Figure 7. 3 Heat released at various stages in a MAC of 9 stages (T=140 °C, [C=C]=550 mM, P=500 psig, [H_2]=140 mM, [Os] =104 μM)

An empirical correlation is used to calculate the heat transfer coefficient, which is suitable for 40< Re <30,000 (Perry, 1997).

$$Nu = 0.6R_e^{2/3}P_r^{0.33}(\frac{\mu_L}{\mu_w})^{0.14}$$ **Equation 7. 2**

where,

$$Nu = \frac{hD}{\kappa}$$ **Equation 7. 3**

$$P_r = \frac{\mu_L C_P}{\kappa}$$ **Equation 7. 4**

$$\mathrm{Re} = \frac{\rho_L N d_I^{\,2}}{\mu_L}$$ **Equation 7. 5**

where Nu is the Nusselt number and Pr is the Prandtl number. h is the heat transfer coefficient, $W/m^2.K$, and *K* is the thermal conductivity, $W.m^{-1}.K^{-1}$. When a 5% NBR solution is considered, it has a viscosity of 0.02 Pa.s and a density of 967.9 kg/m^3. Therefore, the Reynolds number is 6343 and the Prandtl number is 537. As a consequence, the resulting heat transfer coefficient, h, is 484 $W/m^2.K$. In order to remove the heat generated in the first stage, a temperature difference between jacket and the tank bulk of 7 degree is required. It can be seen that the heat removal is not a concern in the current design.

7.5 Concluding Remarks

A MAC of 9 stages with a total volume of 120 L was designed to achieve a HNBR productivity of 50 tons/year based on the success from the bench scale setup. A preview of hydrogenation performance was conducted through numerical simulation and a desired hydrogenation degree of over 95% could be obtained. Heat transfer estimation shows that the reaction heat generated can be immediately removed and no additional heat transfer area is required at the designed operating conditions.

Chapter 8 Conclusions and Recommendations for Future Research

In this project, development of a novel continuous process for hydrogenation of nitrile butadiene rubber has been accomplished. Hydrodynamic study has been carried out with air-water and air-viscous systems in two multistage agitated contactors (MAC) of different scales. A bench-scale prototype was established and hydrogenation performance of the designed process has been explored. A pilot scale unit was also designed based on the results from the bench scale setup.

8.1 Conclusions

8.1.1 Hydrodynamic in Air-water System

The liquid phase backmixing characteristics of the MAC were studied through RTD at a long residence time. The superficial liquid velocity under investigation was from 0.005 m/s to 0.05 m/s, resulting in a residence time from 10 minutes to 50 minutes while the superficial gas velocity was ranging from 0 to 0.088 m/s. The stirring speed employed is from 5 rps to 25 rps. The experimental RTD data are satisfactorily fitted by the CTB model where a back flow ratio is used to characterize back mixing within the reactor. The effects of operating variables on liquid backmixing are also investigated. It is found that with an increase in stirring speed, the back flow ratio increases while increasing liquid flow rate decreases the back flow ratio due to the suppression effect of bulk liquid flow. The presence of gas phase reduces the liquid backmixing between stages due to its two main effects: strengthening effect on liquid flow and entrainment effect in a co-current operation fashion.

For the purpose of interpreting backflow ratio in an air-water system, gas hold-up is also investigated. The gas hold-up achieved in this work is comparable to literature data. In addition, it is found that the gas holdup data from single stage agitated contactors can be applied to MACs with a certain level of confidence.

The back flow ratios obtained in the present study are relatively low and present a design of a MAC with high stage efficiency. Using the present data, a correlation is proposed to predict back flow ratios of the continuous phase in a MAC from the power input point of view.

Volumetric mass transfer coefficients have been studied through a steady state approach. The values obtained in MACs are comparable to the data reported in the SACs under the similar operating conditions.

8.1.2 Hydrodynamics in Air-viscous Systems

Liquid bakmixing in viscous media is not well understood in the literature, especially in a two-phase flow system. Therefore, before using the proposed reactor to perform the continuous process, hydrodynamic behavior in the designed reactor is carried out. Liquid backmixing and gas hold-up have been studied in viscous liquids with a viscosity of up to 0.02 Pa.s. Sugar solutions with up to 60% (w/w) are employed as simulating liquids.

The model discrimination between the CTB model and the AD model shows that the former is still more suitable to describe the flow behavior in the MAC with viscous liquids.

The back flow ratio for the first time is reported for a two phase flow system in viscous media. From the experimental study, it is found that the viscosity helps in reducing liquid backmixing due to the resulting lower level of turbulence. The presence of the gas phase also reduces liquid backmixing by a straightening effect and entrainment effect.

The gas hold-up obtained in viscous media is comparable to previously reported literature data. A similar correlation is proposed to predict back flow ratio by taking into account the influence of the gas phase and the resulting bubble size in viscous media.

8.1.3 RTD Prediction by Computational Fluid Dynamics

The CFD technique is employed to predict RTD curves in MACs of two, four and six stages with different liquids. A suitable strategy has been developed to use CFD to predict liquid RTD in the reactors of interest. In order to account for the turbulence dominating in a stirred vessel, a standard k-ε model and RNG k-ε model are used.

The CFD modeling work is implemented in a commercial CFD package CFX5.7.1. The resulting RTD curves have been compared with experimental data obtained using a conductivity meter. The observed

power number from the simulation show good agreement with the literature value. The observed mean residence time and normalized variance are in a reasonably good agreement with the experimental data. The concentration profile obtained from simulations provides a line of evidence that the CTB model is more suitable to describe the flow behavior in MACs with few stages. However, lower values of back flow ratio (up to 25% compared to experimental data) predicted from CFD simulations are observed presumably due to the inherent deficiency of describing turbulence of two models employed in the present study. Therefore, the improvement is expected by using more advanced turbulence models which can accurately take into account the damping effect of viscosity on turbulence.

Nevertheless, the mixing behavior of MACs can be understood by CFD prediction and the confidence of using CFD to facilitate the reactor design has been established.

8.1.4 Hydrogenation Performance of the Continuous Process

A bench-scale prototype involving a gas liquid MAC of 6 stages (with a reactor volume of around 1 liter) has been designed and established. The hydrogenation behavior of the designed reactor has been investigated by using $OsHCl(CO)(O_2)(PCy_3)_2$ as a selective catalyst.

The primary hydrogenation data acquired from the designed continuous unit have shown the feasibility of the MAC approach. The demands for a high conversion over 95% for hydrogenated NBR can be met by the co-current, upflow MAC approach in two different polymer solutions, 2.5% NBR and 5% NBR. In a 2.5% NBR solution, a minimum of 80 µM osmium loading is required in order to achieve a desired hydrogenation conversion over 95% at a residence time of 40 minutes. On the contrary, a minimum of 100 µM osmium is needed for a residence time of 20 minutes. In a 5% NBR solution, a minimum of 100 µM osmium loading level is required for a residence of 40 minutes while a minimum of 125 µM is sought for a residence time of 20 minutes at the same pressure and temperature conditions. Hence, in order to achieve a desired hydrogenation degree of over 95%, either a combination of a high liquid flow rate with a high catalyst loading level or a low liquid flow rate can be adopted.

An attempt has been made to establish a mathematical model by integrating kinetic data with flow behavior. The CTB model is used to characterize flow behavior and intrinsic kinetics is adopted from

batch experimental studies. The numerical simulation has been conducted and the hydrogenation degree can be predicted by the model by taking into account of catalyst loss and temperature gradient. The apparent catalyst loss suggests that 30% more catalyst is required in order to achieve the desired conversion for an empirical design based on the current experimental data. A revised nCSTRs in series model is proposed to predict hydrogenation degree at steady state.

A continuous process involving a MAC of 9 stage (with a reactor volume of 120 liters) at a pilot scale was designed and the numerical simulation indicates that the pilot scale unit could provide a desired hydrogenation degree over 95% for 5% NBR solution as well as a production capacity of 50 tons/year.

8.2 Future Work

8.2.1 Identification of Catalyst Loss in the Continuous Process

It has been found that a considerable amount of catalyst is deactivated in the continuous process. Approximately 30% to 50% of the catalyst added to system has no activity. It is believed that the impurities within the rubber material and oxygen remaining in the solution contribute to the catalyst deactivation. The portion of the contribution of two factors is required to single out in order to more efficiently utilize the catalyst and provide fundamental data for a large scale production.

8.2.2 Hydrogenation Investigation in Other Efficient Catalysts

One effective catalyst, $OsHCl(CO)(O_2)(PCy_3)_2$, was primarily used to hydrogenate NBR in the present work. It remains to characterize other selective catalyst systems such as rhodium and ruthenium catalysts which have also been demonstrated with high selective hydrogenation efficiency in batch systems.

8.2.3 Bubble Size Investigation and Hydrodynamic Study under Pressure Conditions

Bubble size is also an important critical parameter to describe interfacial area, which in turn determines mass transfer capability. Therefore, knowledge of bubble size and its distribution within the agitated vessel is required.

Hydrodynamics of a MAC under pressure conditions is not studied. The effects of stirring speed, liquid velocity and gas velocity on gas hold-up and liquid backmixing may deviate from the knowledge obtained at ambient conditions. It is demonstrated that a higher pressure helps to increase gas hold-up.

Measurement of gas hold-up and liquid backmixing as a function of stirring speed, liquid velocity and gas velocity under various pressures should be carried out.

8.2.4 Computational Fluid Dynamics for a Reactive Two-phase Flow

The liquid residence time distribution is predicted by CFD simulations. The comparison of simulation prediction to experimental data shows the promise of using this technique to assist reactor design and process optimization. Inherent deficiency of standard k-ε model may lead to the small deviation of model prediction and experimental measurement. Alternative turbulence models will be sought for an improvement of CFD simulation of a single phase system with different liquids.

The confidence of using CFD to predict a two-phase flow based on our experience in a single phase flow is also established. Therefore, further efforts are to be made on simulation of a reactive gas liquid flow in the reactor. The well known phenomena of bubble size distribution may occur in the designed reactor, leading to a deviation of mass transfer prediction from the empirical correlations developed in SACs or MACs. In view of this, a population balance equation may be applied to account for the bubble size distribution within the reactor. Different models of bubble coalescence and bubble breakage may be compared to explain experimental work in practice.

Notations

a: interfacial surface area, m^2/m^3;

A: cross area of the column, m^2;

ACN: content of acrylnitrile in the rubber, w/w%;

AD: axial dispersion model;

A(x): absorption height of characteristic peak, x cm^{-1};

A_{hb}: central opening area, m^2;

B: $B = \frac{Nd_I}{u_L}(\frac{{d_I}^2 A_{hb}}{HDA})^{0.5}$;

BE: backmixing equation;

c_i: oxygen concentration in the i^{th} stage, kg/m^3;

C: tracer concentration, kg/m^3;

CNTB: cascade of non-ideal stirred tanks with back flow;

CSTR: continuously stirred tank reactor;

CTB: cascade of stirred tanks with back flow;

C(t) tracer concentration at an instant, kg/m^3;

C_p: specific heat capacity, kJ/kg.K;

C_μ constant of the k-ε model;

[C=C]: carbon carbon double bond concentration, mM;

d_B: bubble size, m;

d_{vb}: vertical baffles, m;

d_I: diameter of the impeller, m;

D: diameter of the vessel, m;

D_e : axial dispersion coefficient, m^2/s;

D_L: molecular diffusivity, m^2/s;

E(t): residence time distribution, 1/s;

E(θ): normalized residence time distribution;

f: back flow rate, m^3/s;

f^{entr}: back flow rate due to entrainment, m^3/s;

f^{ma}: back flow rate due to mechanical agitation, m^3/s;

f^{Pre}: back flow rate predicted, m^3/s;

F: liquid flow rate, m^3/s;

Fl: Flow number, $\frac{Q_G}{Nd_I^{\ 3}}$;

Fr: Froude number, $\frac{N^2 D}{g}$;

g: gravitational constant, m/s^2;

G_1, G_2: defined in Equation 3.10 and 3.11;

h: heat transfer coefficient, $W/m^2.K$;

H: height of each stage, m;

Ha: Hatta number;

HD: hydrogenation degree;

HNBR: hydrogenated nitrile butadiene rubber;

H_I: impeller location, m;

H_0: liquid Level after aeration, m;

H_1: liquid Level before aeration, m;

ΔH: reaction heat released, kJ/mol;

ΔH_0: reaction heat released at 298 K, kJ/mol;

$[H_2]$: hydrogen concentration, mM;

$[H_2]^*$: hydrogen concentration at equilibrium, mM;

IO: inner-outer approach;

k: turbulent kinetic energy, J/kg;

k': reaction kinetic constant, $mM^{-m}s^{-1}$;

k_L: mass transfer coefficient, m/s;

$k_L a$: volumetric mass transfer coefficient, 1/s;

k_1: rate constant, $mM^{-2}\ \mu M^{-1}s^{-1}$;

L: length of the reactor, m;

m: reactor order with respect to hydrogenation concentration;

m_1,m_2: as defined in Equation 3.13 and 3.14;

M: sum of body forces, N;

MAC: multistage agitated contactor;

MFR: multiple frames of reference;

n: the number of CSTRs;

$n_{G,i}$: number of moles of hydrogen gas per unit liquid volume, mol/L liquid volume;

N: stirring speed, rps;

NBR: nitrile butadiene rubber;

N_0: critical stirring speed, rps;

N_c: the number of stages in a MAC;

N_d: the number of datum points;

N_I: the number of impellers at each stage;

N_p: power number of the impeller;

Nu: the Nusselt number, $\frac{hD}{\kappa}$;

[Os]: osmium catalyst concentration, μM;

p_1, p_2, p_3: coefficients in Equation 3.19 and 3.24;

p_4, p_5, p_6: coefficients in Equation 4.4;

p': modified pressure, Pa;

P: system pressure, Pa;

P_0: power input in unaerated system, W;

P_G: power consumption in aerated system, W;

Pr: Prandtl number, $\frac{\mu_L C_P}{k}$;

q: intra-stage back flow rate, m^3/s;

Q_G: gas flow rate, m^3/s;

r': hydrogenation rate, mM/s;

Re: Reynolds number with respect to an impeller, $\frac{\rho_L N d_I^{\ 2}}{\mu_L}$;

Re_1: Reynolds number based on impeller, $\frac{\rho_L N d_I^{\ 2}}{\mu_L}$;

Re_2: Reynolds number based on the liquid flow, $\frac{\rho_L u_L D}{\mu_L}$;

RTD: residence time distribution;

SM: sliding mesh approach;

t: time, s;

$\bar{t}$: average residence time, s;

T: temperature, K;

u_G: superficial gas velocity, m/s;

u_L: superficial liquid velocity, m/s;

U: mean velocity vector, m/s;

V: volume of each stage, m^3;

w_1,w_2,w_3: coefficients in Equation 7.1;

Greek Symbols

α: back flow ratio, f/F;

a_{GL}: back flow ratio in a gas liquid system;

β: polymer loading level, $\frac{[C=C]_0}{[H_2]^*}$;

δ: exponent with respect to viscosity;

δ(t): Dirac function;

ζ: correction factor for agitators;

ε: eddy energy dissipation in standard turbulence model, J/kg;

ε_G: gas holdup;

$\varepsilon_{L:}$ liquid holdup;

θ_τ: dimensionless residence time, $k_1[Os][H_2]^{*2}\tau$;

κ: thermal conductivity, $W.m^{-1}.K^{-1}$;

λ: as defined in Equation 3.12;

μ: viscosity, Pa.s;

μ_{eff}: effective viscosity, Pa.s;

μ_w: viscosity of water, Pa.s;

μ_L: liquid viscosity, Pa.s;

μ_t: turbulent viscosity, Pa.s;

ξ: dimensionless mass transfer, $\frac{k_L a}{k_1[Os][H_2]^*[C=C]_0}$;

ρ_{air} : air density, kg/m^3

ρ_L : liquid density, kg/m^3;

ρ_G: density of gas, kg/m^3;

σ: surface tension, N/m;

σ_t turbulent Schmidt number;

τ: liquid residence time, s;

Φ: tracer concentration, kg/m^3;

Φ_{outlet}: tracer concentration at the outlet, kg/m^3;

χ: modified back flow ratio;

Ψ: torque, N.m;

Subscripts

0: at the inlet;

B: bubble;

G: gas;

GL: gas-liquid;

L: liquid;

i: ith stage;

w: water;

Superscripts

Cal: calculation;

Entr: entrainment;

Exp*:* experimental*;*

Ma: mechanical agitation;

Pre: prediction;

Appendix A Schematic Reactor Configuration

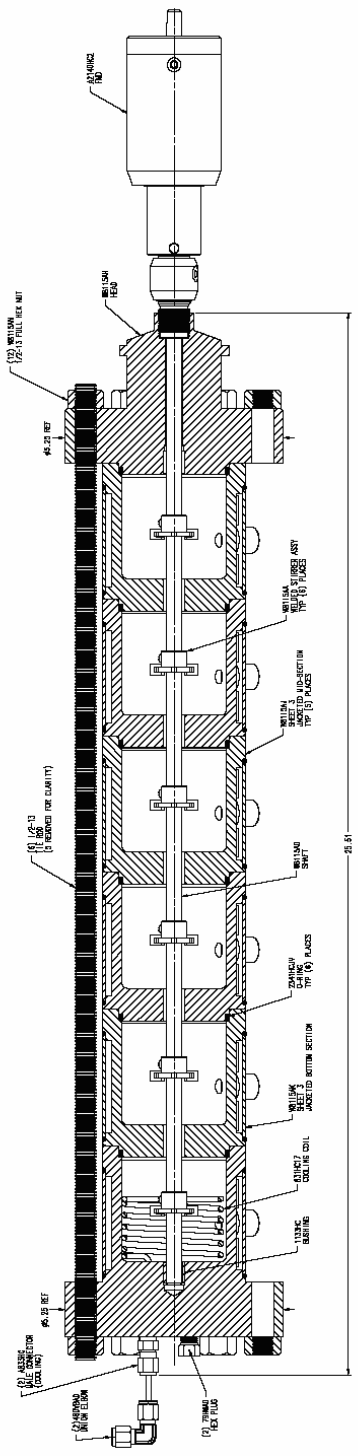

Courtesy of Parr

Appendix B Components of the Continuous Set-up

Component	Supplier	Specifications
A. 10 L carboy	VWR	Polyethylene
B. High pressure metering pump	MiltonRoy	Model RT11-77A1SEM2NN
C. Mass flow controller	Brooks	Model # 5850 1500 psig max
D. Preheater	Parr	Model # 2000 ml capacity, 1500 psig max
E. Relief valve	Swagelok	R3A-C 1500 psig max
F. 1L catalyst bomb	Swagelok	304L-HDF4-1000CC
G. Metering pump	MiltonRoy	RT11-15A1SEM2NN
H. Three way valve	Swagelok	SS-42GXS4
I. Multistage agitated contactor	Custom	Six stages, 1150 ml capacity, 1500 psig max
J. Heat Exchanger	Custom	/
K. Gas liquid separator	Penberthy	Model # IRM8
L. Collection container	VWR	Polyethylene
M. Check valve	Swagelok	Model # SS-4C-TR-1 1psig
N. Bourdon gauge	Weksler	0-3000 psig range
O. back pressure regulator	Tescom	Model# 26-1725-24
P. Low pressure separator	Custom	
Q. Gas rotameter	Brooks	Model#R-25-B-MM

Appendix C Hydrodynamic Data in Air-water System

Table C-1 Effect of stirring speed on liquid back flow ratio under various gas flow rates (D=0.15 m, H=0.15 m, and u_L=0.001 m/s; 6 stages)

Superficial gas velocity, m/s	Stirring speed, rps	Liquid back flow ratio
0	10	0.03
0	12	0.045
0	15	0.07
0	16	0.075
0	20	0.1
0	25	0.14
0.008	12	0.04
0.008	13	0.045
0.008	15	0.06
0.008	17	0.075
0.008	20	0.09
0.008	22	0.1
0.008	25	0.12
0.02	15	0.056
0.02	17	0.066
0.02	20	0.075
0.02	23	0.09
0.02	25	0.1
0.038	15	0.044
0.038	17	0.052
0.038	20	0.063
0.038	23	0.08
0.038	25	0.084
0.055	15	0.04
0.055	17	0.045
0.055	20	0.05
0.055	23	0.06
0.055	25	0.065
0.08	15	0.035
0.08	17	0.04
0.08	20	0.045
0.08	25	0.06

Table C-2 Effect of liquid flow rate on liquid back flow ratio under various gas flow rates (D=0.15 m, H=0.15 m, and N=15 rps; 6 stages)

Superficial gas velocity, m/s	Superficial liquid velocity, m/s	Liquid back flow ratio
0	0.04	0.2
0	0.07	0.12
0	0.1	0.06
0	0.2	0.026
0	0.26	0.017
0	0.36	0.008
0.011	0.05	0.18
0.011	0.1	0.0707
0.011	0.14	0.045
0.011	0.18	0.0156
0.011	0.24	0.01
0.011	0.28	0.0084
0.022	0.14	0.048
0.022	0.37	0.0411
0.022	0.2	0.0482
0.022	0.1	0.0707
0.022	0.28	0.0338
0.038	0.05	0.08
0.038	0.1	0.05
0.038	0.15	0.03
0.038	0.2	0.024
0.038	0.24	0.01
0.038	0.28	0.0048
0.038	0.36	0.0024

Table C-3 Effect of liquid flow rate on liquid back flow ratio under various gas flow rates (D=0.1 m, H=0.1 m, and N=15 rps; 6 stages)

Superficial gas velocity, m/s	Liquid velocity, m/s	Liquid flow ratio
0	0.05	0.6
0	0.1	0.35
0	0.15	0.15
0	0.2	0.0632
0	0.3	0.0375
0.018	0.05	0.25
0.018	0.1	0.0669
0.018	0.15	0.02

0.018	0.2	0.008
0.018	0.3	0.005
0.027	0.05	0.12
0.027	0.1	0.04
0.027	0.15	0.008
0.027	0.2	0.004
0.027	0.3	0.0012
0.035	0.05	0.06
0.035	0.1	0.02
0.035	0.15	0.006
0.035	0.2	0.003
0.035	0.3	0.001
0.055	0.05	0.05
0.055	0.1	0.02
0.055	0.15	0.005
0.055	0.2	0.002
0.055	0.3	0.0015

Table C-4 Effect of impeller position on back flow ratio (D=0.15 m, H=0.15 m, u_L=0.001 m/s; 6 stages)

Stirring speed, rps	H=0.5H	H=0.333 H	H=0.25H
15	0.05	0.056	0.065
17	0.058	0.0663	0.075
20	0.063	0.075	0.085
22	0.074	0.08	0.1
25	0.085	0.1	0.11

Table C-5 Effect of stage number on back flow ratio (D=0.15 m, H=0.15 m, d_I/D=1/3, u_G=0 m/s, and u_L=0.001 m/s)

The number of tages	N= 15 rps	N= 20 rps	N=25 rps
2	0.070	0.11	0.14
3	0.069	0.11	0.15
4	0.067	0.12	0.13
5	0.065	0.10	0.15
6	0.070	0.12	0.14

Table C-6 Effect of stirring speed on gas hold-up, %

(D=0.15m, H=0.15 m, d_I/D=1/3 and u_L=0.001 m/s; 6 stages)

Stirring speed, rps	u_G=0.08 m/s	u_G=0.055 m/s	u_G=0.038 m/s	u_G=0.025 m/s	u_G=0.01 m/s
13	24	19	-	-	7
15	26	21	17	14	8.5
17	28	24	19	15	9.5
20	32	26	21	17.5	10.5
23	35	29	24	19	11.7
25	37	31	25	21	12.5
30	-	-	29	23	14

Table C-7 Effect of gas velocity on gas hold-up, % (D=0.15m, H=0.15 m, d_I/D=0.5 and u_L=0.001 m/s; 6 stages)

Superficial gas velocity, m/s	N=12.5 rps	N=10 rps	N=7.5 rps
0.01	16	14	10
0.022	23	18	14
0.03	27	21	17
0.038	33	25.5	20
0.055	39	32	25
0.08	43	36	32

Table C-8 Effect of stirring speed on volumetric mass transfer coefficient, s^{-1} (D=0.1m, H=0.1 m and d_I/D=0.5, u_L=0.001 m/s; 6 stages)

Stirring speed, rps	u_G=0.008 m/s	u_G=0.018 m/s	u_G=0.025 m/s	u_G=0.038 m/s
6	0.020	0.028	0.035	0.040
8	0.025	0.032	0.040	0.046
10	0.030	0.039	0.045	0.058
12	0.040	0.045	0.052	0.065
14	0.050	0.052	0.060	0.072

Appendix D Hydrodynamic Data in Air/viscous System

Table D-1 Effect of stirring speed on gas hold-up in various liquids (D=0.1 m, H=0.1 m, $d_I/D=0.5$ and $u_L=0.001$ m/s; 6 stages)

25% sugar solution			
Stirring speed, rps	u_G=0.018 m/s	u_G=0.027 m/s	u_G=0.038 m/s
8	12.5	16	19
10	16	18	22
12	17	21	25
14	20	24	29
16	21	26	32
18	24	28	34
20	25	30	36
22	27	33	39
50% sugar solution			
Stirring speed, rps	u_G=0.018 m/s	u_G=0.027 m/s	u_G=0.038 m/s
10	13	16	19
12	15	18	22
14	16	20	24
16	18	21	27
18	20	23	29
20	22	26	31
22	23	29	33
60% sugar solution			
Stirring speed, rps	u_G=0.018 m/s	u_G=0.027 m/s	u_G=0.038 m/s
8	8.3	11.3	19
10	10.3	13.3	21
12	12.5	15.3	22
14	14.7	17.3	23.5
16	16.7	19.3	24.5
18	18.7	22.2	26
20	20	23	27
22	22	24	28

Table D-2 Liquid back mixing data in air/viscous systems (D=0.1m, H=0.1 m and d_I/D=0.5; 6 stages)

25% sugar system			
Stirring speed, rps	**Liquid velocity, m/s**	**Gas velocity , m/s**	**Back flow ratio**
8	0.001	0.018	0.03
10	0.001	0.018	0.06
12	0.001	0.018	0.08
14	0.001	0.018	0.11
16	0.001	0.018	0.14
18	0.001	0.018	0.16
20	0.001	0.018	0.2
22	0.001	0.018	0.24
8	0.001	0.027	0.025
10	0.001	0.027	0.05
12	0.001	0.027	0.07
14	0.001	0.027	0.1
16	0.001	0.027	0.12
18	0.001	0.027	0.13
20	0.001	0.027	0.16
22	0.001	0.027	0.2
8	0.001	0.038	0.025
10	0.001	0.038	0.045
12	0.001	0.038	0.06
14	0.001	0.038	0.1
16	0.001	0.038	0.1
18	0.001	0.038	0.11
20	0.001	0.038	0.13
22	0.001	0.038	0.15
20	0.001	0	0.5
5	0.001	0	0.02
8	0.001	0	0.08
10	0.001	0	0.12
12	0.001	0	0.18
14	0.001	0	0.23
16	0.001	0	0.3
50% sugar solution			
5	0.001	0.018	0.008
10	0.001	0.018	0.05
12	0.001	0.018	0.07
14	0.001	0.018	0.08
16	0.001	0.018	0.12
18	0.001	0.018	0.15
20	0.001	0.018	0.18
22	0.001	0.018	0.2

5	0.001	0.027	0.008
10	0.001	0.027	0.03
12	0.001	0.027	0.04
14	0.001	0.027	0.06
16	0.001	0.027	0.08
18	0.001	0.027	0.1
20	0.001	0.027	0.15
22	0.001	0.027	0.18
8	0.001	0.038	0.008
10	0.001	0.038	0.02
12	0.001	0.038	0.03
14	0.001	0.038	0.05
16	0.001	0.038	0.06
18	0.001	0.038	0.08
20	0.001	0.038	0.10
22	0.001	0.038	0.12
15	0.0015	0	0.12
15	0.002	0	0.08
15	0.0025	0	0.06
15	0.003	0	0.05
15	0.0035	0	0.03
15	0.004	0	0.02
15	0.0005	0	0.33
15	0.001	0	0.05
60% sugar solution			
10	0.00027	0	0.40
9	0.0006	0	0.10
10	0.00067	0	0.12
14	0.00028	0	0.60
10	0.001	0	0.052
12	0.001	0	0.07
14	0.001	0	0.153
16	0.001	0	0.188
18	0.001	0	0.262
20	0.001	0	0.35
5	0.001	0	0.010
15	0.002	0.018	0.05
15	0.0025	0.018	0.04
15	0.003	0.018	0.028
15	0.0035	0.018	0.020
15	0.004	0.018	0.010
15	0.0005	0.018	0.20
15	0.001	0.018	0.12
15	0.002	0.027	0.050
15	0.0025	0.027	0.035
15	0.003	0.027	0.030

15	0.0035	0.027	0.018
15	0.004	0.027	0.008
15	0.001	0.027	0.08
15	0.0005	0.027	0.15
15	0.002	0.038	0.04
15	0.0025	0.038	0.03
15	0.003	0.038	0.02
15	0.0035	0.038	0.01
15	0.004	0.038	0.008
15	0.0005	0.038	0.1
15	0.001	0.038	0.06

Appendix E Hydrogenation Data

Table E-1 Batch reaction data ([C=C]=275 mM, [Os]=80μM, 350 psig and N=10 rps, total liquid volume= 140 ml)

Reaction time, minute	130-1	130-2	Reaction time, minute	140-1	140-2
0	0	0	0	0	0
5	21.46	22.17	3	36.05	-
10	43.2	46.72	5	49.03	50.61
15	62.65	58.6	7	64.7	-
20	77.3	75	10	75.8	74
25	90.1	90	15	91.7	90
30	97.3	97.8	20	96.7	97.3
40	100	100	25	100	100

Table E-2 Batch reaction data ([C=C]=275 mM and N=10 rps, total liquid volume= 140 ml)

Reaction time, minute	[Os]=80 μM	Reaction time, minute	[Os]=20 μM	Reaction time, minute	[Os]=10 μM
0	0	0	0	0	0
2.5	13.77	2.5	0	10	5.74
5	28.61	5	2.7	15	7.76
10	50.21	10	10.88	20	8.67
15	80.08	20	15.59	30	15.08
20	91.99	30	27.93	40	20.5
25	97.78	40	30.09	50	25.56
30	98.78	50	34.98	60	27.77
40	99.34	60	40.59	70	32.57
50	99.63	70	42.84	80	36.24
60	99.78	80	44.58	90	38.02
				100	38.77

Table E-3 Hydrogenation data from continuous set-up

F=24 ml/min; [C=C]=275 mM; 350 psig; [Os]= 80μM; N=10 rps						
Operation time, minute	Stage 1	Stage 2	Stage 3	Stage 4	Stage 5	Stage 6
0	0	0	0	0	0	0
10	3.46	2.1	0	0	0	0
20	3.98	3.86	2.28	2.15	0	0
30	8.21	13.7	11.7	7.1	5.6	3.77
40	12.07	27.36	26.64	16.7	15.89	12.5
50	15.57	30.16	39.8	42	36.7	24.47
60	14.44	36.07	48.4	51.24	54.7	49.2
70	12.79	34.8	50.8	65.65	67.5	68.5

80	18.47	40.94	58.7	72.4	78.2	78
90	21.13	41.74	57	73	85	86
100	20	42	57.3	74.7	85.3	88.9
110	17.85	40.22	61.3	78.84	86.9	90.9
120	20	39.08	59.1	78.25	86	89.9
130	19.5	41.02	57.2	75	85.6	90.5
140	17	39.3	56.5	73	83	89
150	18.4	40.1	58.21	74	84	89.6
F=24 ml/min; [C=C]=275 mM; 500 psig; [Os]= 80µM; N=12.5 rps						
0	0	0	0	0	0	0
10	4.25	5.27	4.35	0	0	0
20	2.37	17.67	13.25	4.92	0	0
30	12.37	42.78	53.22	41.69	26.01	9.42
40	14.81	63.69	86.48	89.7	76.5	51.5
50	15.93	70.66	94.94	98.43	98.8	92.23
60	19.18	74.48	95.05	98.82	99.67	99.67
70	16.57	69.43	94.15	98.65	99.69	100
80	5.83	62.25	91.61	99.28	99.95	100
90	11.81	55.74	88.08	95	98.23	99.7
100	7.67	36.4	74.5	94.9	98.8	98.8
110	5	29.84	59.96	79.83	96.89	98.5
120	3.14	33.99	62.28	79.35	93.93	97.9
130	8.85	42.76	75.08	87.89	95.94	97.36
140	10.82	50.8	71.7	90.1	96.02	98.25
150	13.5	41.5	82.83	94.67	98.6	99.05
160	15	44.89	79.12	94.96	99.44	100
F=24 ml/min; [C=C]=275 mM; 350 psig; [Os]= 27µM; N=12.5 rps						
0	0	0	0	0	0	0
10	0	0	0	0	0	0
20	0	2.58	0	0	0	0
30	1.59	3.95	6.5	3.2	1.66	0
40	3.18	12.01	16.51	11.2	8.86	4.55
50	3.56	13.76	21.19	25.17	25.66	18.46
60	3.54	15.22	27.51	29.64	33.29	28.3
70	4.28	13.7	22.11	33.04	39.54	42.06
80	2.99	17.58	26.95	34.25	44.32	46.58
90	3.58	24.53	26.78	37.16	46.65	52.64
100	3.88	21.58	25.69	41.9	51.76	58.3
110	5.41	18.22	25.44	36.45	51.19	56.09
120	5.68	15	25.79	41.21	52.3	57.6
130	2.43	13.29	24.57	37.3	49.72	58.04
140	2.74	15.26	26.54	33.88	50.2	60.43
150	2.84	14.5	25.52	39.7	49.8	59.25
F=48ml/min; [C=C]=275 mM; 500 psig; [Os]=100 µM; N=12.5 rps						
10	2.17	5.55	2.7	2.61	3.97	0
20	5.74	14.03	21.2	22.55	17.32	8.86

25	6.11	14.68	33.69	44.16	42.35	38.54
30	5.58	18.73	40.72	57.9	65.39	64.43
40	5.46	25.7	47.9	68.54	80.75	87.04
50	6.5	28.21	56.2	77.95	89.38	94.98
60	5.25	28.5	54.5	76.34	87.98	95.92
70	5.78	27.9	56	76.5	84.5	91.84
80	5.4	28.4	56.3	77.8	85.29	94.3
90	5.1	27.8	55.9	79.1	88.3	93.5
F=24 ml/min; [C=C]=550 mM; [Os]=140 µM; N=12.5 rps						
0	0	0	0	0	0	0
10	3.5	1.76	0	0	0	0
20	4.0	15.86	12.44	12.16	6.86	3
30	3.2	21.34	33.61	34.28	27.77	15.2
40	7.96	32.9	53.8	56.8	51.4	42.08
50	6.19	37.2	59.38	69.96	72.77	63.5
60	9.82	38.77	65.67	80.31	85.5	83.6
70	15.18	51.5	74.4	86.62	91.84	91.67
80	20.47	56.25	81.9	92.3	96.2	97.07
90	16.06	55.13	81.45	93.4	97.25	98.122
100	8.49	50.8	80.06	93.9	98.2	99.54
110	14.76	53.4	79.13	93.12	97.85	99.06
120	11.67	49.09	76.35	92.01	97.65	99.36
130	13.29	48.59	76.3	91.81	96.79	98.95
140	12.38	46.19	76.48	90.48	97.35	98.7
150	14.11	48.34	76	91.14	98.32	98.8
F=24 ml/min; [C=C]=550 mM; 500 psig; [Os]= 95 µM; N=12.5 rps						
0	0	0	0	0	0	0
10	1.5	1.76	0	0	0	0
20	3.83	8.25	8.25	8.89	1.31	0.97
30	4.5	11.35	19.25	39.75	28.43	1.65
40	6.3	13.41	26.34	61.35	57.51	12.55
50	11.9	16.92	37.89	65.95	74.74	43.97
60	9.87	19.83	46.54	67.45	76.67	68.45
70	8.69	29.51	52.78	64.33	83.14	78.48
80	10.5	26.15	51.63	65.26	83.16	84.55
90	12.3	30.12	45.45	64.98	82.16	85.3
100	11.9	29.81	43.84	68.42	80.13	84.27
110	9.35	33.01	46.9	65.17	80.52	84.55
120	10.25	29.25	42.13	64.26	81.13	85.19
130	6.54	28.34	44.8	67.5	83.5	83.9
140	8.98	26.19	45.9	68.2	82.9	85.3
F=48 ml/min; [C=C]=550 mM; 500 psig; [Os]= 127µM; N=12.5 rps						
0	0	0	0	0	0	0
5	0	0	0	0	0	0
10	2.53	3.58	1.83	0	0	1.37

15	4.53	20.83	10.33	9.35	10.2	5.79
20	6.07	38.9	33.48	23.7	63	25.6
30	12.75	44.6	48.9	69.7	85.67	43.67
40	15.78	37.8	55.94	82.55	92.82	87.06
50	14.02	45.9	57.5	87.6	95.6	94.5
60	13.81	43.8	62.98	91.06	97.96	98.97
70	12.54	44.23	-	-	-	-

Appendix F MATLAB Code

Solve ODEs and Plot Hydrogenation Profiles

%%

Function MACplot;

[t,c]=ode45('osmium',[0,8400],[275,275,275, 275,275,275,0,0,0,0, 0,0,110,110,110,110,110,110]); % Rugga-Kutta method to solve the established ODEs

Plot (t, (275-c(:,6))/275);

Hold on;

Plot(t, (275-c(:,5))/275);

Plot(t, (275-c(:,4))/275);

Plot(t, (275-c(:,3))/275);

Plot(t, (275-c(:,2))/275);

Plot(t, (275-c(:,1))/275);

xlable('time, minute');

ylabel('Hydrogenation degree, %');

%%%

The following program indicates a function which consists of the established ODEs.

The following function is created for solve a MAC with six stages. If a MAC with more stages, the corresponding number of ODEs should be added.

%%

Function dx=osmium(t, x);

dx=zeros(24, 1); % Initialize matrix

k=0.004/100/110/110; % kinetic constant excluding catalyst concentration and hydrogen concentration

F=24/60; % liquid flow rate, l/min

alpha=0.28; % back flow ratio

c0=275; % inlet polymer concentration, mM

E0=80; % inlet catalyst concentration, μM

V=1135/6; % volume of each stage, ml

toi=V/F; % average residence time at each stage

```
h0=110; % mM, hydrogen inlet concentration
H0=110; % mM, hydrogen equilibrium concentration
e0=0.85; % liquid hold-up
a=2; %  reaction order with respect to hydrogen concentration
P=350/14.7*101325; % system pressure
R=8.314; % gas constant
T=413; % K, temperature
dB=0.0027; % meter, bubble diameter
kl=1*0.001;%  liquid side mass transfer coefficient
dx(1)=(c0-(1+alpha)*x(1)+alpha*x(2))/toi/x(19)-k*x(1)*x(7)*(x(13))^(a);
dx(2)=((1+alpha)*(x(1)-x(2))+alpha*(x(3)-x(2)))/toi/x(20)-k*x(2)*x(8)*x(14)^(a);
dx(3)=((1+alpha)*(x(2)-x(3))+alpha*((x(4)-x(3))))/toi/x(21)-k*x(3)*x(9)*x(15)^(a);
dx(4)=((1+alpha)*(x(3)-x(4))+alpha*(x(5)-x(4)))/toi/x(22)-k*x(4)*x(10)*(x(16))^(a);
dx(5)=((1+alpha)*(x(4)-x(5))+alpha*(x(6)-x(5)))/toi/x(23)-k*x(5)*x(11)*x(17)^(a);
dx(6)=((1+alpha)*(x(5)-x(6)))/toi/x(24)-k*x(6)*x(12)*(x(18))^(a);
dx(7)=(E0-(1+alpha)*x(7)+alpha*x(8))/toi/x(19);
dx(8)=((1+alpha)*(x(7)-x(8))+alpha*(x(9)-x(8)))/toi/x(20);
dx(9)=((1+alpha)*(x(8)-x(9))+alpha*(x(10)-x(9)))/toi/x(21);
dx(10)=((1+alpha)*(x(9)-x(10))+alpha*(x(11)-x(10)))/toi/x(22);
dx(11)=((1+alpha)*(x(10)-x(11))+alpha*(x(12)-x(11)))/toi/x(23);
dx(12)=((1+alpha)*(x(11)-x(12)))/toi/x(24);
dx(13)=(h0-(1+alpha)*x(13)+alpha*x(14))/toi/x(19)-k*x(1)*x(7)*(x(13))^(a)+kl*6*(1-
x(19))/dB*(H0-x(13));
dx(14)=((1+alpha)*(x(13)-x(14))+alpha*(x(15)-x(14)))/toi/x(20)-k*x(2)*x(8)*(x(14))^(a)+kl*6*(1-
x(20))/dB*(H0-x(14));
dx(15)=((1+alpha)*(x(14)-x(15))+alpha*(x(16)-x(15)))/toi/x(21)-k*x(3)*x(9)*(x(15))^(a)+kl*6*(1-
x(21))/dB*(H0-x(15));
dx(16)=((1+alpha)*(x(15)-x(16))+alpha*(x(17)-x(16)))/toi/x(22)-k*x(4)*x(10)*(x(16))^(a)+kl*6*(1-
x(22))/dB*(H0-x(16));
dx(17)=((1+alpha)*(x(16)-x(17))+alpha*(x(18)-x(17)))/toi/x(23)-k*x(5)*x(11)*(x(17))^(a)+kl*6*(1-
x(23))/dB*(H0-x(17));
```

```
dx(18)=((1+alpha)*(x(17)-x(18)))/toi/x(24)-k*x(6)*x(12)*(x(18))^(a)+kl*6*(1-x(24)) /dB*(H0-x(18));

dx(19)=kl*6*P*x(19)*(1-x(19))/dB/R/T*(H0-x(13))+(e0-x(19))/toi;

dx(20)=kl*6*P*x(20)*(1-x(20))/dB/R/T*(H0-x(14))+(x(19)-x(20))/toi;

dx(21)=kl*6*P*x(21)*(1-x(21))/dB/R/T*(H0-x(15))+(x(20)-x(21))/toi;

dx(22)=kl*6*P*x(22)*(1-x(22))/dB/R/T*(H0-x(16))+(x(21)-x(22))/toi;

dx(23)=kl*6*P*x(23)*(1-x(23))/dB/R/T*(H0-x(17))+(x(22)-x(23))/toi;

dx(24)=kl*6*P*x(24)*(1-x(24))/dB/R/T*(H0-x(18))+(x(23)-x(24))/toi;

%%%%%%%%%%%%%%%%%%%%%%%%%%%%%%%%%%%%%%%%%%
```

Appendix G Temperature Profile

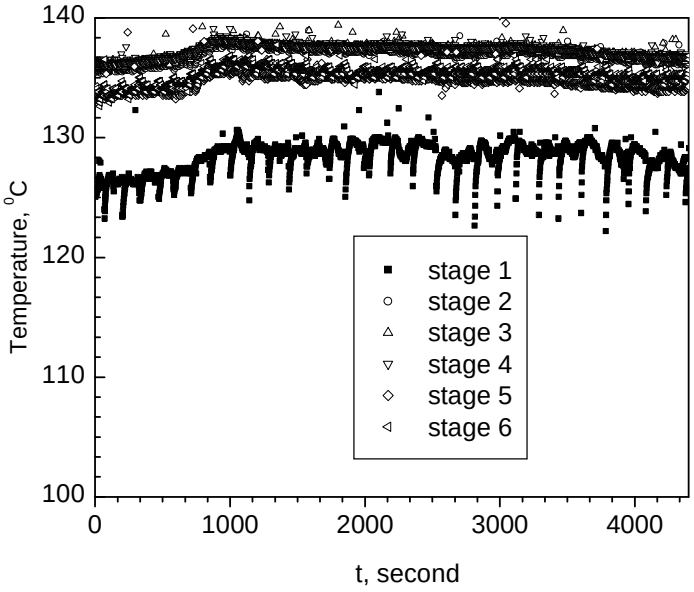

Temperature profile in various stages (above: Run #1; bottom: Run #5)

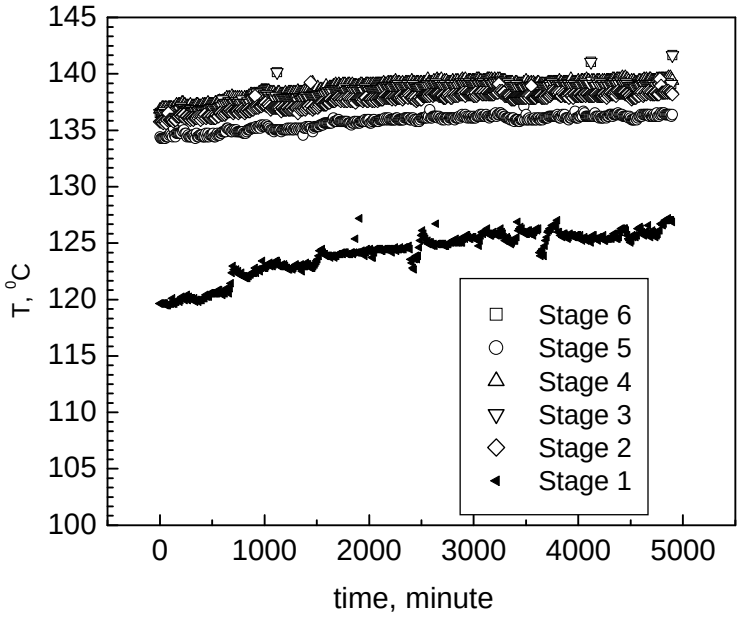

Bibliography

Bakker R.A., Van Den Akker H.E.A., **1994**, Computational Study of Chemical Reactor on the Basis of Micromixing Model, *Chem. Eng. Res. Des.*, 72(A6), 733-738.

Bhattacharjee S., Bhowmick A.K., Avasthi B.N., **1991**, High-Pressure Hydrogenation of Nitrile Rubber: Thermodynamics and Kinetics, *Ind. Eng. Chem. Res.*, 30, 1086-1092.

Bhavaraju S.M., Russell T.W.F., Blanch H.W., **1978**, The Design of Gas Sparged Devices for Viscous Liquid Systems, *A.I.Ch.E.J.*, 24, 454-466.

Bibaud R.E., Treybal R.E., **1966,** Axial Mixing and Extraction in a Mechanically Agitated Liquid Extraction Tower, *A.I.ChE.J*, 12(3), 472-477.

Breman B.B., Beenackers A.A.C.M., Bouma M.J., **1995**, Flow Regimes, Gas Hold-up and Axial Gas Mixing in the Gas-Liquid Multistage Agitated Contactor, *Chem. Eng. Sci.*, 50, 2963-2982.

Breman B. B., Beenackers A.A.C.M., Bouma M.J., Van Der Werf M.H., **1996a**, The Gas-liquid Mass Transfer Coefficient (k_La) in the Gas Liquid Multistage Agitated Contactor (MAC), *Trans IChemE, Part A*, 74(A6), 872-881.

Breman B. B., Beenackers A.A.C.M., Bouma M.J., Van Der Werf M.H., **1996b,** Axial Liquid Mixing in a Gas-liquid Multistage Agitated Contactor, *Trans IChemE, Part A*,74 (A6), 669-678.

Brucato A., Ciofalo M., Grisafi F., Micale G., **1998**, Numerical Prediction of Flow Fields in Baffles Stirred Vessels: a Comparison of Alternative Modeling Approaches. *Chem. Eng. Sci.*, 53, 3653-3684.

Bujaski W., Nienow A.W., Chatwin S., Cooke M., **1987**, Dependency on Scale of Power Numbers of Rushton Disc Turbines, *Chem. Eng. Sci.*, 42(2), 317-326.

Bujalski J.M., Jaworski Z., Bujalski W., Nienow A.W., **2002**, The Influence of the Addition Position of a Tracer on CFD Simulated Mixing Times in a Vessel Agitated by A Rushton Turbine, *Chem. Eng. Res. Des.*, 80, 824-831.

Calderbank P.H., Physical Rate Process in Industrial Fermentation, **1958**, Part I The Interfacial Area in Gas Liquid Contacting with Mechanical Agitation, *Chem. Eng. Sci.*, 36, 443-446.

CFX 5.7.1 User Manual, ANSYS Inc. Waterloo, 2005

Chio B.S., Wan B., Philyaw S., Dhanasekharan K., Ring T.A., **2004,** Residence Time Distribution in a Stirred Tank: Comparison of CFD Predictions with Experiment, *Ind. Eng. Chem. Res.*, 43, 6548-6556.

Dankwerts P.V., **1970**, Gas-Liquid Reactions, McGraw-Hill, NewYork.

Deckwer W., **1992**, *Bubble Column Reactors*, John Wiley and Sons, New York.

Deen N.G., Soberg T., Hjertager B.H., **2002**, Flow Generated by an Aerated Rushton Impeller: Two-Phase PIV Experiments and Numerical Simulations, *Can. J. Chem. Eng..,* 80, 638-652.

Delnoij E., Kuipers J.A.M., van Swaaji W.P.M., **1997**, Computational Fluid Dynamics Applied Gas Liquid Contactors, *Chem. Eng. Sci.,* 52, 3623-3638.

Fajner D., Magelli F., Pasquali G., **1982**, Modeling of Non-Standard Mixers Stirred with Multiple Impellers, *Chem. Eng. Comm*., 17, 285-295.

Garcia-Ochoa F., Gomez E., **2004**. Theoretical Prediction of Gas-liquid Mass Transfer Coefficient, Specific Area and Hold-up in Sparged Stirred Tanks**,** *Chem. Eng. Sci*., 59, 2489-2501.

Greaves M., Barigou M., **1988**. Estimation of Gas Hold-up and Impeller Power in a Stirred Vessel Reactor, *Institute of Chemical Engineers Symposium Series*, 63, 235-255.

Harris C.K., Roekaerts D., Rosendal F.J.J., Buitendijk F.G.J., Daskoplous Ph., Vreenegoor A.J.N, Wang H., **1996**, Computational Fluid Dynamics for Chemical Reactor Engineering, *Chem. Eng. Sci.,* 51, 1569-1594.

Haug H.F., **1971**, Backmixing in Multistage Agitated Contactor-a Correlation, *A.I.Ch.E.J.*, 17(3), 585-589.

He G., Guo, Y., Hsu A.T., **1999**, The Effect of Schmidt Number on Turbulent Scalar Mixing in a Jet-in-crossflow, *Int. J. Heat MassTtran.*, 42, 3727-3738.

Hjertager L.K., Hjertager B.H., Solberg T., **2002**, CFD Modeling of Fast Chemical Reactions in Turbulent Liquid Flows, *Comp. Chem. Eng.,* 26, 507-515.

Hibino S., Tsuge H., **1978,** Mass Transfer in Multistage Bubble Column, *Asahi Glass Found Ind Technol.*, 32, 1.

Hougen O.A., Watson K.M., Ragatz R.A., **1960**, Chemical equilibrium constants, In Chemical Process Principle, Part II, Thermodynamics; Wiley, NewYork, 982-1014.

Ingham.J., **1972**, Backmixing in a Multi-mixer Liquid-liquid Extraction Column, *Trans.Inst.Chem.Eng*, 50, 372-384.

Joshi J.B., Pandit A.B., Sharmar M.M., **1982**, Mechanically Agitated Gas-liquid Reactors, *Chem. Eng. Sci.,* 37(6), 813-844.

Kehl S., **1998**. Catalytic Hydrogenation of Nitrile Butadiene Rubber in a Packed Reactor, M.S. Thesis, Department of Chemical Engineering, University of Waterloo.

Kerdouss F., Bannari A., Proulx P., **2006**, CFD Modeling of Gas Dispersion and Bubble Size in a Double Turbine Stirred Tank, *Chem. Eng. Sci.*, 61,3313-3322.

Kubo et al., **1981**. US 4,275,012.

Kudrewizki, F., Rabe P., Model of the Dissipation of Mechanical Energy in Gassed Stirred Tanks, **1986**, *Chem. Eng. Sci.*, 41, 2247-2252.

Lane G.L., Schwarz M.P., Evans G.M., **2002**, Prediction Gas-liquid Flow in a Mechanically Stirred Tank, *Appied Mathematical Modeling*, 26, 223-235.

Lane G.L., Schwarz M.P., Evans G.M., **2005**, Numerical Modeling of Gas Liquid Flow in Stirred Tanks, *Chem.Eng. Sci.*, 60, 2203-2214.

Lelli U., Magelli F., Sama C., Backmixing in a Multistage Mixer Column, **1972**, *Chem. Eng. Sci.*, 27, 1109-1117.

Lelli U., Magelli F., Pasquali G., **1976**, Multistage Mixer Columns-A Contribution to Fluid-Dynamic Studies, *Chem. Eng. Sci.*, 31, 253-256.

Letellier B., Xuereb, C., Swaels P., Hobbes, P., Bertrand J., **2002**, Scale-up in Laminar and Transiet Regimes of a Multi-stage Stirrer, a CFD Approach, *Chem. Eng. Sci.*, 57, 4617-4632.

Levenspiel O., **1999**, *Chemical Reaction Engineering*, Second Edition, John Wiley & Sons, pp. 270-280.

Loiseau B., Midoux N., Charpentier J.C., **1977,** Some Hydrodynamics and Power Input Data in Mechanically Agitated Gas-Liquid Contactor, *A.I.Ch.E.J.*, 23, 931-935.

Luo, J.Y., Gosman A.D., Issa R.I., Middleton J.C., Fitzgerald M.K., **1993**, Full Flow Field Computation of Mixing in Baffled Stirred Vessels, *Chem. Eng. Res. Des.*, 71(A), 342-344.

Magelli F., Pasquali G., Lelli U., **1982**, Backmixing in Multistage Mixer Columns-II. Additional Results, *Chem. Eng. Sci.*, 37, 141-145.

Meister D., Post T., Dunn I.J., Bourne J.R., **1979**, Design and Characterization of a Multistage Mechanically Stirred Column Absorber, *Chem. Eng. Sci.*, 34, 1367-1374.

Michel B.J., Miller S.A., **1962**, Power Requirement of Gas Liquid Agitated Systems, *A.I.Ch.E.J.*, 20, 445-448.

Miyauchi T., Mitsutake H., Harase I., **1966**, Longitudinal Dispersion in a Rotating Impeller Types of Contactor, *A.I.Ch.E.J.*, 12(3), 508-513.

Montante G., Lee K.C., Brucato A., Yianneskis M, **1999**, An Experimental Study of Double-to-single Loop Transition in Stirred Vessels, *Can.J.Chem.Eng*, 77, 649-659.

Montante G., Lee K.C., Brucato A., Yianneskis M., **2001**, Numerical Simulation of the Dependency of Flow Pattern on Impeller Clearance in Stirred Vessels, *Chem. Eng. Sci.,* 56, 3751-3770.

Montante G., Mostek M., Jahoda M., Magelli F., **2005**, CFD Simulations and Experimental Validation of Homogenization Curves and Mixing Time in Stirred Newtonian and Pseudoplastic Liquids, *Chem. Eng. Sc.*, 60, 2427-2437.

Nagata Shinji, **1975**, Mixing: Principles and Applications, Wiley, NewYork.

Nocentini M., Fajner D., Pasquali G., Magelli F., **1993**, Gas-liquid Mass Transfer and Hold-up in Vessels Stirred with Multiple Rushton Turbines: Water and Water-glycerol Solutions, *Ind. Eng. Chem. Res.*, 32, 19-26.

Paglianti A., Takenaka K., Bujalski W., Takahashi K., **2000**, Estimation of Gas Hold-up in Aerated Vessels, *Can. J. Chem. Eng.*, 78, 386-392.

Pan Q.M., Rempel G.L., **2000**, Numerical Investigation of Semibatch Process for Hydrogeantion of Diene-based Polymers, *Ind .Eng. Chem. Res.*, 39, 277-284.

Pan Q.M., Rempel G.L., NG F.T.T., **2002**, Numerical Investigation of Continuous Processes for Catalytic Hydrogenation of Nitrile Butadiene Rubber, *Poly. Eng. Sci.*, 42(5), 899-910.

Pan Q.M., Rempel G.L., **2003**, Numerical Investigation for Optimal Phase Hold-up of a Continuous Reactor for Hydrogenation of Nitrile Butadiene Rubber, *International Journal of Chemical Reactor Engineering*, 1, A59.

Pan Q.M., Rempel G.L., **2004**, Investigation of Fundemental Data for Nitrile Butadiene Rubber in Monochlorobenzene and o-Dichlorobenzene, *Poly. Eng. Sci.*, 44, 88-95.

Parent J.S, **1996**, Catalytic Hydrogenation of Butadiene Copolymers Ph.D Thesis, Department of Chemical Engineering, University of Waterloo,

Parent J.S; Mcmanus N.T; Rempel G.L. **1996**, RhCl(PPh3)3 and RhH(PP3)4 Catalyzed Hydrogenation of Acrylonitrile-Butadiene Copolymers, *Ind. Eng. Chem. Res.*, 35,4417-4423.

Parent J.S.; McManus N.T.; Rempel G.L., **1998**, OsHCl(CO)(O2)(PCy3)2-Catalyzed Hydrogenation of Acrylonitrile-Butadiene Copolymers, *Ind. Eng. Chem. Res.*, 37, 4253-4261.

Patwardhan A.W., **2001a**. Prediction of Residence Time Distribution of Stirred Reactors, *Ind.Eng. Chem. Res.*, 40, 5686-5695.

Patwardhan A.W., **2001b**. Prediction of Flow Charateristics and Energy Balance for a Variety of Downflow Impellers, *Ind. Eng. Chem. Res*., 40, 3806-3816.

Perry R.H., Green D.W., **1997**, Perry's Chemical Engineer's Handbook (7th Edith), McGraw-hill.

Ranade V.V., Bourne J.R., Joshi J.B., **1991**, Fluid Mechanics and Blending in Agitated Tanks. *Chem. Eng. Sci.*, 46, 1883-1893.

Ranade V.V., **1997**, An Efficient Computational Model for Simulating Flow in Stirred Vessels: A Case of Rushton turbine, *Chem. Eng. Sci.*, 52(24), 4473-4484.

Sahu A.K., Kumar P., Patwardhan A.W., Joshi J.B., **1999**, CFD Modeling and Mixing in Stirred Tanks, *Chem. Eng. Sci.*, 54, 2285-2293.

Rehakova M., Novosad Z., **1968**, Residence Time Distribution and Fractional Conversion for a Multistage Reactor with Backmixing between Real Stages, *Chem. Eng. Sci.*, 23, 139-145.

Rempel G.L, **2000**, Catalytic Hydrogenation of Nitrile Butadiene Rubber, Polymer Preprints, 41(2), 1507-1508.

Smith J.M., **1991**, Simple Performance Correlations for Agitated Vessels, Proceedings of the Seventh European Mixing Conference(Brugge, September 18-20), Koninklijke, Vlaamse Ingenieursvereniging: Antwerpen, 233-241.

Sullivan G.A., Treybal R.E., **1970**, Axial Mixing and Gas Adsorption in a Mechanically Agitated Absorption Tower, *Chem.Eng. J.*, 1, 302-309.

Sawinsky J., Hunek J., **1981**, Methods for Investigating Backmixing in the Continuous Phase of Multiple-mixer Extraction Columns. *Chem. Eng. Res. Des.*, 59, 64-66.

Takriff M.B., Penny W.R., Fasano J.B., **1998**, Insterstage Backmixing of an Aerated Multistage Mechanically-Agitated Compartmented Column, *Can. J. Chem. Eng.*, 76, 365-369.

Tatterson G.B., **1991**, Fluid Mixing and Gas Dispersion in Agitated Tanks, McGraw-Hill, NewYork.

Tsuge H., Yamada T., Terasaka K., Miyakawa S., **1995**, Mass Transfer in Multistage Slurry Bubble Column: Analysis by Back Flow Model, *Trans IChemE, Part A*, 73, 669-675.

Van't Reit. K., **1979**, Review of Measuring Mehods and Results in Non-viscous Gas-liquid Mass Transfer in Stirred Vessels, *Ind Eng Chem Proc Dev.*, 18(3), 357-363.

Vasconcelos J.M.T., Alves S.S., Barata, J.M., **1995,** Mixing in Gas-liquid Contactors Agitated by Multiple Turbines, *Chem. Eng. Sci.,* 50, 2343-2354.

Vasconcelos J.M.T., Barata J.M., Alves S.S., **1996**, Transitional Mixing in Multiple-Turbine Agitated Tanks, *Chem. Eng. J.*, 63, 53-58.

Venneker B.C.H., Derksen J.J., Van Den Akker H.E.A, **2002**, Population Balance Modeling of Aerated Stirred Vessels Based on CFD, *A.I.CH.E.J.*, 48, 673-685.

Vidaurri F.C., Sherk F.T., **1985**, Low Backmixing in Multistage Agitated Contactor Used as Reactor, *A.I.Ch.E.J.*, 31(5), 705-710.

Vidaurri et al., **1983**. US 4,370,470.

Xu B.C., Penney W.R., Fasano J.B., **2005**, Interstage Backmixing for Single-Phase Systems in Compartmented Agitated Columns: Design Correlations, *Ind. Eng. Chem. Res.*, 44, 6103-6109.

Yagi H., Yoshida F., **1975**, Gas Absorption by Newtonian and Non-Newtonian Fluids in Sparged Agitated Vessels, *Ind .Eng. Chem. Proc. Des. Dev.*, 14, 488-493.

Yimer, I., Campbell I., Jiang L.Y., **2002**, Estimation of the Turbulent Schmidt Number from Experimental Profiles of Axial Velocity and Concentration for High-Reynolds-number Jet Flows. *Canadian Aeronautics and Space Journa*l, 48, 195-200.

Zhang L.F., **2004**, Research Proposal, University of Waterloo.

Zhang L.F., Pan Q.M., Rempel G.L., **2005 a**, Liquid Backmixing and Phase Hold-up in a Gas Liquid Multistage Agitated Contactor, *Ind. Eng. Chem. Res.*, 44, 5304-5311.

Zhang L.F., Pan Q.M., Rempel G.L., **2005b** ,A Hydrodynamic Study and Mass Transfer Coefficient on a Multistage Agitated Contactor with Cocurrent Gas Liquid Upflow, Symposium of 7th World Congress of Chemical Engineering, 10-14 July, Glasgow, Scotland, no. 05-003, 10 pages.

Zhang L.F., Pan Q.M., Rempel G.L., **2005c,** Modeling and Simulation of A Multistage Agitated Contactor for Hydrogenation of Nitrile Butadiene Rubber, *International Journal of Chemical Reactor Engineering*, A9.

Zhang L.F., Pan Q.M., Rempel G.L., **2006**, Liquid Phase Mixing and Holdup in a Multistage-Agitated Contactor with Co-current Upflow Air/viscous Fluids, *Chem. Eng. Sci.,* 61, 6189-6198.